United States Environmental Protection Agency

Evaluation and Mitigation of Visible Acidic Aerosol Plumes from Coal Fired Power Boilers

Final Report

EPA/600/R-06/156
September 2006

EVALUATION AND MITIGATION OF VISIBLE ACIDIC AEROSOL PLUMES FROM COAL FIRED POWER BOILERS

FINAL REPORT

EPA Contract No. EP-C-04-056
Work Assignment Numbers 0-3 & 1-4
Southern Research Institute Project No. 11402

By:
Peter M. Walsh, Joseph D. McCain, and Kenneth M. Cushing
Southern Research Institute
2000 Ninth Ave. South
P.O. Box 55305
Birmingham, AL 35255-5305

For:
C. Andrew Miller, Project Officer

U.S. Environmental Protection Agency
Office of Research and Development
National Risk Management Research Laboratory
Air Pollution and Prevention Control Division
Research Triangle Park, NC 27711

Notice

The U.S. Environmental Protection Agency through its Office of Research and Development funded and managed the research described here. It has been subjected to the Agency`s review and has been approved for publication as an EPA document. Mention of trade names, products, or services does not convey, and should not be interpreted as conveying, official EPA approval, endorsement, or recommendation.

Foreword

The U.S. Environmental Protection Agency (EPA) is charged by Congress with protecting the Nation's land, air, and water resources. Under a mandate of national environmental laws, the Agency strives to formulate and implement actions leading to a compatible balance between human activities and the ability of natural systems to support and nurture life. To meet this mandate, EPA's research program is providing data and technical support for solving environmental problems today and building a science knowledge base necessary to manage our ecological resources wisely, understand how pollutants affect our health, and prevent or reduce environmental risks in the future.

The National Risk Management Research Laboratory (NRMRL) is the Agency's center for investigation of technological and management approaches for preventing and reducing risks from pollution that threaten human health and the environment. The focus of the Laboratory's research program is on methods and their cost-effectiveness for prevention and control of pollution to air, land, water, and subsurface resources; protection of water quality in public water systems; remediation of contaminated sites, sediments and ground water; prevention and control of indoor air pollution; and restoration of ecosystems. NRMRL collaborates with both public and private sector partners to foster technologies that reduce the cost of compliance and to anticipate emerging problems. NRMRL's research provides solutions to environmental problems by: developing and promoting technologies that protect and improve the environment; advancing scientific and engineering information to support regulatory and policy decisions; and providing the technical support and information transfer to ensure implementation of environmental regulations and strategies at the national, state, and community levels.

This publication has been produced as part of the Laboratory's strategic long-term research plan. It is published and made available by EPA's Office of Research and Development to assist the user community and to link researchers with their clients.

Sally Gutierrez, Director
National Risk Management Research Laboratory

TABLE OF CONTENTS

LIST OF FIGURES

List of Figures (Continued)

List of Figures (Continued)

LIST OF TABLES

NOMENCLATURE

c_{ad}	mean speed of acid mist droplets, m/s
c_{fg}	mean speed of flue gas molecules, m/s
c_w	mean speed of water vapor molecules, m/s
C_{ad}	concentration of acid mist droplets, kg/m^3
C_{ad0}	initial concentration of acid mist droplets, kg/m^3
C_{bl}	average gas concentration in the boundary layer of a tube or particle, kmol/m^3
C_c	Cunningham correction factor, Eq. (7.9), dimensionless
C_D	drag coefficient for scrubber spray droplets, dimensionless
C_g	total gas concentration, kmol/m^3
$C_{H_2SO_4}$	concentration of H_2SO_4, kg/m^3
C_S	total gas concentration at a deposit or particle surface, kmol/m^3
C_{sd}	concentration of scrubber spray droplets, kg/m^3
$C_{w,ad}$	concentration of water vapor in equilibrium with the surfaces of acid mist droplets, kg/m^3
$C_{w,sd}$	concentration of water vapor in equilibrium with the surfaces of scrubber spray droplets, kg/m^3
$C_{w,\infty}$	concentration of water vapor in the free stream, far from droplet surfaces, kg/m^3
d	characteristic length, diameter, m
d_{ad}	diameter of acid mist droplets, m
d_{ad0}	initial diameter of acid condensation nuclei, m
d_p	mean particle size, m
d_{sd}	diameter of scrubber spray droplets, m
d_t	tube diameter, m
D_{ad}	diffusion coefficient for acid mist droplets, m^2/s

NOMENCLATURE (CONTINUED)

$D_{w,fg}$	pseudo-binary molecular diffusion coefficient for a mixture of water vapor with the other combustion products, m^2/s
D_{SO_3}	molecular diffusion coefficient of SO_3 in combustion products, m^2/s
ESP	electrostatic precipitator
f_{cap}	fraction of initial H_2SO_4 captured by scrubber spray droplets, dimensionless
FGD	flue gas desulfurization
k_B	Boltzmann constant, = 1.38 x 10^{-23} J/K
k	effective rate coefficient for the heterogeneous reaction between SO_2 and O_2, m/s
k_i	global reaction rate constant for compound *i*
k_{ad}	rate coefficient for coagulation, m^3/s
k_t	effective rate coefficient for the heterogeneous reaction between SO_2 and O_2 at tube or ash deposit surfaces, m/s
k_p	effective rate coefficient for the heterogeneous reaction between SO_2 and O_2 at particle surfaces, m/s
k_{sa}	effective overall rate coefficient for transport of water vapor between scrubber spray droplets and acid mist droplets, Eq. (7.24), dimensionless
k_1	rate coefficient for Reaction (5.4), m/s
k_2	rate coefficient for Reaction (5.5), m/s
$Kn_{ad,ad}$	Knudsen number for diffusion of droplets toward each other, dimensionless
$Kn_{fg,ad}$	Knudsen number for acid mist droplets in flue gas, dimensionless
$Kn_{w,ad}$	Knudsen number for water vapor diffusing to and from acid mist droplets in flue gas, dimensionless
LG	liquid to gas feed ratio in the scrubber, gal/1000 scf or dimensionless
m_{ad}	mass of acid mist droplets, kg
N_{ad}	number concentration of acid mist droplets, m^{-3}
N_{ad0}	initial number concentration of acid mist droplets, m^{-3}

NOMENCLATURE (CONTINUED)

$P_{w,ad}$	partial pressure of water vapor in equilibrium with the surfaces of acid mist droplets, Pa
$P_{w,af}$	partial pressure of water vapor in equilibrium with a flat sulfuric acid surface, Pa
$P_{w,sd}$	partial pressure of water vapor in equilibrium with the surfaces of scrubber spray droplets, Pa
r_{SO_3}	rate of sulfur trioxide formation, kmol/m^3·s
R	universal gas constant, = 8314.51 J/(kmol·K)
Re	Reynolds number, dimensionless
S	effective area of catalytic surface per unit of gas volume, m^{-1}
S_{ad}	specific surface area of acid mist droplets, m^2/kg
S_p	external surface area of fly ash particles per unit of gas volume, m^{-1}
S_{sd}	specific surface area of scrubber spray droplets, m^2/kg
S_t	surface area of tube or ash deposits on a tube, per unit of gas volume, m^{-1}
Sc	Schmidt number, dimensionless
SCR	selective catalytic reduction
Sh	Sherwood number for mass transfer, dimensionless
Sh_p	Sherwood number for mass transfer through the external boundary layer of a particle, = 2, dimensionless
Sh_{sd}	Sherwood number for mass transfer to and from scrubber spray droplets, dimensionless
$Sh_{w,ad}$	Sherwood number for transport of water vapor to and from acid mist droplets, dimensionless
Sh_t	average Sherwood number for mass transfer between tube or deposit surface and the free stream, dimensionless$t$ time, s
t	residence time, s
t_o	residence time at the entrance to a row of tubes, s

NOMENCLATURE (CONTINUED)

T	absolute temperature, K
u_{fg}	velocity of flue gas in scrubber, m/s
u_{sd}	terminal fall velocity of scrubber spray droplets relative to the scrubber, m/s
W_{fg}	average molecular weight of flue gas, kg/kmol
$W_{H_2SO_4}$	molecular weight of H_2SO_4, kg/kmol
$W_{H_2SO_4 \cdot H_2O}$	molecular weight of $H_2SO_4 \cdot H_2O$, kg/kmol
W_w	molecular weight of water, kg/kmol
X_i	mole fraction of species i, dimensionless
X_{SO_3}	mole fraction of SO_3 in the free stream, dimensionless
$X_{SO_3,eq}$	mole fraction of SO_3 at equilibrium, dimensionless
$X_{SO_3,eq,p}$	mole fraction of SO_3 at equilibrium at particle surfaces, dimensionless
$X_{SO_3,eq,t}$	mole fraction of SO_3 at equilibrium at tube or ash deposit surfaces, dimensionless
$X_{SO_3,s}$	mole fraction of SO_3 at catalyst surface, dimensionless
$X_{SO_3,o}$	initial mole fraction of SO_3 at the entrance to a row of tubes, dimensionless
Y_a	mass fraction of H_2SO_4 in sulfuric acid, dimensionless
Y_{a0}	initial mass fraction of H_2SO_4 in acid condensation nuclei, dimensionless
$Y_{Fe_2O_3}$	mass fraction of all iron oxides in deposit or particles, from ash analysis, dimensionless
Y_{FeO_X}	mass fraction of higher iron oxide in deposit or ash particles, dimensionless
$Y_{FeO_{X-1}}$	mass fraction of reduced iron oxide in deposit or ash particles, dimensionless

NOMENCLATURE (CONTINUED)

Greek Symbols

β	factor matching droplet diffusion behavior in the continuum and free molecule regimes, Eq. (7.3), dimensionless
Δt	small increment of time, s
λ_{ad}	mean free path of acid mist droplets, m
λ_{fg}	mean free path of flue gas molecules, m
λ_{w}	mean free path of water vapor molecules in flue gas, m
μ_{fg}	viscosity of flue gas, kg/(m·s)
ρ_{a}	density of sulfuric acid, kg/m^3
ρ_{sd}	density of scrubber spray droplets, kg/m^3
σ_{a}	surface energy of sulfuric acid, J/m^2

Subscripts

a	acid
ad	acid mist droplets
af	flat acid surface
c	Cunningham (correction factor)
cap	captured (acid by scrubber spray droplets)
D	drag
eq	equilibrium
fg	flue gas
sa	scrubber spray droplets to acid mist droplets
sd	scrubber spray droplets
w	water vapor
0	initial value at entrance to scrubber
∞	free stream, far from droplet surfaces

ABSTRACT

The formation of sulfur trioxide (SO_3) during the combustion of sulfur-containing fuels, particularly coal, can increase significantly following the installation and operation of selective catalytic reduction (SCR) systems for reduction of nitrogen oxides (NO_x). The increased SO_3 formation can in turn lead to adverse environmental impacts, including visible near-stack plumes and increased fine PM emissions, primarily in the form of sulfuric acid (H_2SO_4) aerosols. The potential extent of the problem in the electric utility sector is estimated based on the population of coal-fired utility boilers, the sulfur content of coal burned by each unit, and the likelihood that units will install SCR and flue gas desulfurization (FGD) systems. Of the 363 large (≥ 250 MWe) generating plants in the eastern U.S., there is a significant potential that as many as 65 could experience visible H_2SO_4 aerosol plumes or more serious problems after installation of SCR and FGD systems, based on the sulfur content of the coal historically used at those plants. As use of FGD systems increases, it is also likely that utilities will turn to higher sulfur coal, which can exacerbate this problem. This report describes the mechanisms of SO_3 and acid aerosol formation and removal across boiler convection sections, air preheaters, and wet FGD systems, and presents information from an exploratory study of the absorption of SO_3 onto coal fly ash. A model of SO_3 formation and emissions based on these mechanisms is shown to accurately predict the stack concentration of SO_3 for a 1300 MWe pulverized coal-fired boiler, indicating that the mechanisms described have captured the fundamental behavior of SO_3 in utility combustion and flue gas treatment systems. This information can provide the basis for developing mitigation approaches to reduce the impacts of SO_3 formation across SCRs and the subsequent formation and emission of acid aerosols.

1. INTRODUCTION

Background

In 2006 the Environmental Protection Agency (EPA) promulgated the "Clean Air Interstate Rule" (formerly called the "Interstate Air Quality Rule") with the goal of reducing sulfur dioxide (SO_2) and oxides of nitrogen (NO_x) emissions in the Eastern U.S. When fully implemented, the rule is projected to reduce SO_2 emissions by over 70% from 2003 levels and reduce NO_x emissions by over 60% from 2003 levels.[1] Achieving these goals is expected to involve widespread use of selective catalytic reduction (SCR) for NO_x control and flue gas desulfurization (FGD) scrubbers for SO_2 control in coal-fired power plants. In fact, current usage of these technologies has already led to substantial reductions in emissions of NO_x and SO_2. However, the use of SCR for NO_x control has the potential to enhance the formation of sulfur trioxide (SO_3).[2] At elevated concentrations, SO_3 forms visible plumes and excessive local concentrations of sulfuric acid (H_2SO_4) aerosols.

Elevated SO_3 concentrations are of concern due in part to associated potential adverse health effects. Particularly in areas that can be affected by sinking plumes that fall to ground level near the stack, increases in PM smaller than 2.5 μm in aerodynamic diameter ($PM_{2.5}$) caused by high H_2SO_4 concentrations are of concern. At typical ambient concentrations, the health impacts of H_2SO_4 aerosols are unclear. Some evidence of impaired mucociliary clearance and modest changes in lung function has been identified,[3] but there is limited evidence of significant airway inflammation or altered bronchial responsiveness as a result of exposure to typical ambient levels of H_2SO_4 aerosol.[4] In sensitive populations[5] or in combination with other pollutants,[6,7] exposure to H_2SO_4 may lead to more serious problems compared to exposure to H_2SO_4 alone.

Where plumes intercept the ground, effects associated with the higher concentrations associated with occupational exposure levels may be more applicable than effects associated with ambient concentrations. A significant difference is that near-stack plume contact incidents can result in concentrations much higher than typical ambient levels, but much shorter in duration and less frequent than occupational exposures. At elevated occupational levels, exposure to SO_3 can cause lung irritation, fluid build-up in the lungs (pulmonary edema), third-degree burns to the skin, and blindness. Long-term, lower level occupational exposure can lead to bronchitis, emphysema, chronic runny nose, tearing of the eyes, nosebleeds, headaches, nausea, dizziness, and erosion of the stomach and teeth.[8]

There have not been any reported instances of the more serious effects associated with non-occupational exposure to SO_3 or H_2SO_4 aerosol, although physiological responses such as eye, nose, and throat irritation and breathing difficulty have been reported for episodes involving plumes containing sulfuric acid aerosols at ground level.[9,10] In an incident documented in 2001 involving the American Electric Power Gavin Power Plant, residents downwind of a plant having a plume that touched the ground complained of irritation of the eyes, nose, and throat; shortness of breath; and asthma-like symptoms. Measurements of H_2SO_4 levels in the area were found to be between 35 and 120 $\mu g/m^3$.[11] At the same time, ground-level SO_2 concentrations were measured at 20-50 $\mu g/m^3$, so it is not clear whether the effects were caused by H_2SO_4, SO_2, or the combination of the two along with the other pollutants in the plume. In either case, the presence

of increased levels of acid aerosols and SO_3 is associated with adverse health impacts at concentrations that have been measured in plumes that have contacted the ground.

In addition to the public health impacts of increased SO_3 formation, plant components can be adversely impacted as well.[12,13] Increases in SO_3 formation and emissions can clearly cause problems that need to be addressed for several reasons, but as noted above can also be a consequence of efforts to achieve significant reductions in SO_2 and NO_x. This report will discuss efforts to better understand SO_3 formation processes, information that can lead to cost-effective mitigation approaches and minimization of the adverse impacts of SO_3.

Project Description

The purpose of this project was to conduct research that would improve EPA's understanding of the formation mechanisms of SO_3 and the means by which power plants can minimize the formation of sulfuric acid emissions. These included characterizing the potential significance of the problem and assessing interactions between coal type, pollution control system design and operation, and emissions of SO_3, H_2SO_4, NO_x and SO_2.

This research is important to efforts to achieve targeted reductions in emissions of NO_x and SO_2 while minimizing adverse consequences of control technology application. Combined use of SCR for NO_x control and FGD for SO_2 control in coal-fired power plants has the potential to enhance the formation of SO_3. At elevated concentrations, SO_3 forms visible plumes and excessive local concentrations of sulfuric acid aerosols. Such indirect effects of SCR use must be more fully understood in order to meet regulatory goals of reducing ambient levels of SO_2, NO_x, and particulate matter (PM) in a way that does not create new air pollution problems. In particular, states need information related to SO_3 emissions and its mitigation for the purpose of developing State Implementation Plans (SIPs). The tasks performed during this research were intended to provide that information to EPA and the states.

Earlier work conducted by Southern Research Institute (SRI) for EPA produced an interim report that described the current state of understanding of SO_3 formation and mitigation.[2] The report concluded that "the difficulty faced by utility plant operators is that guidelines are not presently available to define the extent of the problem that may occur at a given site. In the absence of such guidelines, it is not possible to determine in advance the control strategies that are technically and economically feasible for a particular plant site." This lack of guidelines is primarily the result of a lack of sufficient credible data on which to base models for control of SO_3 emissions. In particular, SO_3 collection by combustion air preheaters, electrostatic precipitators and scrubbers were poorly characterized.

The current report describes research conducted by SRI to characterize methods to measure SO_3, develop model plant specifications, estimate acid droplet growth rates, and characterize absorption and adsorption of SO_3 by fly ash. The results reported here provide the basis for more accurate estimates of SO_3 formation and emissions and identify research needs for further improvement in understanding SO_3 formation and removal across different plant components.

Report Overview

Chapter 2 describes a survey of the potential extent of SO_3 emissions in the electric utility industry under current regulations, including the Clean Air Interstate Rule. The chapter includes a state-by-state tabulation of potential SO_3 emissions from individual power plant units and identified those areas where the greatest uncertainties exist (e.g., SCR conversion rates versus scrubber removal efficiencies).

Chapter 3 addresses the methods used to measure SO_3 in combustion flue gases, and describes efforts to develop improved measurement methods. In particular, Chapter 3 discusses tests of a modified sampling probe which permits extraction of a filtered gas sample without passing the sample through a layer of ash. Results are presented on exploratory tests of this probe for use with the controlled condensation method. The tests, conducted at SRI's Coal Combustion Research Facility, demonstrate improvements in SO_3 measurements using the modified probe. Additional, preliminary results are presented for tests at a full-scale operating power plant.

Chapter 4 covers the absorption and adsorption of SO_3 by coal fly ash for coals with significantly different ash properties. Absorption and adsorption of SO_3 and H_2SO_4 can be a major controlling factor in the overall process. Chapter 4 reports on tests that passed an SO_3 laden gas stream over an ash layer in a temperature and moisture controlled environment. Ashes from various coals were tested, and analyses are presented on the soluble sulfate levels for the untreated ashes and the ash specimens after exposure to SO_3. Test conditions were chosen to be representative of those found in typical economizer and air preheater sections.

Chapters 5 and 6 describe, respectively, the behavior of SO_3 in boiler convection sections and air preheaters. Chapter 5 provides quantitative results on the formation and removal of SO_3 across the convection sections (e.g., convective sections, superheaters, reheat sections, economizer). Chapter 6 presents results of estimates for SO_3 removal across four preheaters and compares the estimates to measured SO_3 concentrations at the preheater exits. These results can be used to model SO_3 formation, removal, and emissions for plants with different configurations and operating conditions to more effectively estimate impacts of equipment, fuel, and operating changes on SO_3 emissions and identify mitigation approaches.

Chapter 7 presents the development of an algorithm to describe the evolution and behavior of acid mists in wet FGD units, including mist eliminators, and plant stacks. The algorithm is used to evaluate how changing parameters such as H_2SO_4 concentration, scrubber droplet size, and the size of droplets exiting the mist eliminator influence the mass fraction of H_2SO_4 in the stack aerosol and the scrubber droplets, as well as the acid droplet number concentration and volume fraction. These results are then used to estimate the impacts of changing scrubber type and are compared to measurements from a full-scale plant.

The models presented in Chapters 5-7 are in the developmental stages and have had only minimal validation with measurements. Although they can be used to address performance at specific plants to identify where SO_3 is most likely to be formed or removed, there has not been adequate comparison with measurements to allow significant certainty in the predictions.

Additional measurements are needed along the entire flue gas path at several plants and with different coals to enable more certain estimates to be made.

2. EVALUATION OF THE POSSIBLE EXTENT OF THE SO_3 EMISSIONS PROBLEM IN THE ELECTRIC UTILITY INDUSTRY

With the promulgation of the Clean Air Interstate Rule (CAIR), the electric utility industry is beginning to install technologies for control of NO_x and SO_2. These newly installed technologies have the potential to increase emissions of SO_3 above current levels. To determine whether such changes would be likely to impact a significant fraction of plants, and if so, the degree of such impacts, a simple spreadsheet-based model was developed to evaluate the possible extent of the issue. The model collected data on basic plant size and design parameters and on coal use patterns. These data were coupled with reasonable average rates of SO_2 conversion to SO_3 and removal of SO_3 by common pollution control systems to develop an overall picture of what broad application of SCR and wet FGD scrubbers may mean for SO_3 emissions. This evaluation can provide some overview information on the extent to which SO_3 mitigation measures may be needed.

However, these estimates are highly uncertain and cannot be used to develop estimates for a specific plant. The uncertainties stem from the use of "reasonable average" values for SO_2 conversion and SO_3 removal, and particularly from an inability to predict how plants will work to meet the CAIR requirements. It is likely that the pattern of coal use will change as some plants meet the SO2 requirements by switching to lower sulfur coal, while others switch to higher sulfur coal following installation of FGD systems. Some plants may install either SCR or wet FGD, while others install both. Use of spray dryer systems or installation of fabric filters will also reduce a plant's SO_3 emissions compared to what would be estimated from the spreadsheet model. Finally, the trading approach used by CAIR will likely result in combinations of control efficiencies that cannot be incorporated into a simple spreadsheet model. Each of these factors combine to increase the uncertainties associated with the estimated results. Even so, the model does provide some order-of-magnitude estimate of the extent to which the SO_3 issue may be significant for the electric utility industry.

The evaluation conducted by Southern Research Institute is based on data from the Department of Energy (DOE) Federal Energy Regulatory Commission (FERC) Annual Steam-Electric Plant Operation and Design Database for 2002,[14] augmented when possible with additional information obtained from the U. S. EPA[15] and an industry database[16] to fill gaps in the FERC database. For each coal-fired power plant surveyed, SO_3 emissions after anticipated technology additions for control of NO_x by SCR and SO_2 by wet scrubbers were predicted. These emissions are referred to here as "collateral SO_3 emissions."

To compute the predicted SO_3 concentrations, SO_2 concentrations were calculated from the reported sulfur content of the coals being burned at each plant. The rate of oxidation of SO_2 to SO_3 depends on many factors, including the sulfur content of the fuel, the amount of excess air, and the presence of a catalyst. For this methodology, SO_3 concentrations produced by the boilers were estimated using SO_3/SO_2 ratios developed by Hardman, Stacy and Dismukes for eastern bituminous, western subbituminous, and lignite coals.[17] These ratios are based on measurements

taken during 16 field tests and are shown in Table 2.1 below and are considered to be reasonably representative of existing information. The coal types used in the calculations were the predominant fuels for each unit as reported in the database. Subsequent production and removal of SO_3 was calculated for the configuration of downstream controls at each site.

Table 2.1. Ratio of SO_3/SO_2 Based on 16 Field Tests[17]

Coals Burned	SO_3/SO_2 Ratio	
	Average	Standard Deviation
9 Eastern Bituminous Coals	0.004	0.003
7 Western Subbituminous and Lignite Coals	0.0011	0.0005

Table 2.2 summarizes the projected impact of collateral SO_3 emissions from coal-fired power plant units in the Mississippi Valley and the Eastern U.S. after anticipated technology additions for control of NO_x and SO_2. The table summarizes the number of units exceeding the specified concentrations of SO_3 in their stack emissions broken down by unit generating capacity. The column labeled "Missing Data" refers to units in the database for which critical information such as fuel sulfur was missing. The tabulations show the effect of retrofit of SCR and wet scrubbers on all units. Based on a simplified assumption that the proposed regulations would result in controls on approximately 75% of the total coal-fired generating capacity, all units larger than roughly 250 MW would operate with SCR/scrubber combinations. The total capacity for 250 MW and larger plants is estimated here to be 200 GW. The more detailed EPA analysis done for the Clean Air Interstate Rule (CAIR) estimates 178 GW of capacity will be retrofit with SCR and slightly higher than that, 187 GW, will be retrofit with scrubbers.[18]

Table 2.2 has columns for five SO_3 emissions levels of increasing regulatory or health impacts. The rows in the table for unspecified unit loads, designated as Unknown, refer to units in the database for which unit load information was unavailable. Units with scrubbers having stack SO_3 concentrations of about 4 ppm and higher may have difficulty meeting 20% opacity limits if, as is becoming more common, the opacity limits are applied to the stack plumes. At stack concentrations of about 10 ppm and higher, visible "blue" plumes will exist even in the absence of a scrubber. Plumes from units equipped with scrubbers reach ground level much closer to stacks than those without scrubbers, given equal stack heights. Because stack gases are less diluted close to the stack than at greater distances, ground level SO_3 concentrations near the stack will be higher for a unit with a scrubber than for the same unit without a scrubber.[2] The Gavin Power Plant and the Cinergy/PSI Gibson Generating Station are two plants that have been faced with substantial difficulties with local citizens and regulatory agencies because of such ground level concentrations of SO_3.[9,19] Potential health effect problems have led to concern at both the Gavin and Gibson plants where stack concentrations are approximately 13 ppm or higher. Another potential issue is complying with particulate mass emission rate standards. If the particulate emission standards were to change such that condensables (such as H_2SO_4 aerosols) are included as part of emissions of particulate matter, SO_3 aerosol concentrations in some stacks could contribute significantly to the overall particulate loading (1 ppm is equivalent to about 4 mg/dncm).

Table 2.2. Number of units predicted to exceed selected values of SO_3 stack concentration under scenario assumptions. Data cover all coal-fired plants in the Mississippi Valley and Eastern U.S. Note that each column listing the predicted number of affected plants is a subset of the columns to its right.

	Load Range (MW)	Total # of Units in Range	Approx. Total Capacity (MW)	Approx. % of Total Capacity Included in Range	$SO_3 \geq$ 25 ppm "Gavin-like" conc.	$SO_3 \geq$ 20 ppm	$SO_3 \geq$ 13 ppm "Gibson-like" conc.	$SO_3 \geq$ 10 ppm "Blue plume" w/o scrubber	$SO_3 \geq$ 4 ppm Opacity problems with scrubber	Missing Data
1% SCR Conversion	≥1,200	14	18,989	7%	0	3	5	5	6	0
	900 – 1,199	13	13,378	5%	2	3	3	3	7	0
	700 - 899	67	52,803	20%	0	6	12	15	42	0
	400 - 699	136	74,345	28%	0	10	32	49	102	2
	250 - 399	133	40,690	15%	0	7	19	33	78	0
	<250	957	65,887	25%	23	62	163	266	590	17
	Unknown	30			0	3	7	11	20	2
	Totals	1,350	266,092		25	94	241	382	850	
	Totals ≥ 250 MW	363	200,205		2	32	78	116	255	
0.75% SCR Conversion	≥1,200	14	18,989	7%	0	0	3	5	5	0
	900 – 1,199	13	13,378	5%	0	2	3	3	7	0
	700 - 899	67	52,803	20%	0	1	10	12	40	0
	400 - 699	136	74,345	28%	0	3	24	40	98	2
	250 - 399	133	40,690	15%	0	2	14	22	77	0
	<250	957	65,887	25%	8	26	124	197	564	17
	Unknown	30			0	0	5	7	20	2
	Totals	1,350	266,092		8	34	183	286	812	
	Totals ≥ 250 MW	363	200,205		0	8	59	89	247	
0.5% SCR Conversion	≥1,200	14	18,989	7%	0	0	3	4	5	0
	900 – 1,199	13	13,378	5%	0	0	3	3	5	0
	700 - 899	67	52,803	20%	0	0	6	10	32	0
	400 - 699	136	74,345	28%	0	0	13	26	85	2
	250 - 399	133	40,690	15%	0	0	9	15	69	0
	<250	957	65,887	25%	0	8	64	129	496	17
	Unknown	30			0	0	3	7	11	2
	Totals	1,350	266,092		0	8	101	194	703	
	Totals ≥ 250 MW	363	200,205		0	0	37	65	207	

In Table 2.2, SO_3 from SCR conversion was calculated for conversion rates of 0.5%, 0.75%, and 1.0%. This range of scenarios was selected to address the effects of catalyst aging as well as differences in production rate with new SCR installations. As SCR catalysts age, their NO_x reduction efficiencies decline; however, their SO_3 oxidation rates remain essentially constant. Thus, at some point in time additional catalyst volume will need to be installed on each unit in order to maintain the required NO_x performance (the usual approach taken to extend the service

time of installed catalysts). This means that a unit with a 0.5% SO_2 oxidation catalyst would be expected to eventually behave like the 0.75% catalyst in the table. Similarly, a 0.75% catalyst unit would be expected to eventually produce somewhat more SO_3 than that shown for a 1% catalyst in the table. Because of the issue of SO_3 formation, utilities are strongly pushing for the absolute minimum SO_3 conversion, to avoid this problem. So while the additional beds will result in an increase in conversion, the competing trend is to begin with a catalyst that generates as little SO_3 as possible. That pressure will push toward the 0.5% (or even lower) conversion catalysts.

A summary of the coal sulfur contents in the databases used to generate Table 2.2 are provided in Table 2.3. It is worth noting that there are reports that several utilities are considering switching from low sulfur coals to higher sulfur coals after retrofitting units with scrubbers.[20-25] Such actions would result in higher SO_3 emissions than those shown in Table 2.2 for the same SCR conversion rates and would offset reductions otherwise achievable by use of lower conversion rate catalysts.

Table 2.3. Sulfur contents of coals fired in plants in the Mississippi Valley and Eastern U.S.

Load Range (MW)	Total Number in Range	Total Capacity (MW)	Percentage of Capacity Included in Range	S >3%	S 2% to 3%	S 1% to 2%	S < 1%	Missing Data
≥1,200	14	18,989	6%	3	2	0	9	0
900 – 1,199	13	13,378	4%	3	0	0	10	0
700 - 899	67	52,803	17%	4	6	14	43	0
400 - 699	138	74,345	24%	23	15	42	56	2
250-399	133	40,690	13%	12	6	42	73	0
200 - 249	74	16,482	5%	11	7	26	30	0
<200	882	65,887	21%	82	105	288	389	18
Unknown	24			2	5	4	11	2
Totals	1,345	282,574		140	146	416	621	
Totals ≥250	365	200,205		45	29	98	191	
Totals ≥ 200	439	216,687		56	36	124	221	

The estimated SO_3 removal efficiencies provided by pollution abatement systems are summarized in Table 2.4, with comparison to previously reported reference values .[17,26] Air pre-heaters were assumed to reduce SO_3 by 30%. Units with fabric-filter fly ash collectors were credited with an additional 90% reduction in SO_3. Units with cold-side electrostatic precipitators (ESP) were credited with an additional 25% reduction in SO_3. For these calculations no effect was attributed to either hot-side electrostatic precipitators or wet scrubbers.

Comparison of the columns in Table 2.4 shows the control efficiency values selected are more conservative than those used in the previous references. Air heaters are commonly estimated to remove 50% of the SO_3 reaching them. However, when the above removal percentages were

applied to three plants which have both cold-side precipitators and scrubbers, two plants with only cold-side precipitators, and two plants with only scrubbers, the predicted values for the SO_3 concentrations in the stack gases fell far below the observed values. This led to a reconsideration of these removal efficiencies to better match measured values. This is shown in Table 2.5.

Table 2.4. Estimated SO_3 removal efficiencies (in percent) for control system components

	Data Source		
Device	HSD (a)	MH (b)	Used in This Report
Air Heater	50	50	30
Hot ESP	0	0	0
Cold ESP	25	50	25
Fabric Filter	90	90	90
Wet FGD scrubber	0	50	0

(a) Hardman, Stacey, and Dismukes[17]
(b) Monroe and Harrison[26]

Table 2.5. Comparisons of observed and predicted SO_3 concentrations

Location	Percent Sulfur in Coal	Measured SO_3 (ppm)	SO_3 Predicted Here			Predictions Based on MH[(a)] Removal Efficiencies	Control System
			No SCR	0.5% SCR	1% SCR	1% SCR	
Plant 1	2.6	14		8.3	13	3.4	Cold-side ESP & Scrubber
Plant 2	3.75	~35		11.9	18.5	4.9	Cold-side ESP & Scrubber
Plant 3	2.9	~13		9.2	14.3	3.7	Cold-side ESP & Scrubber
Plant 4a	0.92	7.7		3.9	6.1	3.1	Cold-side ESP
Plant 4b	0.92	9.6		3.9	6.1	3.1	Cold-side ESP
Plant 5a	0.99	4.0		3.2	4.9	2.5	Cold-side ESP
Plant 5b	0.99	7.7		3.2	4.9	2.5	Cold-side ESP
Plant 6	3.35	2.6	6.3			2.3 (No SCR)	Scrubber
Plant 7	3.6	10.7	6.8			2.4 (No SCR)	Scrubber
Plant 8	0.86	6.5		5.8	6.3	2.2	Cold-side ESP

a. Monroe and Harrison[26]

Review of data obtained at several installations tends to show air heater removal efficiencies in the range of 20% to 50% with typical values of about 25%. Removal efficiencies across cold-side precipitators in these same data sets were typically about 25% as well. Similarly, removal efficiencies as low as 15% to 20% have been measured across some fabric filters and removal efficiencies across wet scrubbers have been measured as low as 12% to 15%. In the case of air heaters, the removal efficiencies would be expected to be higher for lower exit gas temperatures, as illustrated in Figure 2.1. Similarly, removal across precipitators and fabric filters increases substantially as the gas temperature decreases to and below the acid dew point. Conversely, if the

gas temperature through a precipitator or fabric filter is substantially above the acid dew point, little removal will take place.

It is clear that the commonly cited estimated removal efficiencies result in under-predicting stack SO_3 concentrations. In Table 2.4, the value of zero for removal efficiency in scrubbers is not meant to imply that no removal takes place in them. Rather, it simply means that the removal by preceding components was over-estimated so much that the results would have been biased severely low if another 30 to 50 percent reduction were applied. The values in Table 2.2 are believed to be reasonable estimates of the emissions from units using their current particulate control systems followed by wet scrubbers.

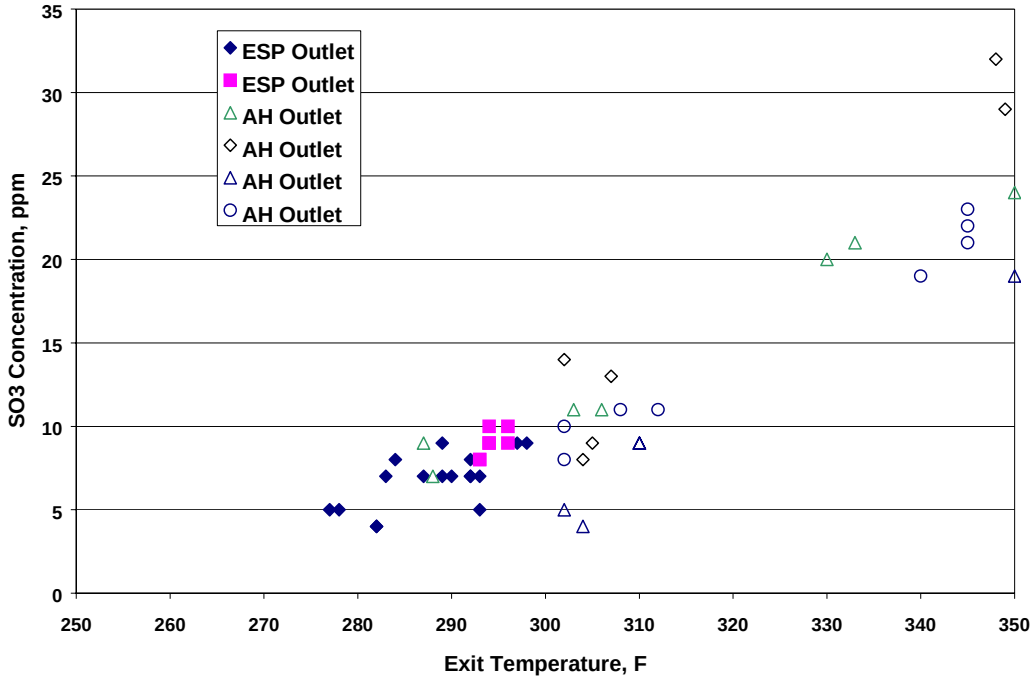

Figure 2.1. Measured SO_3 concentrations versus temperature at the exit of an air heater and cold-side electrostatic precipitator.

Table 2.6 and Figure 2.2 show state-by-state tabulations of estimated SO_3 emissions from individual power plant units in the Mississippi Valley and Eastern U.S. Only units with capacities of 200 MW or more were included, as these are the units that will be most likely affected by the upcoming regulations. While not specifically related to the pertinent issues of opacity, ground effects, or local acidic deposition, these data demonstrate the potential for a significant increase in fine PM emissions relative to the filterable fraction (fly ash). The SO_3 emissions estimates were made using the SO_3/SO_2 ratios developed by Hardman, Stacy, and Dismukes for eastern bituminous and western subbituminous coals.[17] In applying the correlations it was assumed that the fuels in the 2002 Annual Steam-Electric Plant Operation and

Design Database[14] are still in use and that the units operate at an average annual load of 75% of capacity (allowing for some reduced load operation and outages). Table 2.6 and Figure 2.2 show that of the 17 states included in the state-by-state tabulations, six states (OH, PA, IN, TN, KY, and FL) account for nearly 70% of the total projected SO_3 emissions.

Table 2.6. State-by-state tabulation of estimated SO_3 emissions from individual power plant units in the Mississippi Valley and Eastern U.S.

State	1 % SCR Conversion		0.75 % SCR Conversion		0.5 % SCR Conversion	
	SO_3 Emissions (kg/yr)	State % of Total	SO_3 Emissions (kg/yr)	State % of Total	SO_3 Emissions (kg/yr)	State % of Total
AL	5.79E+06	2.70%	4.86E+06	2.71%	3.94E+06	2.72%
AR	1.24E+05	0.06%	1.05E+05	0.06%	8.50E+04	0.06%
CT	7.19E+05	0.34%	6.05E+05	0.34%	4.92E+05	0.34%
DC	6.04E+05	0.28%	5.09E+05	0.28%	4.14E+05	0.29%
DE	8.80E+05	0.41%	7.41E+05	0.41%	6.03E+05	0.42%
FL	1.24E+07	5.76%	1.04E+07	5.78%	8.43E+06	5.82%
GA	7.66E+06	3.57%	6.43E+06	3.58%	5.21E+06	3.60%
IA	1.26E+06	0.59%	1.00E+06	0.56%	7.46E+05	0.52%
IL	4.90E+06	2.29%	4.03E+06	2.25%	3.16E+06	2.19%
IN	2.13E+07	9.92%	1.78E+07	9.89%	1.43E+07	9.85%
KY	1.68E+07	7.85%	1.42E+07	7.89%	1.15E+07	7.96%
LA	1.29E+06	0.60%	1.05E+06	0.58%	8.11E+05	0.56%
MA	6.09E+04	0.03%	5.13E+04	0.03%	4.17E+04	0.03%
MD	6.35E+06	2.96%	5.35E+06	2.98%	4.35E+06	3.00%
ME	1.02E+05	0.05%	8.60E+04	0.05%	6.99E+04	0.05%
MI	5.44E+06	2.54%	4.52E+06	2.52%	3.60E+06	2.49%
MN	1.23E+06	0.57%	9.74E+05	0.54%	7.16E+05	0.49%
MO	6.71E+06	3.13%	5.47E+06	3.04%	4.22E+06	2.92%
MS	1.37E+06	0.64%	1.16E+06	0.64%	9.40E+05	0.65%
NC	9.02E+06	4.21%	7.60E+06	4.23%	6.18E+06	4.27%
NH	0.00E+00	0.00%	0.00E+00	0.00%	0.00E+00	0.00%
NJ	1.02E+06	0.48%	8.56E+05	0.48%	6.92E+05	0.48%
NY	6.82E+06	3.18%	5.74E+06	3.20%	4.67E+06	3.22%
OH	4.00E+07	18.64%	3.35E+07	18.67%	2.71E+07	18.72%
PA	3.09E+07	14.39%	2.60E+07	14.48%	2.11E+07	14.60%
RI	0.00E+00	0.00%	0.00E+00	0.00%	0.00E+00	0.00%
SC	4.86E+06	2.26%	4.09E+06	2.28%	3.33E+06	2.30%
TN	1.75E+07	8.15%	1.47E+07	8.17%	1.19E+07	8.18%
VA	5.11E+06	2.38%	4.30E+06	2.39%	3.50E+06	2.41%
VT	0.00E+00	0.00%	0.00E+00	0.00%	0.00E+00	0.00%
WI	4.28E+06	2.00%	3.50E+06	1.95%	2.72E+06	1.88%
WV	5.37E+04	0.03%	4.52E+04	0.03%	3.68E+04	0.03%

Summary

More than half of the units expected to be affected by the new regulations could reasonably require mitigation of SO_3 emissions to meet opacity requirements and about a quarter could require mitigation to alleviate problems related to ground level SO_3 concentrations. Evidence in the trade press suggests that several utilities are considering returning to the use of high sulfur coals after they install scrubbers. If they do, SO_3 emissions would be expected to increase to levels higher than those projected in this report. This study dealt with only coal-fired units. It should also be noted that similar SO_3 emission problems would be experienced at heavy oil-fired

units, if NO_x control using SCR is applied to them. This analysis suggests that mitigation of SO_3 emissions will be needed in some cases to address plume visibility issues, increased acid aerosol emissions, and $PM_{2.5}$ emission levels, particularly at plants that install SCR and FGD and use high sulfur coal. The remainder of this report discusses measurement methods and SO_3 formation and removal processes across different plant components. This information can provide useful guidance for plant operators who are interested in a range of approaches to avoiding excess collateral SO_3 emissions.

It should be noted that there is a significant lack of actual measurements of the conversion rate of SO_2 to SO_3 in the boiler. This lack makes predictions highly uncertain because of the inability to validate prediction results against actual measurements. Although the predictions made in the following chapters are in line with measured results, the scarcity of measurements makes it very uncertain whether such results can be repeated for the range of units in service. Further measurements of boiler exit SO_3 concentrations are key to advancing our understanding of, and ability to predict, SO_3 emissions.

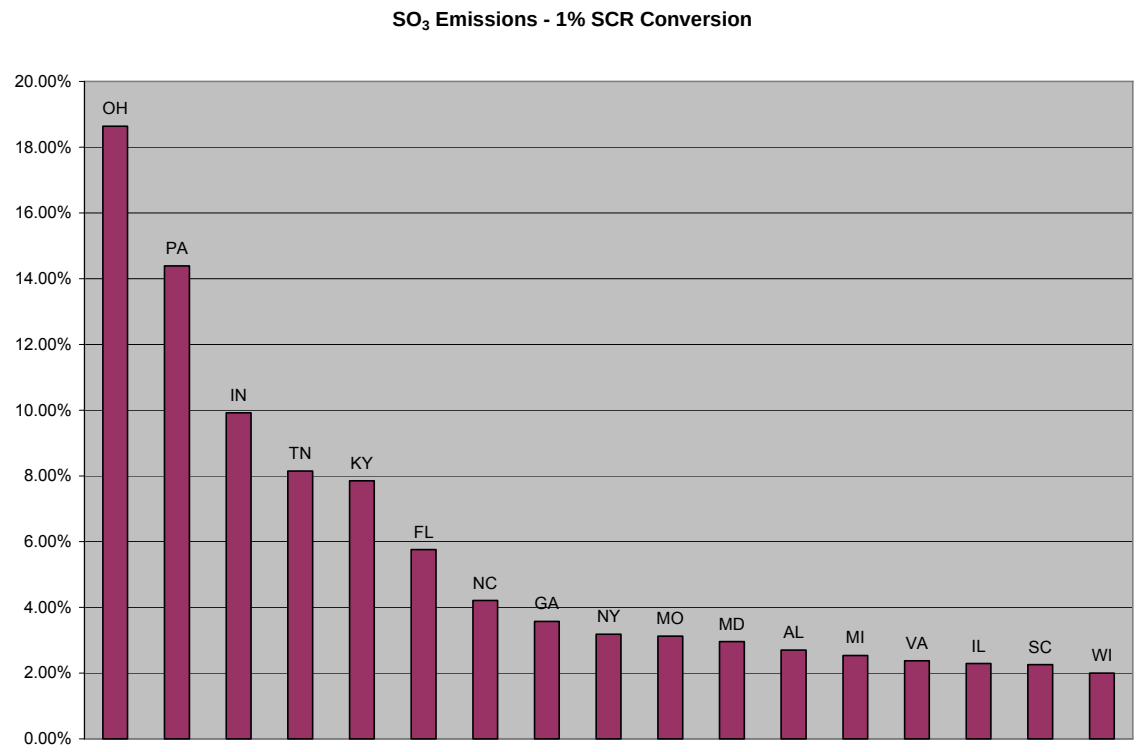

Figure 2.2. SO_3 emissions for states in the Mississippi Valley and Eastern U.S. emitting > 1% of total projected SO_3 emissions for the region (215,000 tonne/year total).

3. IMPROVEMENTS IN SO_3 MEASUREMENT TECHNOLOGIES

Current SO_3/ H_2SO_4 Measurement and Monitoring Methods

Method 8, the EPA promulgated method for measuring emissions of sulfuric acid mist,[27] has a lower detection limit of about 50 mg/m^3, thus it lacks the sensitivity needed for measurements at electric utility plants. The manual controlled condensation method (CCM) developed by Cheney and Homolya[28] is generally recognized as the most reliable method for measuring SO_3/ H_2SO_4 at the levels encountered at power plants.[29] In the CCM, a sample gas stream is conveyed through a heated quartz-lined probe, through a quartz fiber filter and then through a condenser in which the acid vapor is removed. The probe and filter holder are held at a temperature at or above 550 °F to evaporate condensed H_2SO_4 and ensure that the SO_3/H_2SO_4 in the sample is entirely in vapor form before reaching the filter. The condenser is maintained at a temperature above the moisture dew point but well below the sulfuric acid dew point so that all of the acid is collected in it. A second filter downstream of the condenser ensures that any aerosolized acid is retained for analysis with that collected in the condenser itself. After each sample is collected, the condensor is washed to recover the collected acid. The amount of acid collected is later quantified in the laboratory by titration. Over the past few years several improvements have been made to the method as it is applied to coal-fired utility installations.[30,31] The changes deal with minimizing problems arising from the acid vapor being adsorbed on or reacting with ash collected on the filter upstream of the condenser or the filter medium itself, together with the problem of ensuring that any sulfuric acid mist in the sampled gas is completely volatilized in the probe. The first problem is significant upstream of particulate control devices and the second is especially important downstream of a scrubber where the H_2SO_4 is, for practical purposes, entirely in the condensed phase. Both problems must be addressed in automated as well as manual systems. The CCM as described above was used as a manual reference measurement for comparison with the results of measurements reported here.

Design and Fabrication of Sample Extraction and Transport System for SO_3/H_2SO_4

A semi-continuous SO_3/H_2SO_4 monitor was developed by Southern Research Institute under Cooperative Agreement No. DE-FC26-02NT41593 with the U.S. Department of Energy. A significant part for that project addressed a major requirement for a field-useable monitor: a sample extraction system that separates SO_3/H_2SO_4 vapor from in-stack particulate matter (PM) and transports it efficiently as vapor to the sensor.[32]

The sample extraction and transport system (SETS) had to extract and maintain or heat the flue gas to >550 °F, transport the sample stream, separate SO_3/H_2SO_4 from particulate matter, deliver SO_3/H_2SO_4 to the analyzer, and return excess flue gas and PM to the duct. Heating of the sample gas is accomplished primarily by the injection of very hot dilution gas (at a dilution ratio of approximately 1:1) near the probe entrance as well as from contact heating. Flow through the SETS is driven by an eductor, with the hot sample gas being extracted from the probe through an annular filter upstream of the eductor. Because of proven performance in similar applications, a commercially-available probe designed for use in monitoring mercury emissions, the Apogee Scientific QSIS, was purchased and modified to include the hot dilution gas injection for heating

the sample gas as illustrated in Figure 3.1. The QSIS probe and filter element are fabricated from stainless steel with a proprietary coating applied to all surfaces to minimize reactions with the sample gas.

The exhausts of some wet FGD scrubbers contain significant quantities of droplets that are too large (on the order of tens of microns) to evaporate quickly which would lead to their being lost on internal surfaces of the sampling nozzle and transport line. Over time, such droplets deposited on surfaces would dry, leaving a residue that would accumulate and interfere with normal operation of the system. Therefore, when monitoring downstream of wet FGD scrubbers the SETS should incorporate an inertial collector at the probe inlet to remove these droplets. In the past this approach has been found necessary for sample extraction in wet streams. In particular, SRI developed a series of such procedures for the California Air Resources Board for making particle size measurements in wet process streams that have been successfully utilized for over 10 years.[33] Fortunately, the condensed acid tends to reside in droplets having diameters of a few micrometers and smaller.

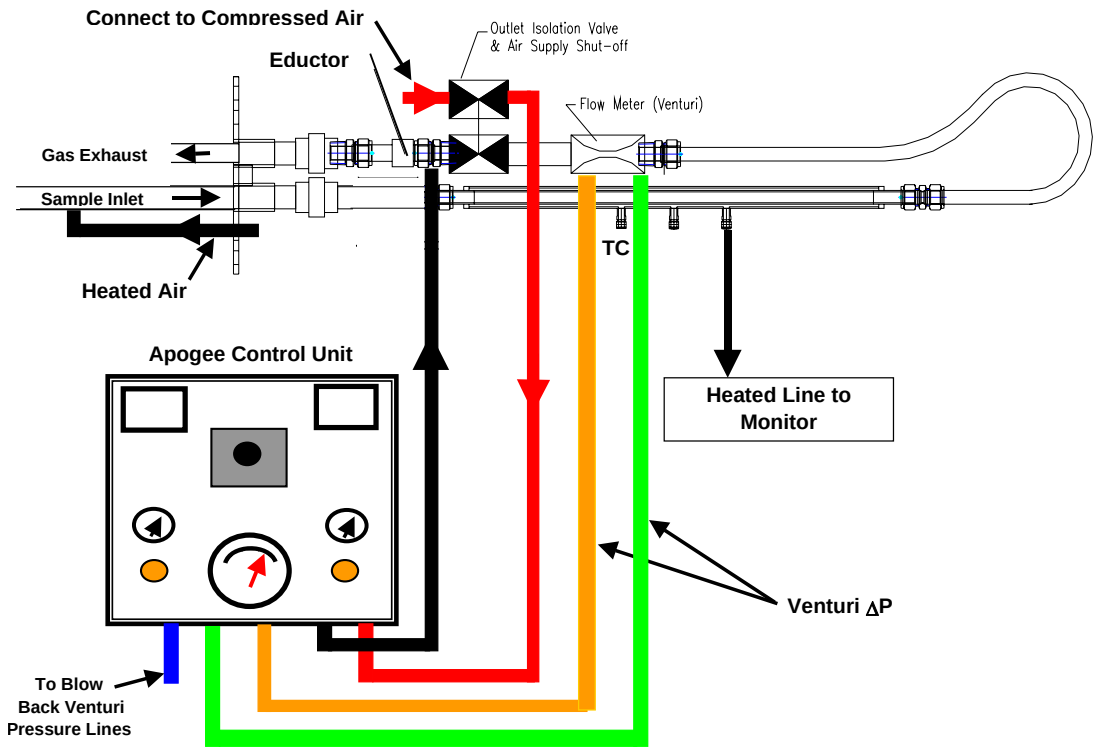

Figure 3.1 Schematic diagram of the Apogee QSIS probe modified for use with the SO_3 monitor.

The QSIS probe extracts a flue gas sample at a flow rate of approximately 10 to 12 acfm through a ¾-inch diameter sample probe. The extracted gas then passes axially along the length of a ½-inch ID cylindrical porous filter element. A slipstream of sample gas is pulled radially through the filter element at a flow rate of a few liters per minute and directed to the sample collection and measurement system. Due to the high axial velocities in the sample probe and core of the

cylindrical filter element, particles entrained in the gas stream are prevented from depositing on the inner walls of the filter. However, fine particles are capable of being trapped in the filter element over time. As a result, the filter element must be periodically removed for cleaning by backwashing. As in the original SETS design, flow through the Apogee system is driven by an eductor, with the analyzer extracting about 2 slpm of hot sample gas upstream of the eductor. The excess gas not used for the actual measurement is returned to the host duct.

Prior to proceeding with the purchase and modification of a QSIS probe for use with the monitor, a brief series of tests was performed to check for any obvious problems with the use of the probe for SO_3/H_2SO_4 sampling. These tests were carried out in SRI's Coal Combustion Research Facility (CCRF) in conjunction with an ongoing mercury measurement program which utilized two such probes, one sampling at a point in the CCRF at which the gas temperature was about 550 °F and the second down stream of the first, following two heat exchangers, at which the gas temperature was about 325 °F. A heated hose like that to be used between the probe and condensor for the SO_3 monitor was used at each location to convey a sample stream to a conventional controlled-condensation condensor setup. Data obtained with this setup were then taken for comparison with data obtained with conventional controlled condensation setups that were being operated to obtain information for the mercury emissions program. The results of these tests are shown in Figure 3.2. The agreement was excellent at the 550 °F location and was reasonably good at the 325 °F location although the results with the QSIS probe were slightly higher than those from the conventional probe at the 325 °F location, perhaps due to a bias introduced by particulate matter on the filter of the CCM sampler. (The differences in concentrations between the two locations results from losses in the heat exchangers.) These results were deemed satisfactory enough to proceed with the purchase and modification of a QSIS probe for use with the SO_3/H_2SO_4 monitoring system.

Tests conducted as part of the current project compared measurements made utilizing the modified probe with those obtained using a conventional CCM setup. These tests were conducted at two conditions: (1) with a flue gas stream in which the H_2SO_4 present would be entirely in the vapor phase and (2) a gas stream in which the majority of the H_2SO_4 present would be in the condensed phase. Condensation of the H_2SO_4 in the flue gas for the second test condition was induced by means of a water spray in the duct upstream of the sampling location. An Illinois Basin coal with a 3.5 % sulfur content was fired in the CCRF for these tests.

Sampling was done at a location about 30 feet downstream of the 325 °F location of Figure 3.2. As is the case for air preheaters on full-scale utility boilers, the air preheaters of the CCRF remove significant fractions of the SO_3/ H_2SO_4 formed in the furnace. The air preheaters were operated to provide less cooling than that used in normal CCRF operations in order to obtain higher H_2SO_4 concentrations and to provide assurance that the H_2SO_4 was entirely in the vapor phase for the first test condition. A nominal temperature of 400 °F was selected as the air preheater exit temperature based on the amount of cooling expected from the water spray to be used to induce condensation by cooling for the second test condition. A target temperature of 270 °F was selected for the second test condition. The saturation vapor pressure of H_2SO_4 at 270 °F was low enough that the majority of the H_2SO_4 vapor could be expected to condense.

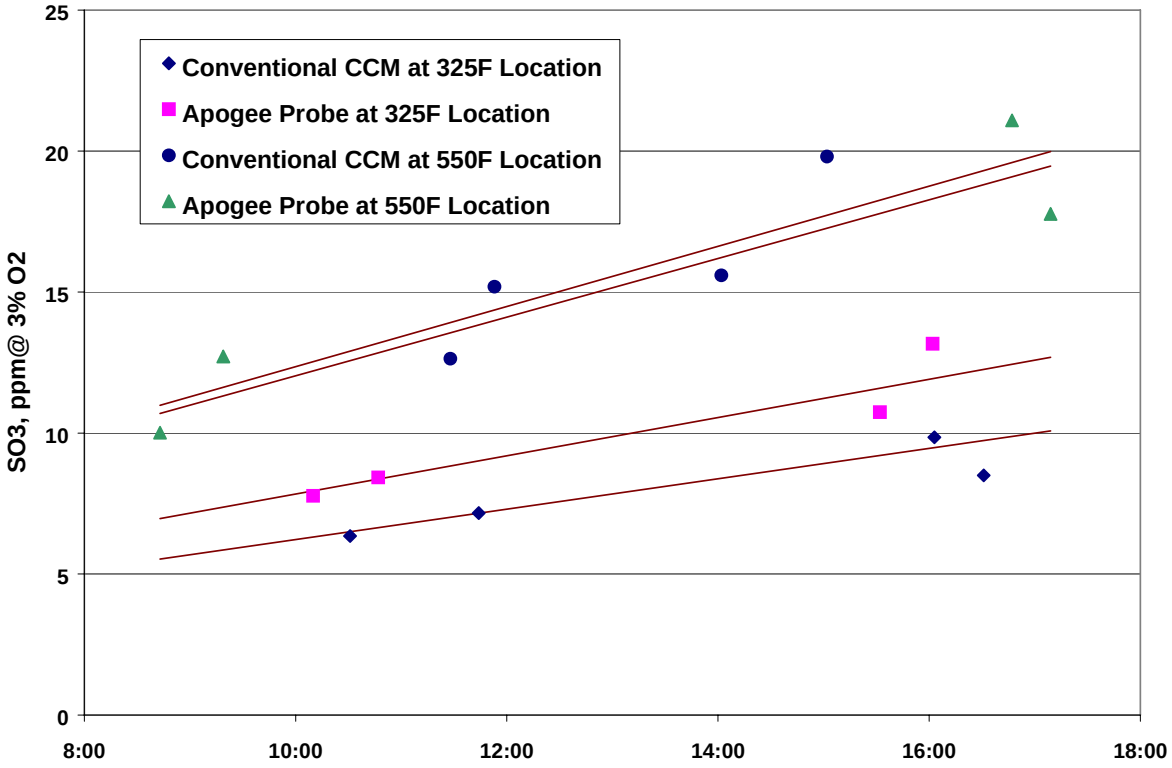

Figure 3.2. Comparison of SO_3 concentrations measured by conventional controlled-condensation methods (CCM) with those measured using Apogee QSIS probes and a heated hose to deliver samples to a controlled-condensation condenser.

Three Apogee probe operating conditions were used during the tests without the water spray with a flue gas temperature of 393 °F. During this phase of the testing the probe was operated without dilution and with dilution of flue gas with filtered hot air; first with the dilution air at 394 °F and then with the dilution air at 1113 °F. The mixed gas temperature was 559 °F at the higher dilution air temperature. The dilution ratio used in these tests was 1:1 on a mass basis. The dilution air temperatures cited here are those measured at the exit of the dilution air heater. The actual temperature of the dilution air as it enters the probe is somewhat lower. No change was noted in the dilution-corrected concentrations under these conditions as illustrated by the first block of data points in Figure 3.3. The temperatures of the dilution air and the mixed sample and dilution gas are given on the figure for each test condition. The initial rise in the SO_3/ H_2SO_4 concentration seen at the beginning of the test was the result of losses in the air preheater that diminished as an ash coating built up on the heat exchanger surfaces which were initially clean.

The amount of cooling provided by the water spray was less than expected at the sampling location, perhaps because of incomplete evaporation in the transit time between the point of injection and the sampling location. Therefore the air preheater exit gas temperature was adjusted

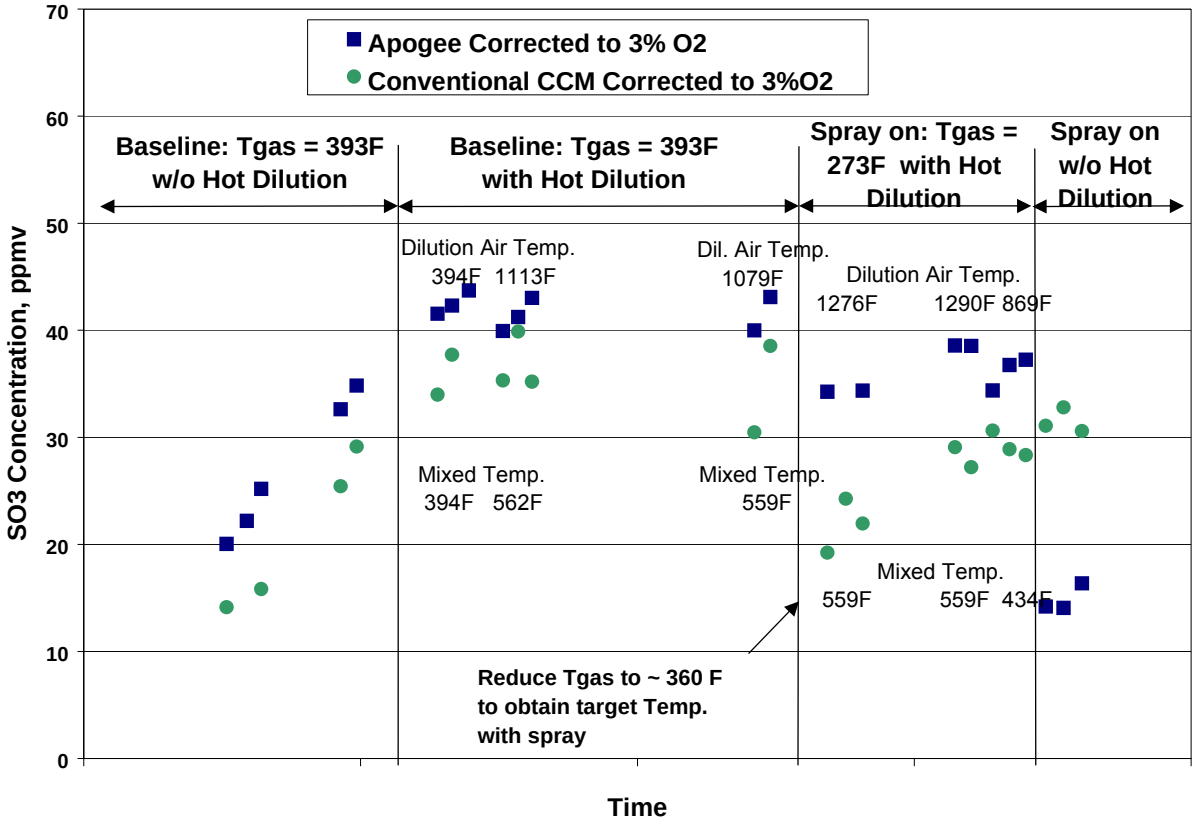

Figure 3.3. Comparisons of SO_3 concentrations measured by the conventional controlled-condensation method (CCM) with those measured using the modified Apogee QSIS probe incorporating the hot gas dilution approach to evaporating condensed H_2SO_4.

downward somewhat to about 360 °F in order to obtain an acceptably low gas temperature at the test location. This resulted in a noticeable decrease in the total SO_3/ H_2SO_4 in the duct.

The dilution air temperature had to be raised to about 1280 °F when the water spray was employed in order to obtain the target 560 °F temperature for the mixed gas. The Apogee probe was also operated with a nominal 870 °F dilution gas temperature, resulting in a mixed gas temperature of 434 °F. At the latter condition a very slight drop in the measured SO_3/ H_2SO_4 concentration was noted as compared to that measured with the 560 °F mixed temperature. Finally, the Apogee probe was operated without the hot dilution gas at which point the measured concentration fell to a value close to the saturation concentration at the flue gas temperature, reflecting the loss of the condensed phase SO_3/ H_2SO_4 in the filter. The large drop in the value measured with the QSIS probe without the hot dilution air while the spray remained on at the end of the test series resulted from condensed acid no longer being evaporated in the probe.

It appears to have taken about five hours after the water spray was turned on for the conventional CCM probe to reach steady-state conditions and provide reliable results. Evidently it took that long for the internal surfaces of the CCM probe to get hot enough to evaporate the condensed phase acid. Again, the lower steady-state values measured with the conventional CCM as compared to those obtained with the Apogee probe through most of this test series are believed

to have resulted from adsorption onto particulate matter which collects on the CCM filter. The QSIS probe as adapted for SO_3 measurements is shown in Figure 3.4.

Following the tests conducted at the SRI pilot-scale Coal Combustion Research Facility, a short series of tests were conducted on a stack downstream of a scrubber on a large coal-fired utility boiler. Results of measurements using a standard controlled condensation probe and filter setup with results using the inertial-separation hot-gas-dilution probe are given in Table 3.1. All values have been corrected to 3% oxygen. The intended value of mixed gas temperature in the dilution probe, 550 °F to 600 °F, was never obtained during these tests. Too much of the transport tubes and mixing zone were in the flue where they were cooled beyond the capability of the dilution gas heater. A mixed gas temperature of 445 °F was as great a value as could be achieved on Test 1. At that temperature the dilution probe results approached those of the conventional probe but were clearly low when the mixed gas temperature was only 419 °F. During Test 2, additional insulation was added to the dilution probe, but the target mixed gas temperature still could not be reached. A simple solution to the problem has been found: simply add a spool piece and probe extension so that the hot gas transport tubes and mixing zone can be located outside the flue. Had the mixed gas been as hot as intended, one could be reasonably certain that all of the condensed acid in the flue was evaporated and thus would have been measured. However, complete evaporation may or may not have been achieved during the tests when the temperature was 445 °F to 490 °F, so it is uncertain as to whether all of the acid present in the sample was available for measurement downstream of the filter.

Table 3.1 Comparison of measurements made using a conventional CCM probe with those made with the hot-gas dilution probe downstream of a full-scale utility scrubber.

Standard Controlled Condensation Probe				Hot-gas Dilution Probe		
	SO_3, ppm @ 3% O_2				SO_3, ppm @ 3% O_2	
Test Run	Average	Range		Mixed Gas Temperature, °F	Average	Range
1	19.3	18.7 – 20.7		419	14.1	12.7 – 15.5
				445	18.4	18.4 - 18.4
2	18.0	17.6 – 18.6		480 – 490	17.0	16.2 – 17.9

Recommended future work includes:

1. Performing tests utilizing the hot gas dilution system to check for artifact SO_3 formation by oxidation of SO_2.
2. Performing tests downstream of a scrubber to verify performance when the predominant form of SO_3 is condensed-phase H_2SO_4 in a low temperature gas stream.

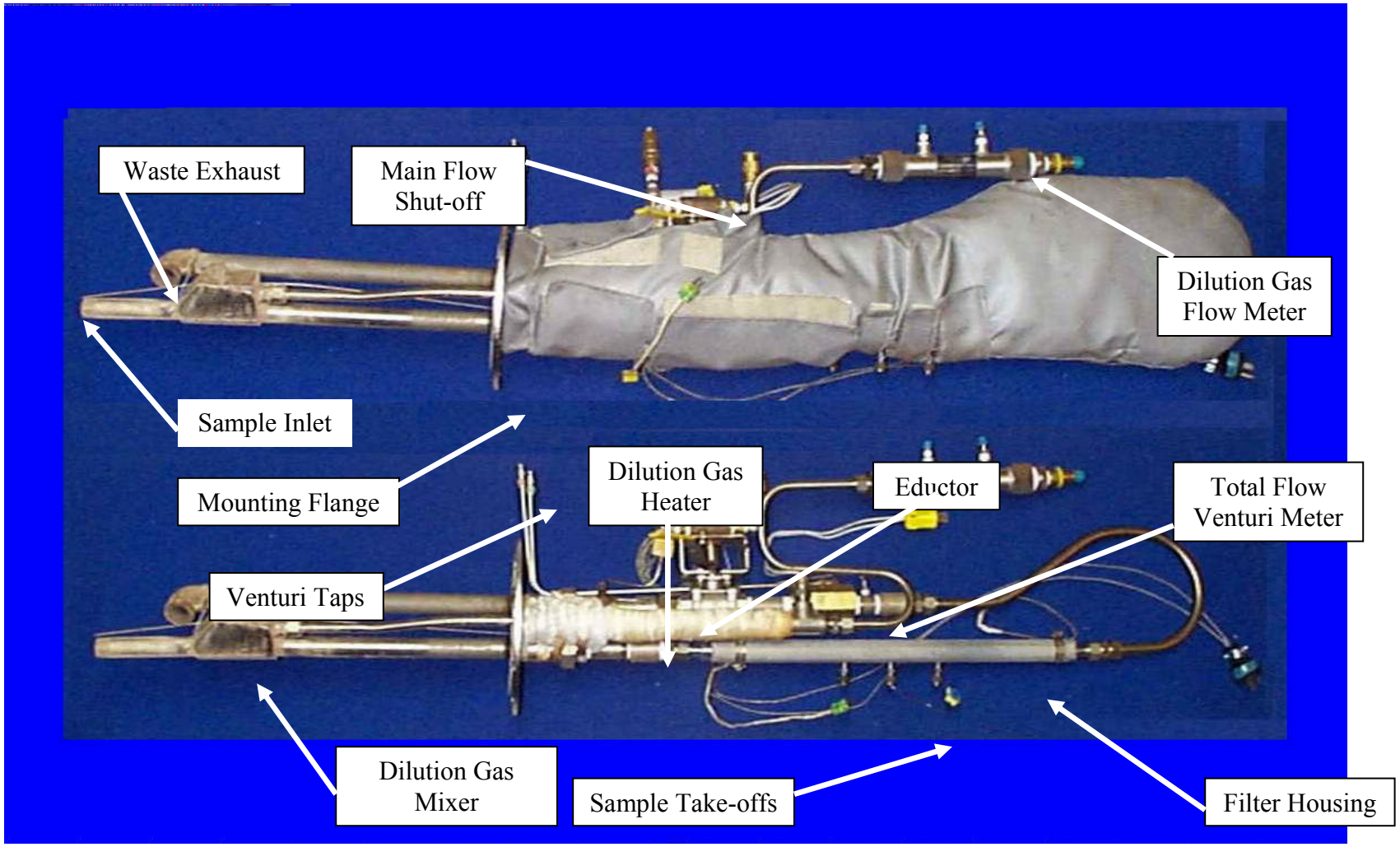

Figure 3.4. Modified Apogee QSIS sampling probe. Upper: probe with insulating jacket in place. Lower: Probe with jacket removed to show principal components. (The waste exhaust normally points opposite the direction shown.)

4. EXPLORATORY STUDY OF SO_3 ADSORPTION BY COAL FLY ASH

Introduction

Removal of SO_3 or H_2SO_4 from the flue gas can take place through a number of mechanisms: by uptake by fly ash, by condensation on the heat exchanger surfaces in air preheaters, by reaction with reagents injected for control of vapor phase SO_3/H_2SO_4, or by condensation and subsequent collection in the form of particles. Significant removal can result from uptake by fly ash but the mechanisms are not fully understood and at present cannot be well predicted. This study was undertaken to provide data which might be used to aid in the development of a predictive model for uptake of SO_3/H_2SO_4 by fly ash from coal-fired utility boilers.

Approach

Nine sets of ash samples from a wide range of coal types were selected from an inventory of ashes that had previously been characterized during studies related to resistivity modification by SO_3 injection. These ashes had been collected either by EPA Method 17[34] directly from flue gas streams or as hopper samples from dry particulate control devices (either electrostatic precipitators or fabric filters). All had been previously exposed to flue gas streams having unknown concentrations of SO_3 prior to collection. The ashes selected included ashes from high and low sulfur eastern bituminous coals, low and moderate sulfur western sub-bituminous coals, a Powder River Basin coal, and a North Dakota lignite.

The ashes were exposed to synthetic flue gas atmospheres in an apparatus normally used for studies related to fly ash resistivity and ash resistivity modification by moisture and sulfur trioxide.[35] The apparatus consisted of a continuous-flow generator which produces a synthetic flue gas stream which was passed through a bell jar containing the samples in a temperature controlled oven. The synthetic flue gas was humidified, and heated to a temperature above that at which SO_3 and moisture combine to form H_2SO_4, after which controlled amounts of SO_3 were added to obtain the desired SO_3 concentration. Previous experience in resistivity work with this apparatus had indicated that over a 72 to 96 hour exposure time SO_3 would permeate and apparently approach equilibrium in a 1 mm thick ash layer.[36] Fresh ash samples were spread as 1 mm thick layers in the bottoms of 12 petrie dishes and placed in the bell jar for each exposure condition. The layout of the samples in the bell jar is illustrated in Figure 4.1. The arrows shown in Figure 4.1 show the positions of the SO_3 inlet and outlet gas streams. Duplicate samples of three of the nine ashes were included in each test to provide information on the reproducibility of the results. Experiments were performed at four temperatures (350 °F, 375 °F, 450 °F, and 850 °F) and two SO_3 concentrations (20 ppmv and 70 ppmv). In each test, prior to adding SO_3 to the gas stream, the samples were cycled up to 850 °F and held at that temperature overnight. In addition to the exposure tests, one baseline run was made in which the samples were subjected to the 850 °F temperature cycle but not exposed to SO_3. Following the exposure to SO_3, the samples were removed from the bell jar as rapidly as

possible and the covers were placed on the petrie dishes after which they were individually extracted for measurement of soluble sulfates.

A typical set of SO_3 concentrations at the inlet and outlet of the bell jar are shown over the course of a test in Figure 4.2. As can be seen, the uptake of SO_3 by the ash was initially fairly high, but declined fairly rapidly over the course of about two days, after which it continued to decline but at a much slower rate, indicting that the limiting capacity of the samples was never reached.

Results

The exposure conditions and results of the measurements are provided in Table 4.1. The percentage of the total entering the bell jar that was taken up by the ash is provided in the table together with the SO_3 mass balance for each set of exposures. The mass balances indicate that the recovery in the analyses of SO_3 taken up by the ash was essentially complete. The results are shown plotted versus the base:acid ratios of the ashes in Figure 4.3. The curves in Figure 4.3 are present only for purposes of tying the results for each test condition together and have no physical or chemical significance. Given the strong correlation between SO_3 uptake and the base:acid ratios of the ashes, it appears that chemi-sorption rather than physical adsorption dominates the process and that temperature plays a strong role as well. Based on rather crude extrapolations of the concentrations of SO_3 at the outlet of the exposure chamber, it is estimated that the limiting capacities of the ashes are perhaps twice the maximum uptakes found in these experiments with the uptake rates being concentration and temperature dependent.

Following the general approach used in developing predictive equations for ash resistivity,[36] ash compositions based on atomic percentages of cations were calculated from the weight percentages as oxides shown in Table 4.2. The resulting atomic percentages are given in Table 4.3. Multiple regression was then used to obtain fitting coefficients for use as a predictive tool for SO_3 uptake by ash based on the ash chemistry. Results of the regression are provided in Table 4.4. A plot of values predicted by the regression equation versus those measured in this study is shown in Figure 4.4.

Table 4.1. Exposure conditions and results

	Experiment	Baseline	Exposure	Exposure	Exposure	Exposure	Exposure
	Duration, hours	12	96	74.75	74.72	93.4	96.5
	Oven Temperature, °C	454	177	190	232	232	454
	Oven Temperature, °F	850	351	374	450	450	850
	Nominal SO_3 Conc., ppm	0	20	20	20	70	70
	Percent Capture by Ash		21.5	26.7	26.3	19.2	25.8
	Mass Balance, %		96.7	96.1	94.4	100.9	99.5
Ash ID	Ash Type	Post Exposure Soluble Sulfate, %					
301	Low S W SB (a)	0.44	2.16	1.95	2.46	3.62	3.21
9896-1-68	E Bit (b)	1.58	4.05	3.67	4.51	7.31	8.82
303	Low S W SB	0.88	2.82	2.55	2.94	4.73	11.43
143	Low S W SB	0.88	2.76	3.46	3.36	6.10	10.25
304	Low S E Bit (c)	0.10	0.86	0.95	1.32	1.78	1.19
304 dup			0.83	0.91	1.24	1.81	1.00
9896-1-69	W SB (d)	1.51	4.16	3.98	4.54	8.39	10.71
129	ND Lignite (e)	4.04	6.55	6.19	6.56	14.36	14.27
129 dup			6.15	6.01	6.47	12.91	13.45
305	Hi S E Bit (f)	0.78	1.59	1.59	1.99	2.72	2.87
305 dup			1.68	1.71	2.15	2.70	3.21
9896-1-57	PRB (g)	2.49	4.69	4.54	4.99	10.22	13.92

(a) Low sulfur western subbituminous coal
(b) Eastern bituminous coal
(c) Low sulfur eastern bituminous coal
(d) Western subbituminous coal
(e) North Dakota lignite
(f) High sulfur eastern bituminous coal
(g) Power River Basin coal

Table 4.2. Properties of ashes used in adsorption study

			Ash mineral analyses, wt%										
Ash ID.	Coal Type	Base/Acid Ratio(a)	Li_2O	Na_2O	K_2O	MgO	CaO	Fe_2O_3	Al_20_3	SiO_2	TiO_2	P_2O_5	SO_3
301	Low S W SB (b)	0.149	0.03	0.51	1.7	1.3	4.4	5.0	25.8	59	1.70	0.31	0.35
9896-1-68	E Bit (c)	0.354	0.04	1.20	2.40	1.80	7.4	13.1	25.5	45.6	2.10	0.32	1.60
303	Low S W SB	0.462	0.05	0.34	0.42	6.30	19.5	4.3	24.1	41.2	1.50	0.31	0.94
143	Low S W SB	0.535	0.01	1.13	0.70	4.00	22.7	4.8	21.6	38.8	1.90	1.40	1.70
304	Low S E Bit (d)	0.092	0.04	0.19	2.70	0.85	0.56	4.1	32.2	56.4	2.30	0.15	0.18
9896-1-69	W SB (e)	0.698	0.01	4.00	1.90	5.70	19.9	9.0	14.4	42.7	0.92	0.27	1.60
129	ND Lignite (f)	1.558	0.02	1.58	0.20	8.90	32.2	12.6	12.3	22.6	0.70	0.30	7.90
305	Hi S E Bit (g)	0.242	0.05	0.34	3.10	1.10	2.20	12.5	27.1	50.5	1.80	0.33	0.57
9896-1-57	PRB (h)	0.901	0.02	1.70	0.52	4.40	27.9	9.9	19.3	27.4	2.60	1.10	3.10

(a) Base/Acid ratio = $(Na_2O+K_2O+MgO+CaO+Fe_2O_3)/(Al_2O_3+SiO_2+TiO_2)$
(b) Low sulfur western subbituminous coal
(c) Eastern bituminous coal
(d) Low sulfur eastern bituminous coal
(e) Western subbituminous coal
(f) North Dakota lignite
(g) High sulfur eastern bituminous coal
(h) Power River Basin coal

Table 4.3. Atomic concentrations of cations for ashes used in adsorption study

Ash ID	Li	Na	K	Mg	Ca	Fe	Al	Si	Ti	P	S
301	0.047	0.385	0.844	1.126	2.739	0.875	7.068	22.626	0.490	0.044	0.076
9896-1-68	0.066	0.952	1.253	1.639	4.843	2.409	7.343	18.383	0.637	0.048	0.367
303	0.075	0.245	0.200	5.219	11.612	0.719	6.315	15.112	0.414	0.042	0.196
143	0.015	0.830	0.338	3.370	13.745	0.816	5.755	14.471	0.533	0.194	0.361
304	0.065	0.149	1.395	0.766	0.363	0.746	9.178	22.505	0.690	0.022	0.041
9896-1-69	0.015	2.839	0.887	4.643	11.651	1.480	3.710	15.398	0.250	0.036	0.328
129	0.030	1.132	0.094	7.318	19.032	2.092	3.199	8.228	0.192	0.041	1.635
305	0.085	0.278	1.667	1.031	1.483	2.366	8.036	20.962	0.562	0.051	0.135
9896-1-57	0.031	1.288	0.259	3.826	17.437	1.738	5.308	10.548	0.753	0.158	0.679

Table 4.4. Results of multiple regression to obtain predictive equation for uptake of SO_3

Regression Statistics	
Multiple R	0.973909
R Square	0.948498
Adjusted R Square	0.942555
Standard Error	0.081164
Observations	59

Analysis of Variance (ANOVA)

	df	*SS*	*MS*	*F*	*Significance F*
Regression	6	6.308791	1.051465	159.6114	1.1E-31
Residual	52	0.342558	0.006588		
Total	58	6.651349			

	Coefficients	*Standard Error*	*t Stat*	*P-value*	*Lower 95%*	*Upper 95%*
Intercept	-2.99121	0.512215	-5.83974	3.44E-07	-4.01904	-1.96337
log(SO_3 conc., mg/am^3)	0.513845	0.062655	8.20119	6.13E-11	0.388119	0.639571
log(T, R)	0.785485	0.185629	4.231475	9.45E-05	0.412993	1.157977
Log(Li+Na)(a)	0.270711	0.077058	3.513064	0.000926	0.116082	0.42534
Log(K)	-0.1177	0.05934	-1.98347	0.052606	-0.23677	0.001375
Log(Mg+Ca)(b)	0.292563	0.081426	3.592989	0.000725	0.12917	0.455956
Log(Fe)	0.288818	0.056989	5.068003	5.43E-06	0.174462	0.403174

(a) Li + Na = Sum of atomic concentrations of Li and Na
(b) Mg + Ca = Sum of atomic concentrations of Mg and Ca

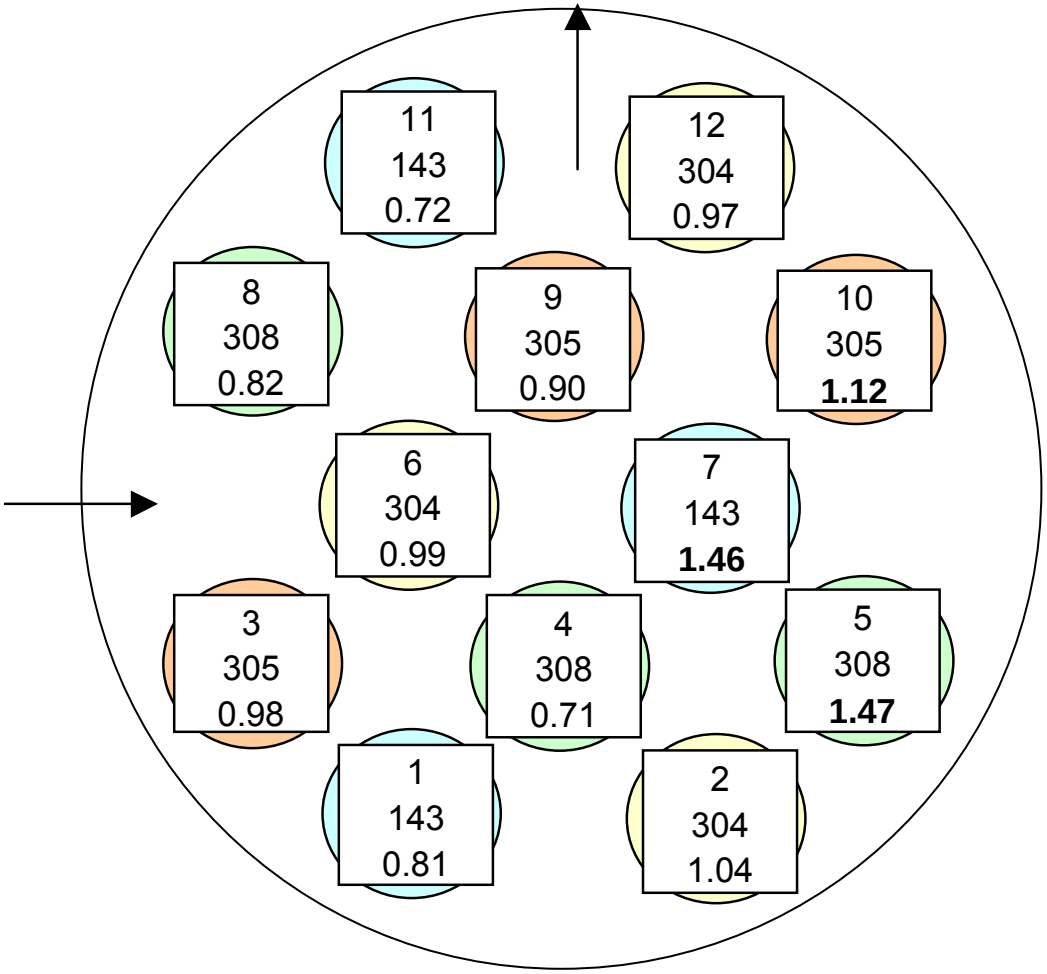

Figure 4.1. Layout of ash samples in the exposure chamber as seen from above. Simulated flue gas enters as shown by the arrow at the left of the figure and exits as shown by the arrow at the top of the figure. The upper number is the sample position number. The center number is the ID of the ash exposed in that position during an initial check for reproducibility and positional dependence and the third value is the SO_3 uptake by the ash in that position in this initial check.

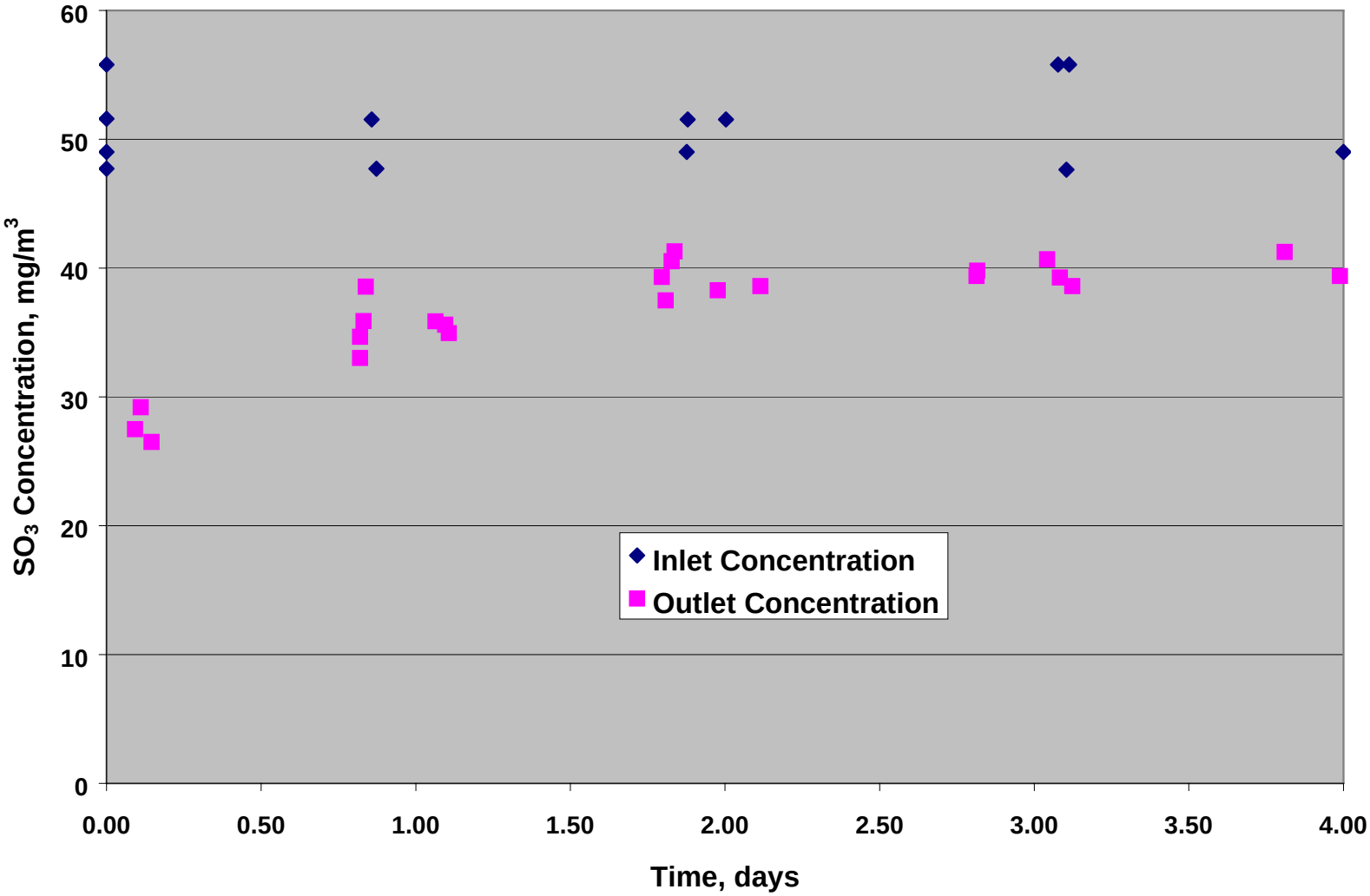

Figure 4.2. Typical concentration *versus* time measurements at the inlet and outlet of the SO_3 exposure chamber.

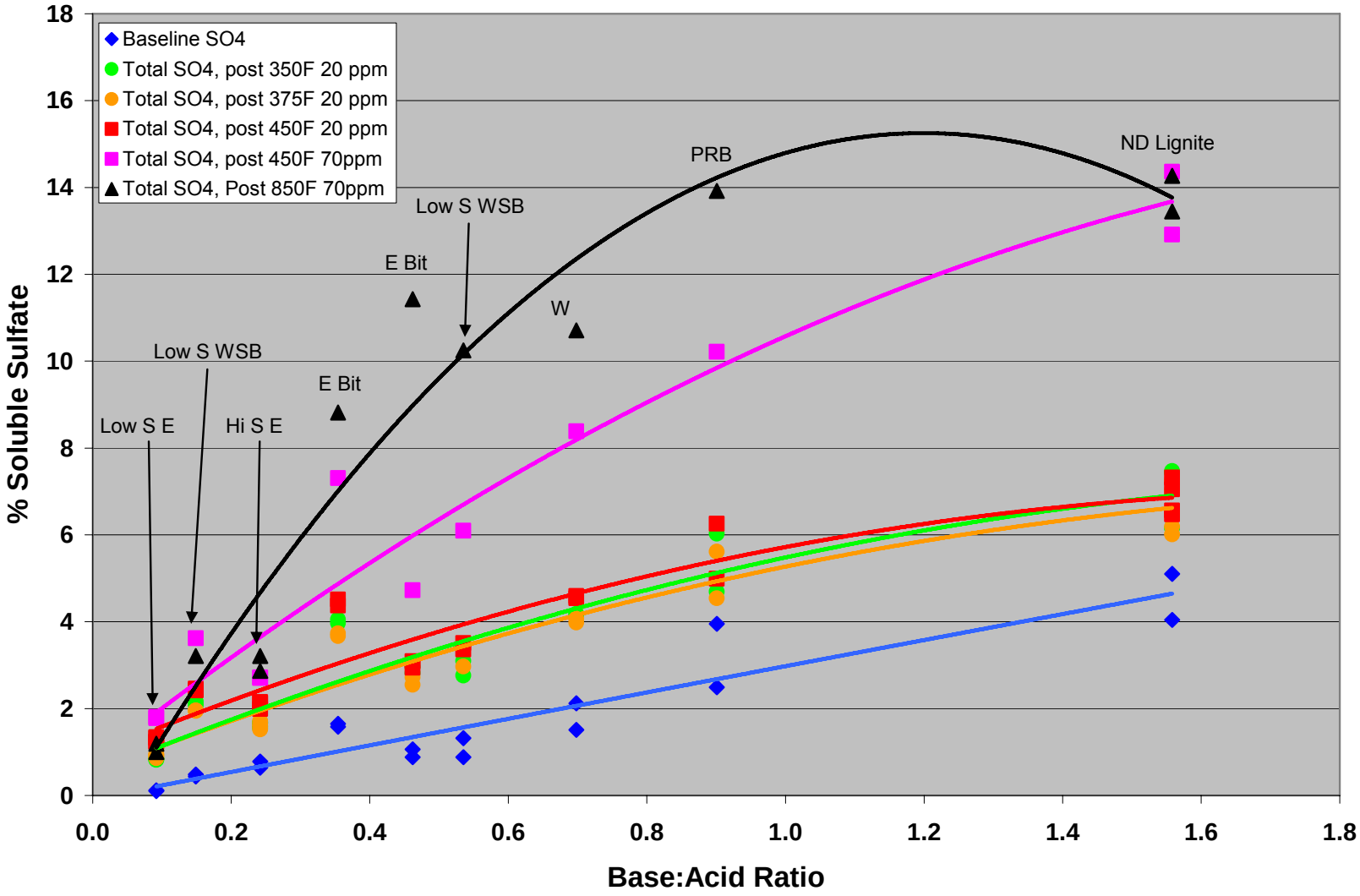

Figure 4.3. Total soluble sulfate found in ash samples after exposure to SO_3 at the conditions indicated *versus* ash base:acid ratios.

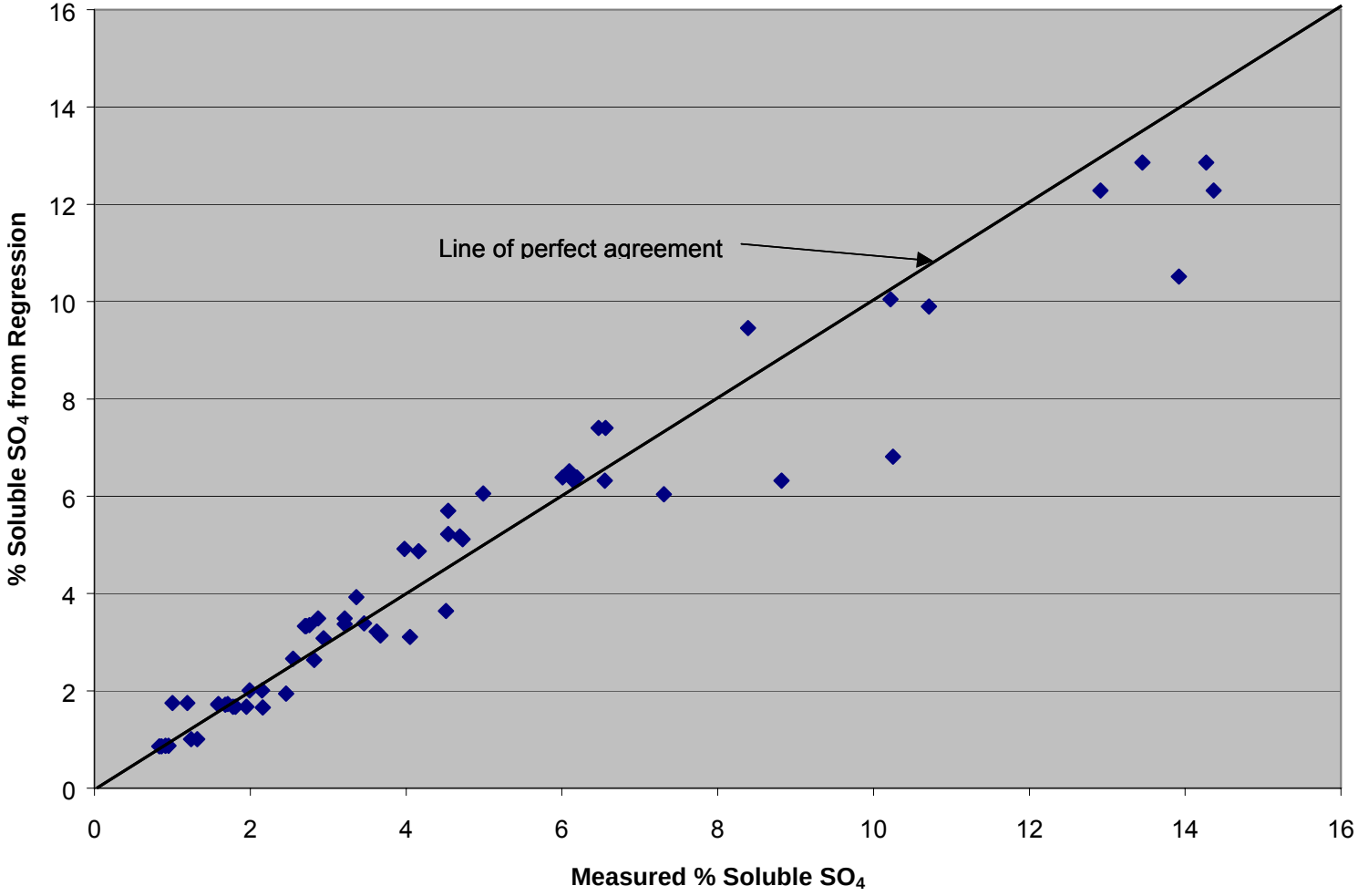

Figure 4.4 Plot of SO_4 on ash as predicted by the regression equation and the values measured in this study.

5. FORMATION OF SULFUR TRIOXIDE IN THE CONVECTION SECTION OF COAL-FIRED ELECTRIC UTILITY BOILERS

Formation of SO_3 in the Convection Section

Southern Research Institute, working in cooperation with the U.S. Environmental Protection Agency, Electric Power Research Institute, and Tennessee Valley Authority, is developing a model relating SO_3 formation in the convection sections of pulverized coal-fired boilers to coal properties, convection section design, and operating conditions. The model is intended to provide electric utilities with guidance on coal specification, sootblowing schedule, and excess air adjustment to minimize the contribution of convection section processes to formation of sulfuric acid, subject to the other constraints on fuel selection and system operation.

The processes incorporated in the model are: catalytic oxidation of SO_2 to SO_3 by oxide scale on convection section tubes, catalytic oxidation of SO_2 by ash deposits on the tubes, catalytic oxidation of SO_2 by suspended fly ash particles, and adsorption of SO_3 and H_2SO_4 by fly ash. The model is a refinement and significant extension of one developed by Peter Walsh and coworkers at Pennsylvania State University, working with the Consolidated Edison Co. of New York, Electric Power Research Institute, Empire State Electric Energy Research Corp., and Florida Power & Light Co. on particulate emissions from residual oil-fired boilers, and with the New York State Electric and Gas Corp. on the blue plume at Hickling Station in Corning, NY. That work is documented in two reports and an article.[37-39]

The basis for the calculation of catalytic oxidation of SO_2 to SO_3 by tube scale, ash deposits, and fly ash is a chemical mechanism in which SO_2 is oxidized by iron oxide. The oxide, which is reduced in the process, is returned to its higher oxidation state by reaction with oxygen. This system of reactions, coupled with diffusion of SO_3 from its point of formation on the iron-containing surfaces of tubes, deposits, or suspended fly ash to the free stream, reproduces the complex dependence of SO_3 formation on temperature, excess oxygen, coal sulfur content, heat exchanger surface area, extent of fouling of the tubes, and boiler load. The calculation includes flue gas, tube, and deposit surface temperatures; reaction rates, including approach to equilibrium; contact times; and transport of SO_3. There is no diffusion limitation on the supply of the reactants, SO_2 and O_2, because they are present in great excess. The calculation is done for each row of convective section tubes from the furnace exit through the economizer.

Measurements at an oil-fired boiler showed that a situation that leads to excessive SO_3 formation was the growth of fouling deposits on the usually relatively cool surfaces of the primary superheater toward the back end of the convection section, where tube spacing is relatively close and the tube surface to gas volume ratio is high. The growth of deposits in this region eventually leads to deposit surface temperatures in the most active temperature range, and the combination of these temperatures with high surface to volume ratio generates high levels of SO_3.

A related problem is illustrated in Figures 5.1, 5.2, and 5.3, for the case of the stoker-fired boiler at Hickling Station.[38] The top panel in Figure 5.1 shows the surface temperature distribution on clean superheater tubes without fouling deposits on either the steam or fire sides. Sulfur trioxide

formation is most rapid in the range of catalyst temperatures from 900 to 1400 ^{o}F. The catalyst, in the case of clean tubes, is iron oxides in tube scale, nearly 100% iron oxides on the SA213 T11 and T22 tubing. Sulfur trioxide formation over clean tubes, shown in the bottom panel of Figure 5.1, is most rapid near the entrance to the superheater where the temperature is at or above 900 ^{o}F. At the lower temperatures further back, SO_3 formation is negligible.

The case of tubes heavily fouled on the fire side is shown in Figure 5.2. Surface temperatures through almost the entire superheater are in the most active range. The catalyst is now the relatively low concentration of iron oxides (~ 0.13 wt%) in the ash deposits. The combined effect of higher temperature and lower iron oxide concentration is a modest increase in SO_3 leaving the superheater, from about 25 to 30 ppmv.

The case of tubes moderately fouled on the steam side but clean on the fire side is shown in Figure 5.3. Temperatures through much of the superheater are in the most active range and most of the surface exposed to flue gas is catalytic tube scale. This combination results in a marked increase in SO_3 leaving the superheater, to approximately 75 ppmv. These examples illustrate some of the complexity of the SO_3 formation process and the usefulness of a mechanistic model in providing rational explanation for observations in the field.

Comparisons of model predictions in the Hickling report[38] with measured values at various locations through the plant are shown in Figure 5.4. As can be seen, the model as it existed at the time appeared to provide plausible results.

Mechanisms of SO_3 Formation

Sulfur trioxide is formed by oxidation of sulfur dioxide according to the overall reaction,

$$SO_2 + 1/2\ O_2 \text{ --> } SO_3 \qquad (5.1)$$

Two distinct reaction mechanisms are possible under conditions in boilers: homogeneous (gas) and heterogeneous (solid-catalyzed). In the flame and postflame regions, above about 1200 K (1700 ^{o}F), the steady-state concentration of SO_3 is approximately described by formation and destruction reactions of SO_2 and SO_3 with oxygen atoms:[40]

$$SO_2 + O + M \text{ --> } SO_3 + M \qquad (5.2)$$

$$SO_3 + O \text{ --> } SO_2 + O_2 \qquad (5.3)$$

"M" is any molecule, such as N_2, CO_2, H_2O, O_2, etc., that collides with SO_2 and the O atom at about the same time and carries away energy, stabilizing the product. All of the possible collision partners are not equally efficient, a refinement that a detailed treatment might take into consideration. Discussions of this homogeneous reaction system are given by Merryman and Levy,[40] Cullis and Mulcahy,[41] and Smith, Wang, Tseregounis, and Westbrook.[42]

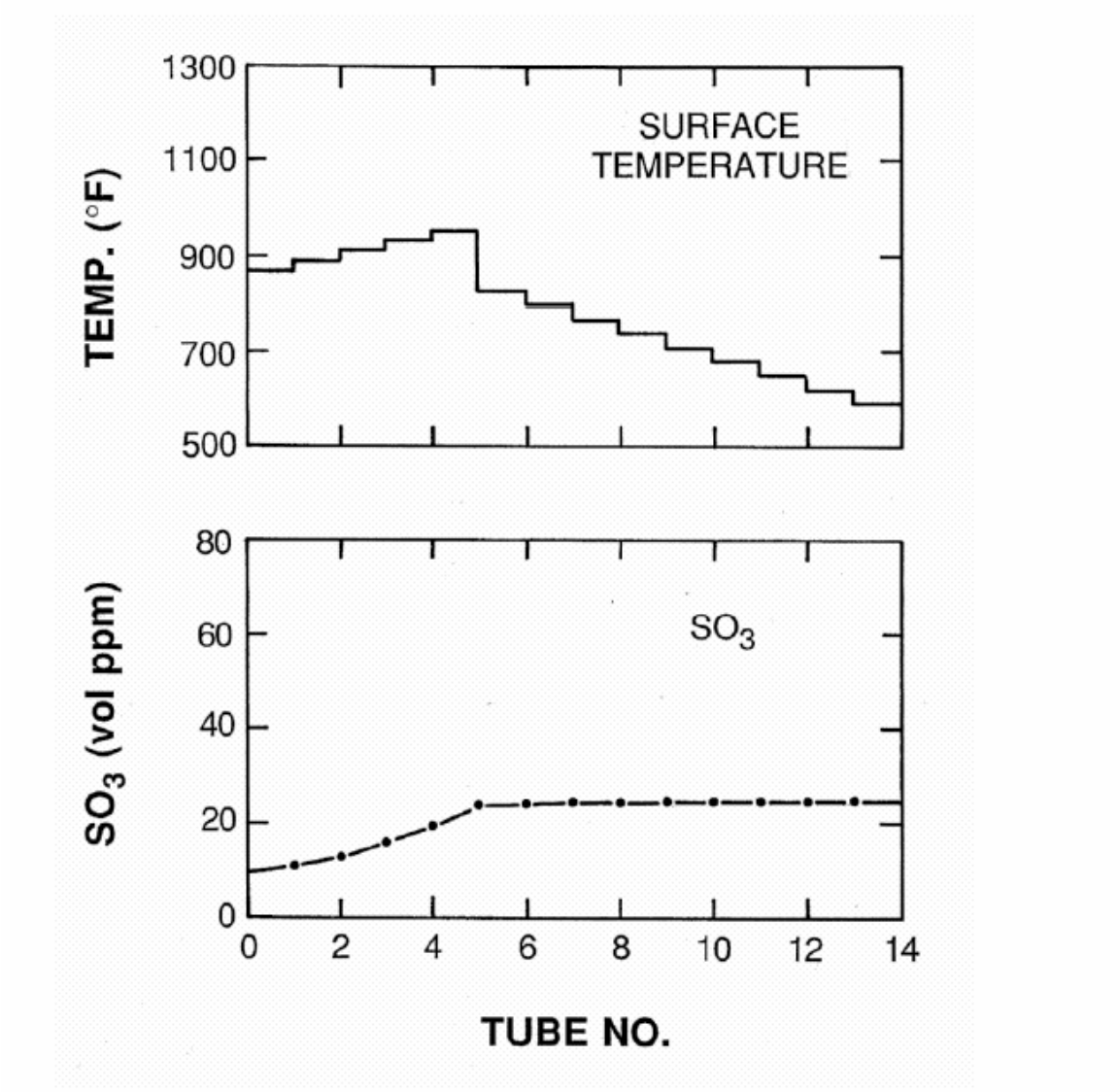

Figure 5.1. Surface temperature and SO_3 formation in the superheater under the assumption of negligible fouling and tube scale exposed to flue gas.[38]

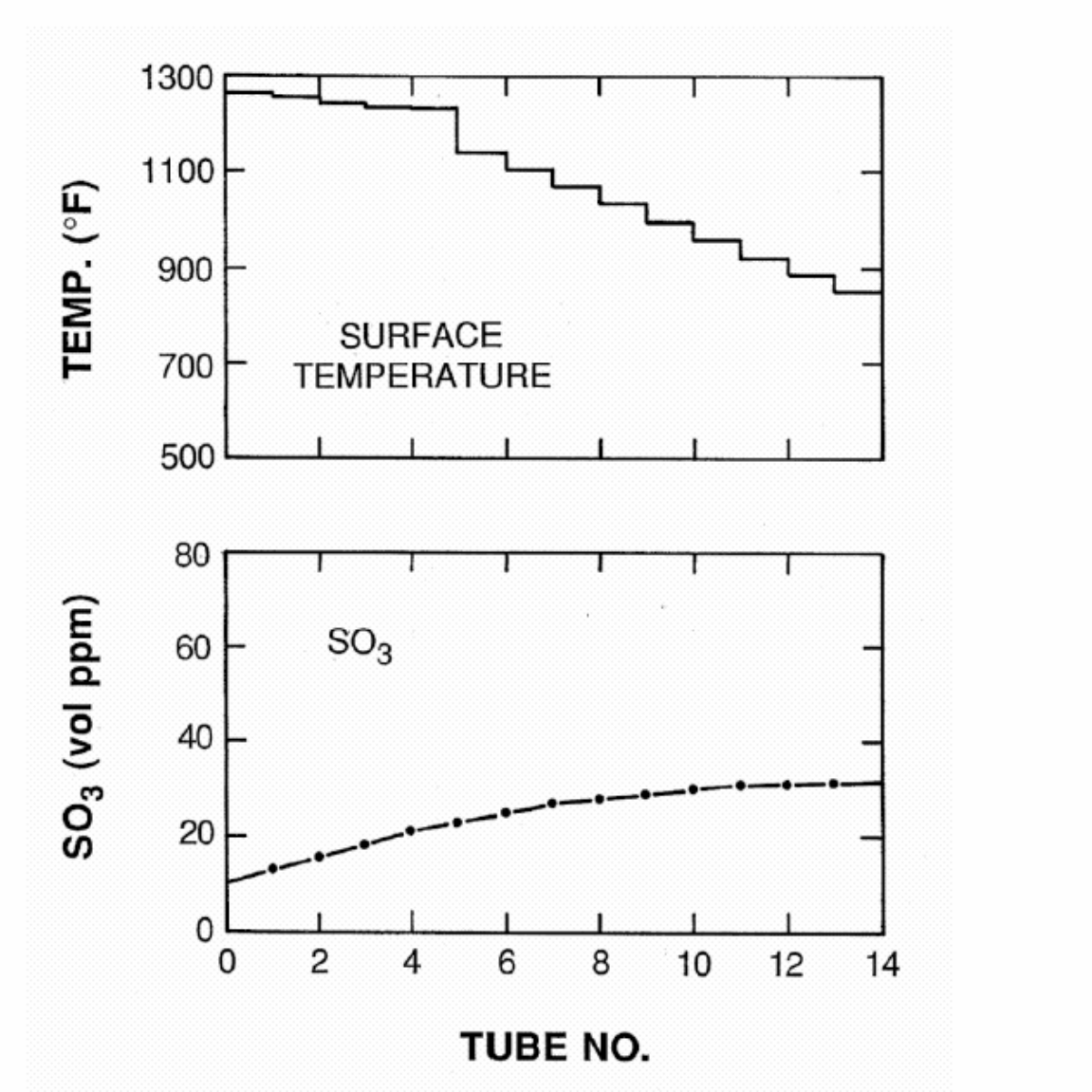

Figure 5.2. Surface temperature and SO_3 formation in the superheater under the assumption of heavy fouling on the fire side, with ash deposits exposed to flue gas.[38]

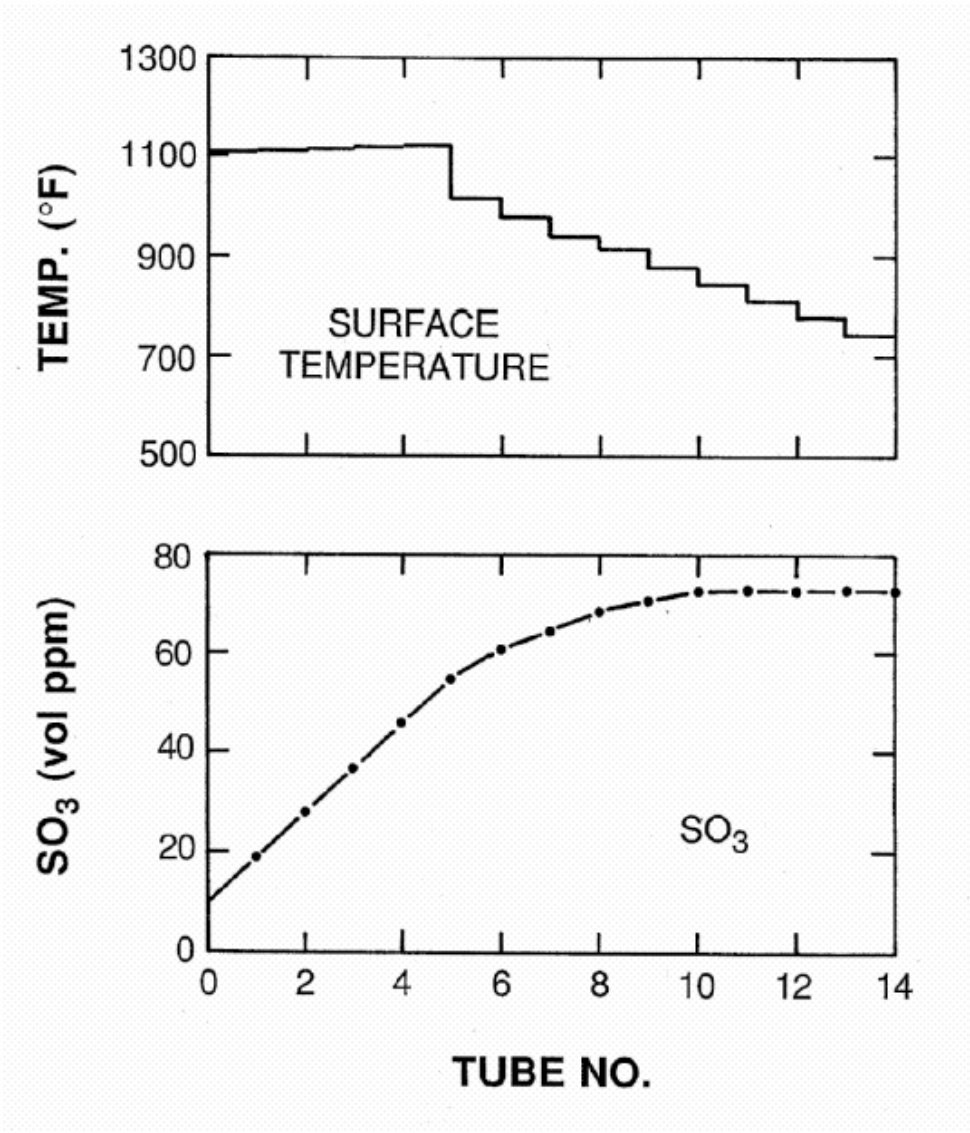

Figure 5.3. Surface temperature and SO_3 formation in the superheater under the assumption of moderate fouling on the steam side, with tube scale exposed to flue gas.[38]

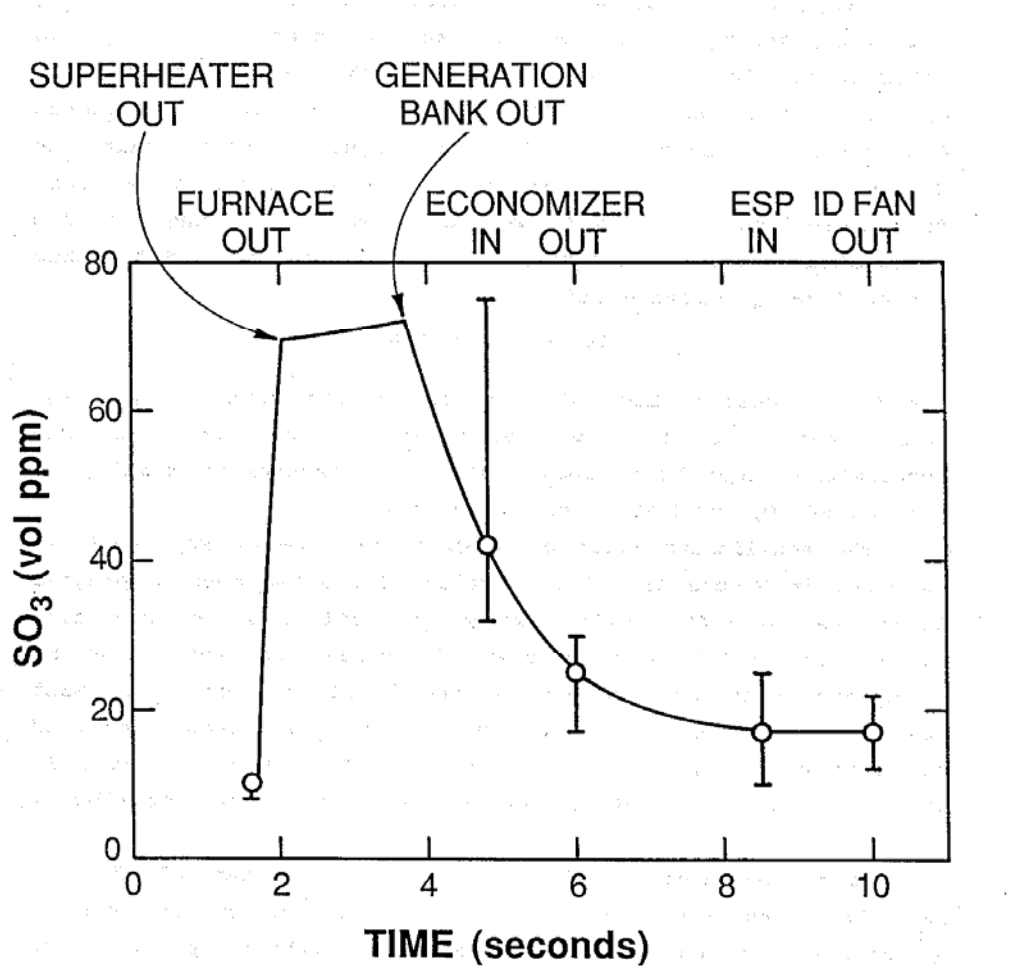

Figure 5.4. Comparison of the calculated SO_3 formation to measurements for the Hickling Station modeling.[38] The model calculations were done under the assumptions of moderate fouling and a mixture of tube scale and ash deposits exposed to flue gas.

In a region where conditions are not changing too rapidly, the system of reactions (5.2) and (5.3) approaches a steady state in which the ratio of SO_3 to SO_2 is constant, independent of the oxygen atom concentration.[40] At the furnace exit, far from the flame zone, where the oxygen atom concentration might reasonably be assumed to approach equilibrium at the local temperature, a useful approximation, in the absence of a direct measurement, may be to assume that SO_2 and SO_3 are also in equilibrium at that temperature. This would typically give an SO_3 volume fraction on the order of 10 to 20 ppmv in combustion products from fuel containing 1 to 2 wt % sulfur at temperatures in the vicinity of 1560 K (2350 ^{o}F). Measurements in a pilot-scale combustion tunnel firing residual fuel oil[43] support the assumption that SO_3 volume fractions in a boiler furnace and at the furnace exit are of roughly this magnitude.

The equilibrium distribution of the sulfur oxides shifts toward SO_3 as temperature decreases. Therefore, as combustion products cool, near the furnace exit and further downstream,

equilibrium favors additional conversion of SO_2 to SO_3, but the rate of the homogeneous reactions decreases with decreasing temperature, closing off this route for SO_3 formation. The rate of SO_2 oxidation may still be appreciable, however, in the presence of a heterogeneous catalyst. Solid-catalyzed reactions are thought to be the source of the high levels of SO_3 sometimes observed at the economizer outlet.

The best-known catalyst for SO_2 oxidation is vanadium pentoxide, V_2O_5, used to generate SO_3 in the manufacture of sulfuric acid. V_2O_5 is a component of selective catalytic NO_X reduction (SCR) catalysts and the ash constituent typically making the greatest contribution to catalytic SO_3 formation in high-sulfur residual oil firing. Because of the importance of catalytic oxidation of SO_2 in the manufacture of a major industrial chemical, this reaction has been the subject of numerous investigations.[44]

A comparison of the catalytic activities of iron and vanadium oxides for SO_2 oxidation, for the specific purpose of understanding SO_3 formation in oil-fired boilers, was made in laboratory experiments performed by Wickert.[45] His results demonstrated two important features relevant to boilers: (1) iron oxide was an active catalyst, only slightly less active than vanadium pentoxide, and with peak activity shifted to slightly higher temperatures than that for vanadium oxide, and (2) during a fixed residence time in contact with iron pentoxide, conversion of SO_2 to SO_3 was greatest over the range of temperatures from roughly 760 to 1030 K (900 to 1400 ^oF). The evident activity of iron oxide and the abundance of iron oxide in coal ash and tube scale suggest that it is likely to be the principal catalyst for SO_3 formation in coal-fired boilers. Iron oxides are present in tube scale, in ash deposits on tubes, and in suspended fly ash. Significant conversion is observed only over a limited range of temperature because at higher temperatures formation of SO_3 is limited by the equilibrium distribution of sulfur oxides and at lower temperatures by the rate of the solid-catalyzed reaction.

Models for both homogeneous formation of SO_3 and heterogeneous formation catalyzed by ash deposits in oil-fired boilers were developed by Squires.[46] Squires treated the temperature dependence of conversion in the presence of catalyst by incorporating, in the rate coefficient for the heterogeneous reaction, a temperature dependence derived from the measurements of Wickert.[45] This approach has the disadvantage that calculated SO_2 oxidation could proceed to unrealistically high conversion in a system having long gas-catalyst contact time, regardless of the equilibrium constraint.

Development of the model described below also began with a study of SO_3 formation in the convection sections of residual-oil-fired boilers.[37,39,47] The reactions were described using rate coefficients having Arrhenius temperature dependence, with conversion limited by the equilibrium between sulfur oxides. The oil-fired case did not require that a contribution from suspended ash be considered, because the ash concentration and its surface area per unit of gas volume are small. The model was applied to a coal-fired stoker boiler by Walsh, DeJohn, Bower, and Rahimi.[38] These authors included an approximate treatment of the contribution to SO_3 formation from catalysis by fly ash, which was small, but significant. In pulverized coal firing, the fly ash concentration and contribution to SO_3 formation are expected to be larger than in a stoker-fired boiler, therefore a more rigorous treatment of the contribution to SO_3 formation

by catalytic reaction on suspended fly ash has been implemented in the present version of the model.

Model for Catalytic SO_3 Formation in the Convection Section

The kinetics of heterogeneous oxidation of SO_2 were reviewed by Urbanek and Trela.[44] The essential features of the system are oxidation of SO_2 by a metal oxide, accompanied by reduction of the metal to a lower oxidation state having little or no catalytic activity. The active higher oxide is regenerated by reaction with oxygen. The cycle can be represented as follows:

$$SO_2 + FeO_X \xrightarrow{k_1} SO_3 + FeO_{X-1} \tag{5.4}$$

$$FeO_{X-1} + 1/2\ O_2 \xrightarrow{k_2} FeO_X \tag{5.5}$$

Equations 5.4 and 5.5 are the overall reactions, not elementary steps, and k_1 and k_2 are global rate coefficients. The reactions are assumed to be first order with respect to the gaseous species and the iron oxides. The rate of formation of SO_3 by reaction 5.4 is then (please see the list of nomenclature for definitions of the symbols):

$$r_{SO_3} = k_1\, Y_{FeO_X}\, S\, C_s\, X_{SO_2} \tag{5.6}$$

When the catalyst composition is steady, the mass fraction of the higher oxide, FeO_X, can be written in terms of the total mass fraction of iron oxides, $Y_{Fe_2O_3}$, from an ash analysis, or any other measure of total iron content, and the relative rates of formation and destruction of the higher and lower oxides:

$$r_{SO_3} = \frac{Y_{Fe_2O_3} S\, C_s}{\dfrac{1}{k_1 X_{SO_2}} + \dfrac{1}{k_2 X_{O_2}}} \left[1 - \frac{X_{SO_3,s}}{X_{SO_3,eq}} \right] \tag{5.7}$$

The factor in brackets is introduced to account for the approach of the rate to zero as the SO_3 concentration adjacent to the catalyst surface approaches its equilibrium value. At steady state, the rate of SO_3 formation at the deposit surface equals its rate of transport from the surface to the free stream:

$$r_{SO_3} = \frac{Sh\, D_{SO_3}}{d} S\, C_{bl}\, (X_{SO_3,s} - X_{SO_3}) \tag{5.8}$$

Combining Eqs. 5.7 and 5.8 to eliminate the unknown concentration of SO_3 at the deposit surface:

$$r_{SO_3} = k\, S\, C_g\, (X_{SO_3,eq} - X_{SO_3}) \tag{5.9}$$

in which the effective rate coefficient is:

$$k = \frac{1}{\dfrac{1}{\dfrac{Sh\ D_{SO_3}}{d}\dfrac{C_{bl}}{C_g}} + \dfrac{C_g\ X_{SO_3,eq}}{C_s\ Y_{Fe_2O_3}}\left[\dfrac{1}{k_1\ X_{SO_2}} + \dfrac{1}{k_2\ X_{O_2}}\right]} \tag{5.10}$$

Under conditions of interest in boilers the extent of conversion of SO_2 to SO_3 is small, so the changes in SO_2 and O_2 concentrations accompanying SO_3 formation may be neglected. The rate of SO_3 production, Eq. 5.9, is equated to the rate of change in molar flux of SO_3 with position in the convection section. Integration of the resulting expression, with the boundary condition $X_{SO_3} = X_{SO_3,o}$ at $t = t_o$, gives an expression for the change in SO_3 mole fraction with residence time in a row of tubes in which deposit composition and surface temperature are uniform:

$$X_{SO_3} = X_{SO_3,eq} - (X_{SO_3,eq} - X_{SO_3,o}) \exp[-k\ S\ (t - t_o)] \tag{5.11}$$

Inspection of the rate expression, Eq. 5.9, and effective rate coefficient, Eq. 5.10, shows that there are four regimes of SO_3 formation: (1) equilibrium; (2) control by diffusion through the concentration boundary layer adjacent to the deposit (near equilibrium at the surface); (3) control by O_2; and (4) control by SO_2.

The temperature dependence of SO_3 at equilibrium in the products of combustion of 1.41 wt % sulfur coal with 5 vol % excess oxygen is shown in Figure 5.5a and the temperature dependence of the effective rate coefficient and its components is shown in Figure 5.5b, as functions of the reciprocal of absolute temperature. The total volume fraction of sulfur oxides (SO_2 + SO_3) is 1170 ppmv. The equilibrium volume fraction of SO_3 (Figure 5.5a) is the ultimate value reached if the mixture were allowed to stand at the specified temperature, with or without catalyst, for a long period of time. Referring to the Fahrenheit temperature scale at the top in Figure 5.5a, we see that at equilibrium at 2200 ^oF (1478 K), the gas would contain 10 ppmv SO_3; at 1800 ^oF (1255 K) it would contain 40 ppmv SO_3; at 1400 ^oF (1033 K) it would contain 300 ppmv SO_3; and at 1000 ^oF (811 K) it would contain 1000 ppmv SO_3.

In the flow of combustion products through a convection section, in which the volume fraction of SO_3 is rising from a low value but unable to keep up with the increase in equilibrium

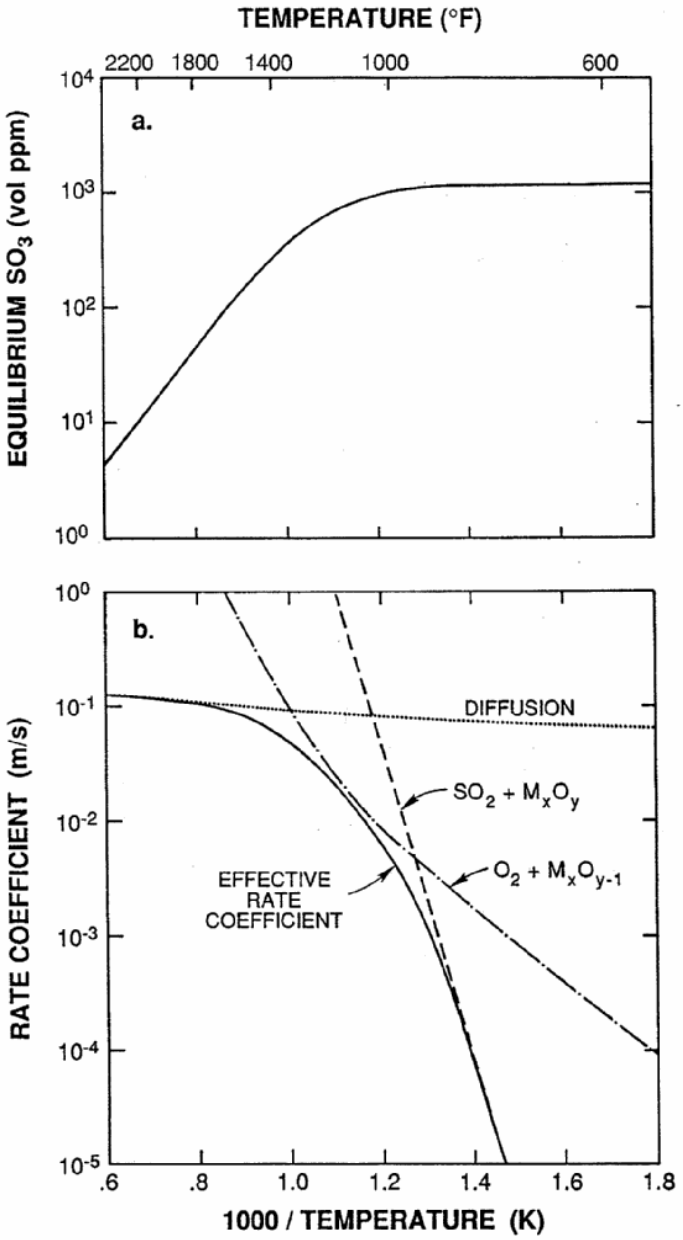

Figure 5.5. Equilibrium and kinetic constraints on SO_3 formation.[38] (a) Equilibrium mole fraction of SO_3 in the products of combustion of Lee coal (wt %, as received: moisture, 11.62; ash, 17.51; volatile matter, 22.92; fixed carbon, 47.95; sulfur, 1.41; and 10,508 Btu/lb HHV, as received). (b) Rate coefficients for: diffusion of SO_3 from the surface of a tube or deposit to the free stream; oxidation of SO_2 by reaction with metal oxide, Reaction (5.4); reoxidation of reduced metal oxide to the active state, Reaction (5.5); and the overall reaction, when these three processes all occur simultaneously.

concentration associated with the decrease in temperature, the equilibrium concentration at the local temperature of the point of formation (the catalyst surface) will not be exceeded. The curve shown in Figure 5.5a therefore represents the maximum possible SO_3 that could be found in flue gas adjacent to a catalytic surface at the specified temperature.

Walsh, Mormile, and Piper[39] proposed the rate coefficients shown in Figure 5.5b to simulate SO_3 formation in a residual-oil-fired boiler. The line labeled "diffusion" is the mass transfer coefficient for SO_3 formed at the surface of a tube or ash deposit to the free stream. The dashed and dot-dash curves are effective rate coefficients for reactions (5.4) and (5.5). They are termed "effective" because the concentration of catalytic metal oxide on the surface and the distribution of the oxides between the higher and lower oxidation states are also incorporated in the coefficients. The solid curve is the overall effective rate coefficient governing the formation of SO_3. The overall rate coefficient is never greater than the rate coefficient for the slowest process at a given temperature, which shifts from SO_2 oxidation at low temperatures, to catalyst (metal oxide) regeneration at intermediate temperatures, to mass transfer at the highest temperatures. At high temperatures equilibrium also limits the conversion of SO_2 to SO_3. A connection between diffusion control and equilibrium at the catalyst surface is expected because, when both reactants (SO_2 and O_2) are present in excess, a limitation by mass transfer implies that the chemical reaction at the deposit surface is much faster than diffusion and, therefore, that the concentration of the product, SO_3, at the surface approaches its equilibrium value.

Combination of the upper limit imposed by equilibrium (Figure 5.5a) with the limit imposed by the rate coefficient for SO_3 formation and the residence time of gas in contact with catalyst, results in the characteristic behavior observed by Wickert,[45] i.e. conversion of SO_2 to SO_3 is greatest over a narrow range of temperatures. At lower temperature, the rates of the reactions are too slow and at higher temperatures the equilibrium concentration (the maximum possible concentration in the situation under consideration) of SO_3 is low.

The choice of active surface area is a question where little guidance is available. Several possible assumptions were examined by Shareef, Homolya, and Mormile.[48] In the present work, the surface area of the convective tubes was used as the basis for the estimate of catalyst surface area, and the mass fraction of vanadium oxides in deposits provided an estimate of the fraction of the surface which was active. Measurements of the vanadium content of the outer surface of deposits from the boiler showed little variation in vanadium content through the convective section.[49]

Simultaneous SO_3 Formation on Ash Deposits and Suspended Particles

The equations describing SO_3 formation catalyzed by iron oxide in suspended fly ash particles and by iron oxide in stationary deposits or tube scale are the same, Eq. (5.11), but with their respective external surface areas per unit of gas volume, S, Sherwood numbers, Sh, characteristic lengths, d (tube and mean particle diameters), mass fractions of iron oxides, $Y_{Fe_2O_3}$, and temperatures, T (flue gas temperature for fly ash and surface temperature for deposit or clean tube). The total rate of SO_3 formation, including the reaction on tube surface or ash deposits, subscript "t," and the reaction on suspended fly ash, subscript "p," is the sum of the contributions from the two parallel processes:

$$r_{SO_3} = k_t \; S_t \; C_g \; (X_{SO_3,eq,t} - X_{SO_3}) + k_p \; S_p \; C_g \; (X_{SO_3,eq,p} - X_{SO_3}) \qquad (5.12)$$

A derivation parallel to that for a single catalytic surface, above, gives the following expression for the mole fraction of SO_3 in flue gas at the outlet from the space surrounding a row of tubes, in the presence of suspended fly ash, when the mole fraction at the inlet to the space is $X_{SO_3,o}$:

$$X_{SO_3} = \frac{k_t S_t X_{SO_3,eq,t} + k_p S_p X_{SO_3,eq,p}}{k_t S_t + k_p S_p} - \left[\frac{k_t S_t X_{SO_3,eq,t} + k_p S_p X_{SO_3,eq,p}}{k_t S_t + k_p S_p} - X_{SO_3,o} \right] \exp[-(k_t S_t + k_p S_p)(t - t_o)] \tag{5.13}$$

The first term on the right-hand side, which also appears as the first term inside the large brackets, is an average equilibrium SO_3 mole fraction, weighted by the relative rates of formation of SO_3 over deposit or tube surface and fly ash.

Calculations

Design data and operating conditions for the boiler of a large coal-fired electric generating unit were provided by the utility to which it belongs. The model described above was used to calculate SO_3 formation in the convection section between the furnace exit and the inlet to the economizer at full load. This region included, in order, beginning at the furnace exit, the secondary superheater, reheat superheater, primary superheater, and horizontal reheat superheater, a total of 140 rows of tubes. For the present, preliminary calculations the flue gas temperature change from the furnace exit to the economizer inlet was divided into 140 equal increments, corresponding to a temperature change of approximately 5 K (9 ^{o}F) across each row of tubes. The resulting distribution of gas temperatures through the region under consideration is shown in Figure 5.6. The temperature drop shown in the figure for the economizer was estimated simply by dividing the overall temperature change and residence time into four equal increments.

The difference between steam inlet and outlet temperatures for each tube bank was divided into a number of increments equal to the number of rows of tubes in the bank to estimate the steam temperature in each row. The general direction of steam flow in each bank was taken into consideration, where an overall direction could be identified, but finer details of the flow were not considered, for example in some sections of the secondary and reheat superheaters, where the steam flow enters through tubes in the middle of a bank, then goes to upstream and downstream tubes in the same bank. The actual volumetric flow rate of flue gas was calculated at each tube row and used, with the tube diameter, to determine the residence time in the empty space associated with that row, the Reynolds, Nusselt, and Sherwood numbers for the tubes, and the tube surface area per unit of gas volume. The tubes were assumed to be covered with ash to the extent that the heat transfer resistance from the deposits plus tube metal plus steam film was equal to the external film resistance in the flue gas. The deposit surface temperature was assumed to be uniform around the perimeter, along the height or length, and over the width of a given row of tubes.

A mean particle size of 10 micrometers was assumed for the fly ash. Its concentration in the flue gas was calculated from the coal analysis and local flue gas volumetric flow rate, assuming that 20% of the ash feed was retained in the boiler. Loss of ash by deposition and fall-out in the convection section was not considered. The fly ash temperature was set equal to the flue gas temperature at every point. The formation of SO_3, catalyzed by fly ash, in the cavities within and between convective tube banks was included, as well as in the space surrounding the tubes.

The calculation was begun at the furnace exit, with the equilibrium SO_3 in flue gas containing SO_2 and O_2 corresponding to the coal analysis and typical excess air, at the furnace exit gas temperature. The calculated volume fraction of SO_3 at this point is 12 ppm. The increment in the volume fraction of SO_3 was calculated for each of the 140 rows of tubes using Eq. (5.13) and local values for the geometry, temperatures, and flow conditions, with the results shown in Figure 5.7, as the volume fraction of SO_3 versus flue gas residence time. The rate coefficients, k_1 and k_2, for the iron-oxide-catalyzed reactions (5.4) and (5.5), respectively, were given the same values used by Walsh, DeJohn, Bower, and Rahimi[38] to explain their measurements in Boiler No. 1 at Hickling Station. The values assigned to the parameters used in the calculations are listed in Table 5.1.

Table 5.1 Conditions for the SO_3 model run whose results are shown in Figures 5.6 and 5.7.

Parameter	Value
Barometric pressure, inch Hg	29.50
Excess air	0.24
Stoichiometric air/fuel mass ratio, kg/kg	8.570
Coal feed rate, kg/s	145.56
Mass fraction sulfur in coal, kg/kg	0.03
Mass fraction ash in coal, kg/kg	0.08
Mass fraction iron oxides in ash, SO_3 free	0.2
Mass fraction iron oxides in tube scale	1.0
Average mass fraction iron oxides presented to flow over tubes	0.2000
Ratio of heat transfer coefficients, (steam+deposits)/gas	1
Pressure at furnace exit, inch water column	0
Furnace exit gas temperature, ^oF	2350
Average molecular weight of flue gas, wet, kg/kmol	29.1
External surface area-weighted mean particle size, m	0.000010
Fly ash apparent density, kg/m3	2500
Weight fraction of ash feed to furnace bottom	0.2
Weight fraction of ash feed to economizer hopper	0.05
Volume fraction O_2 in furnace exit gas, wet	0.038
Catalyst deactivation rate, activation energy, J/kmol	2.40E+08
Catalyst deactivation rate, preexponential factor	4.794461E+14
Catalyst regeneration rate, activation energy, J/kmol	5.00E+07
Catalyst regeneration rate, preexponential factor	0.959806

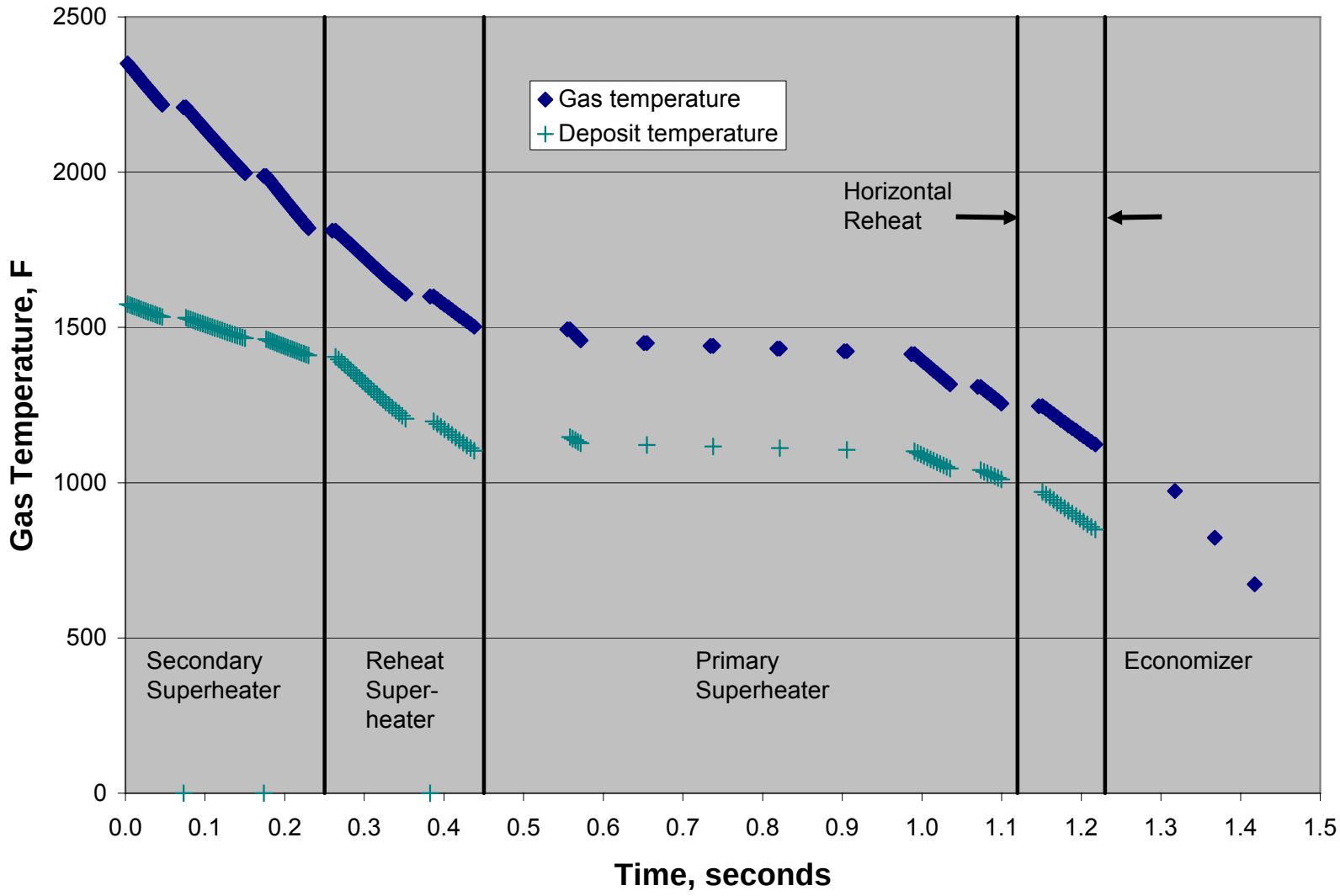

Figure 5.6. Modeled temperature profiles through a 1300 MW pulverized coal-fired utility boiler.

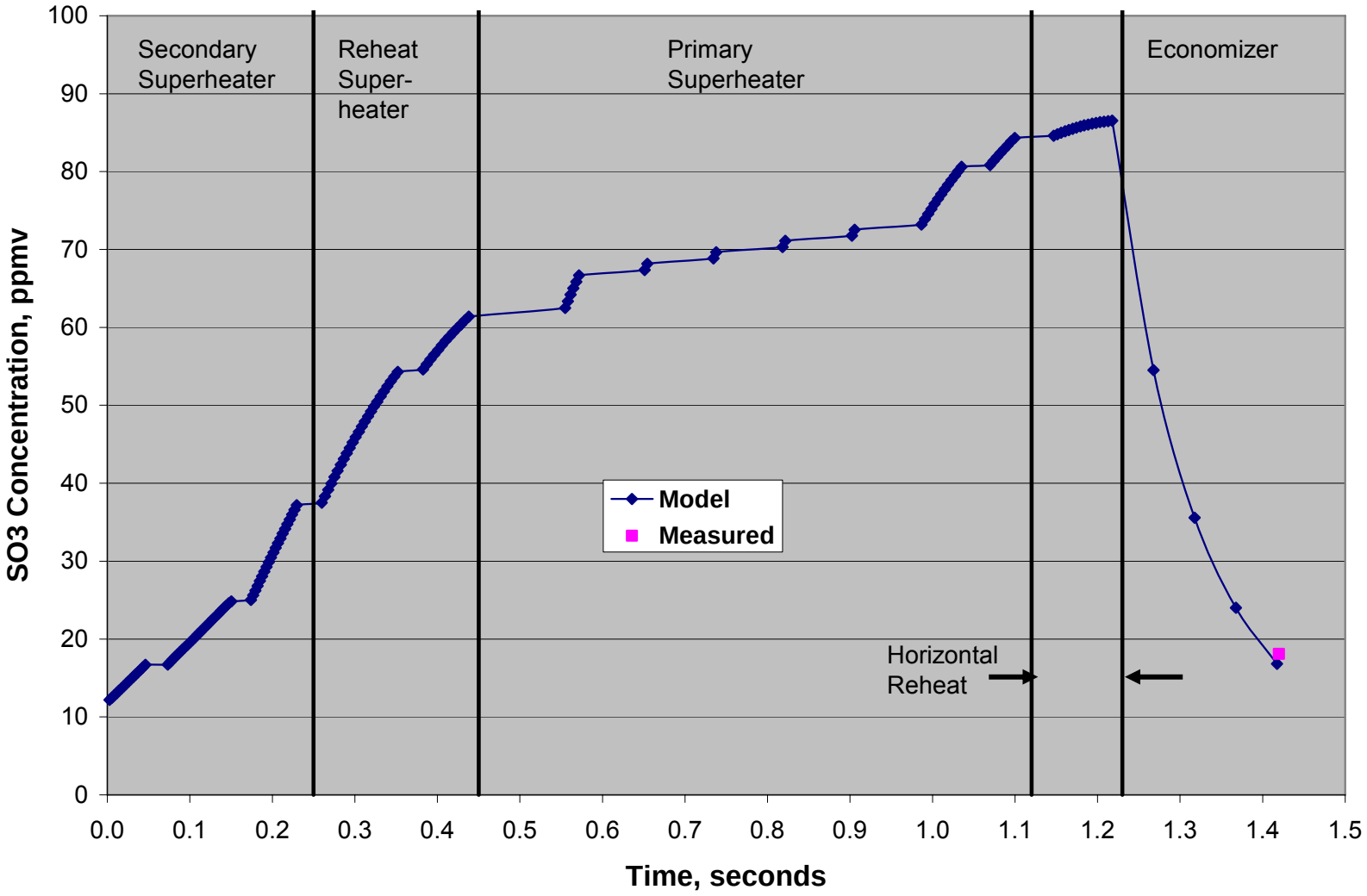

Figure 5.7. SO_3 concentration profile through a 1300 MW pulverized coal-fired utility boiler as predicted by the model.

Results and Discussion

The surface temperature of the deposit on the first row of secondary superheater tubes, at the furnace exit, was estimated to be 1130 K (1574 ^{o}F), above the high end of the temperature range in which catalytic SO_3 formation is thought to be most rapid. Nonetheless, the formation rate is significant. The discontinuities in the SO_3 profile in the figure are cavities between tube bundles. The small positive slopes of the line segments in these regions are indicative of the contributions to SO_3 formation by suspended fly ash. Its contribution is small throughout the convective section because the concentration and external surface area of fly ash are low.

At the entrance to the outlet (third) section of the secondary superheater, the deposit surface temperature is 1068 K (1463 ^{o}F), still above the most favorable range for SO_3 formation, but the side-to-side spacing of the tubes has been reduced by half and the number of tube assemblies doubled, compared to that in the first two secondary superheater sections, so the surface area per unit of gas volume is doubled, with a corresponding increase in the rate of SO_3 formation.

At the entrance to the reheat superheater the deposit surface temperature is 1036 K (1405 ^{o}F) and the tube density is the same as at the exit from the secondary superheater. The rate of SO_3 formation in this region remains high. In the second section of the reheat superheater, however, the rate is still high but beginning to decline. The deposit surface temperature at the exit from this section is 868 K (1103 ^{o}F), near the temperature at which the highest conversion was observed by Wickert[45] in the presence of iron oxide. Evidently, the temperature dependence of the activity obtained by fitting the Hickling Station measurements is not the same as that of the iron oxide samples examined by Wickert.

In the short section at the entrance to the primary superheater (the entrance with respect to the flue gas flow, it is actually the outlet with respect to the steam flow) the rate of SO_3 formation again shows a marked increase, due to another reduction in side-to-side tube spacing and near doubling of the surface area of ash deposits per unit of gas volume. From the slopes of the line segments between the following widely spaced (in the flow direction) tubes, one can see the contribution to SO_3 formation from the heterogeneous reaction on suspended fly ash. In the last two sections of the primary superheater, the rate of SO_3 formation remains high.

The deposit surface temperature at the entrance to the horizontal reheat superheater is 794 K (970 ^{o}F). At this point the rate of SO_3 formation shows a large decline, due at least in part to a factor of two reduction in the side-to-side tube spacing. Also, surface temperature is evidently approaching the lower end of the most active range, because the rate of SO_3 formation leaving this section has practically dropped to zero. The surface temperature is now 727 K (849 ^{o}F), in agreement with the lower end of the active range of temperatures observed by Wickert.[45]

Absorption of SO_3 and H_2SO_4 by Fly Ash

Walsh, DeJohn, Bower, and Rahimi[38] inferred a rapid decline in SO_3 at temperatures below about 700 K (800 ^{o}F) in the flue of Boiler No. 1 at Hickling Station. This is approximately the temperature at which reaction with water vapor begins to convert SO_3 to H_2SO_4. A preliminary treatment of this process was incorporated in the present calculation by considering the rate of diffusion of H_2SO_4 to suspended fly ash, in combination with the capacity of ash for SO_3/H_2SO_4 uptake described in another section of this report. For this calculation the temperature drop and

residence time in the economizer were divided into four equal increments, as mentioned briefly above. The results of these calculations, also shown in Figure 5.7, agree favorably with the measured value at the economizer exit. The comparison of the predicted and measured values at the economizer outlet using reasonable values for the controlling parameters in this instance is encouraging. However, substantially more testing is needed for validation of the model before it can be relied upon as a useful tool for predicting SO_3 emissions from coal-fired boilers.

6. DEVELOPMENT OF AN ESTIMATOR FOR REMOVAL OF SO_3/H_2SO_4 ACROSS AIR PREHEATERS

Condensation of H_2SO_4 on the surfaces of combustion air preheaters can remove significant amounts of the incoming SO_3/H_2SO_4, depending on the incoming concentrations and the air preheater exit temperatures. Although a detailed model of the processes related to the behavior of H_2SO_4 in air preheaters exists, an easily used, reasonably accurate means of estimating losses across rotary air preheaters would be useful. Such a method is described here.

The surface temperatures of the heat exchange elements in the air preheater are cooler than the incoming flue gas. As the elements of the air preheater rotate the surfaces are heated by the incoming flue gas, resulting in a gradient in the outlet flue gas outlet temperatures. For the purposes of this estimator it is assumed that the effective surface temperature for H_2SO_4 condensation at any point in the rotation has some constant offset from the exit gas temperature at that point. The acid dewpoint at any point on the exit face is then taken to be equal to the flue gas temperature at that point less this offset and the H_2SO_4 concentration is taken to be the saturation concentration at that temperature. Typical ranges of gas temperatures across the exit faces of air heaters from the cold end to the hot end are 50 °F to 100 °F.

Table 6.1 shows measured average concentrations at the exits of four rotary air heaters together with values predicted as described above using two offset temperatures. Figure 6.1 shows plots of estimated losses versus average exit temperature for a range of air heater inlet concentrations using a value of 35 °F for the temperature offset between the local exit gas temperature and the local exit saturation temperature. Curves are shown for two ranges of gas temperature variation across the exit faces of the preheaters: 50 °F and 100 °F. Figure 6.2 shows plots of the estimated average H_2SO_4 exit concentrations for the same conditions used in generating Figure 6.1. The flue gas moisture concentration will have some affect on the exit H_2SO_4 concentrations as illustrated in Figure 3. Figures 6.4 and 6.5 show curves similar to those in Figures 6.1 and 6.2 resulting from the use of a 30 °F offset temperature rather than the 35 °F offset. Figures 6.6 through 6.9 show plots of measured air heater exit H_2SO_4 concentrations together with concentrations predicted by the model using a 30 °F offset temperature.

Table 6.1. Measured and predicted average exit SO_3 concentrations for four rotary air heaters.

	Measured, ppm		Predicted, ppm	
Site	Inlet	Outlet	30 degree offset	35 degree offset
Rotary No. 1	3.1	0.9	1.7	1.4
Rotary No. 2	50	23	30	26
Rotary No. 3	42	18	17	13
Rotary No. 4	50	24	30	26

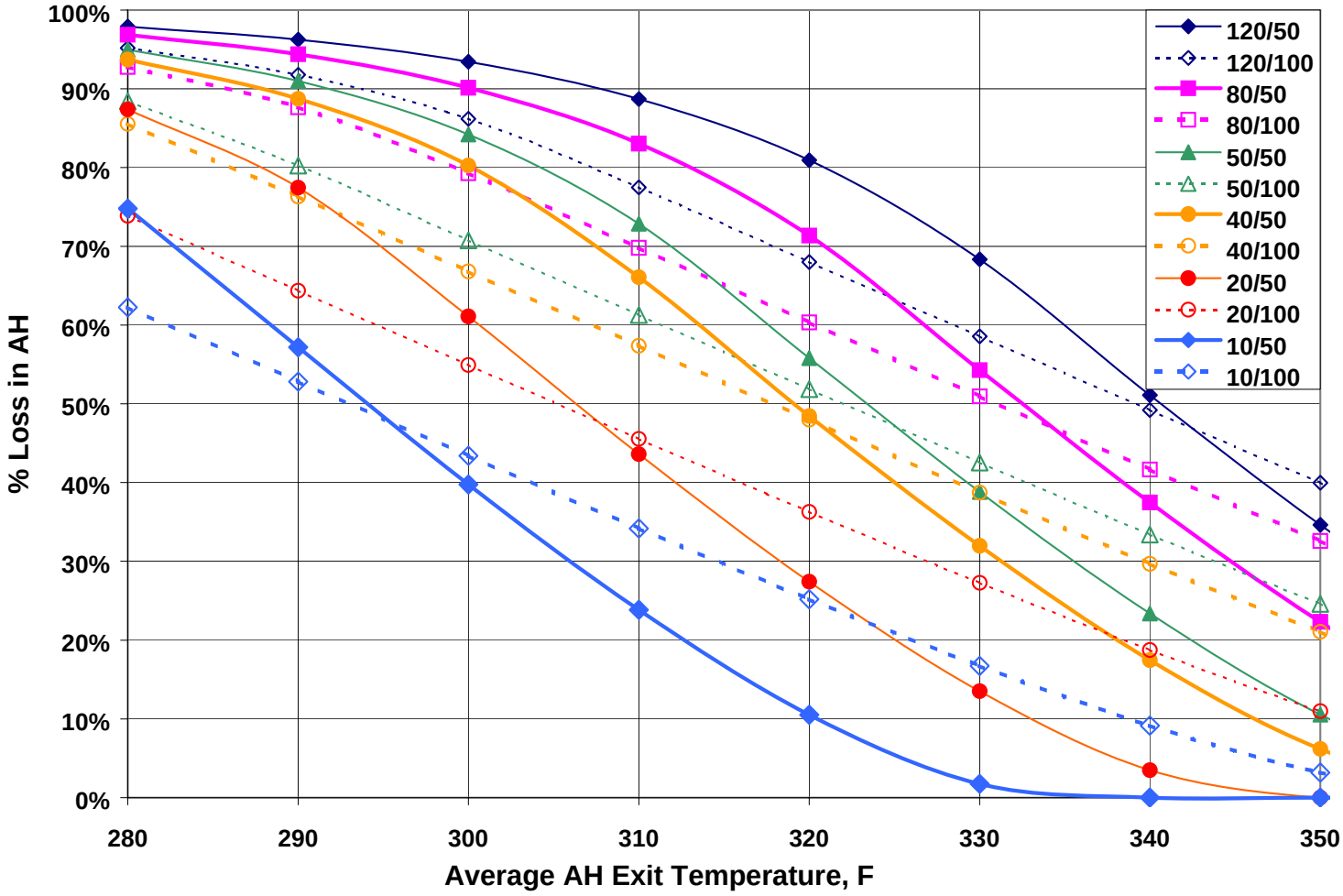

Figure 6.1. Estimated SO_3/H_2SO_4 losses across combustion air preheaters versus average air preheater exit temperature for a temperature offset of 35 °F. The first value of each pair in the legend is the preheater inlet SO_3/H_2SO_4 concentration in ppm and the second value of the pair is the spread in exit gas temperature between the cold side and the hot side of the preheater exit.

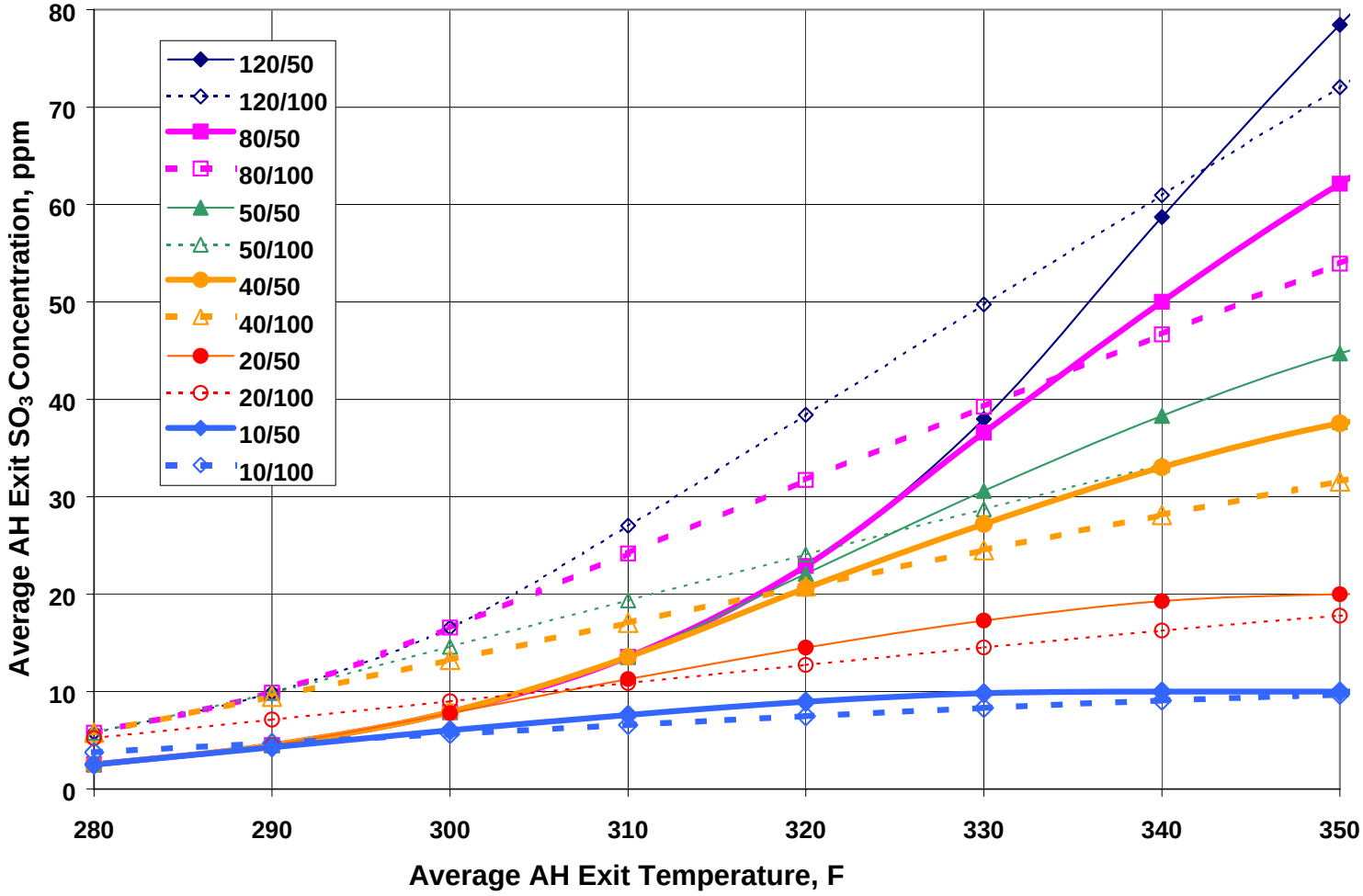

Figure 6.2. Estimated air preheater exit SO_3/H_2SO_4 concentration versus average air preheater exit temperature for a temperature offset of 35 °F. The first value of each pair in the legend is the preheater inlet SO_3/H_2SO_4 concentration in ppm and the second value of the pair is the spread in exit gas temperature between the cold side and the hot side of the preheater exit.

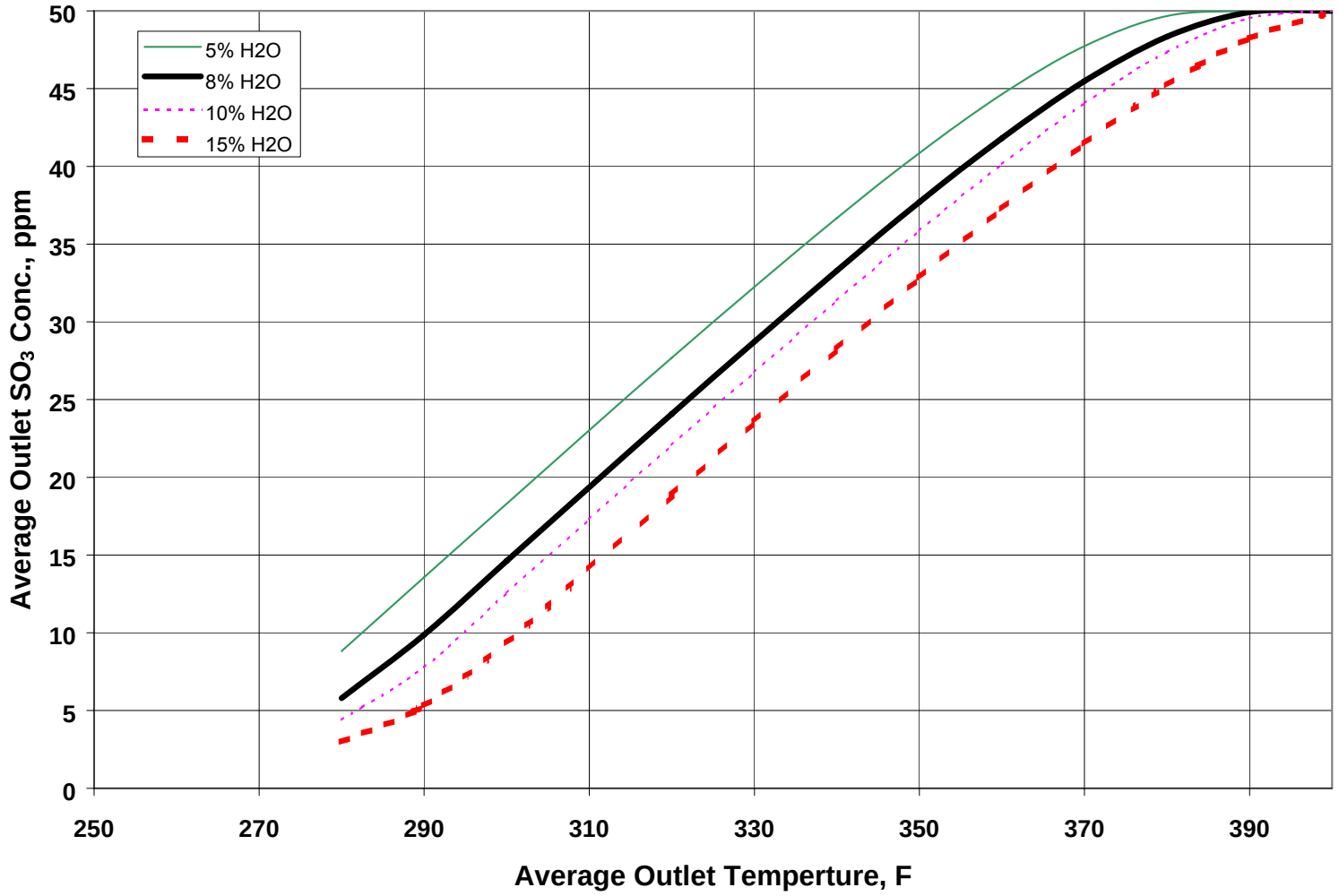

Figure 6.3. Effect of flue gas moisture content on the estimated air preheater exit SO_3/H_2SO_4 concentration for a temperature offset of 35 °F. Values shown are calculated for an inlet concentration of 50 ppm with an air preheater exit temperature spread of 100 °F.

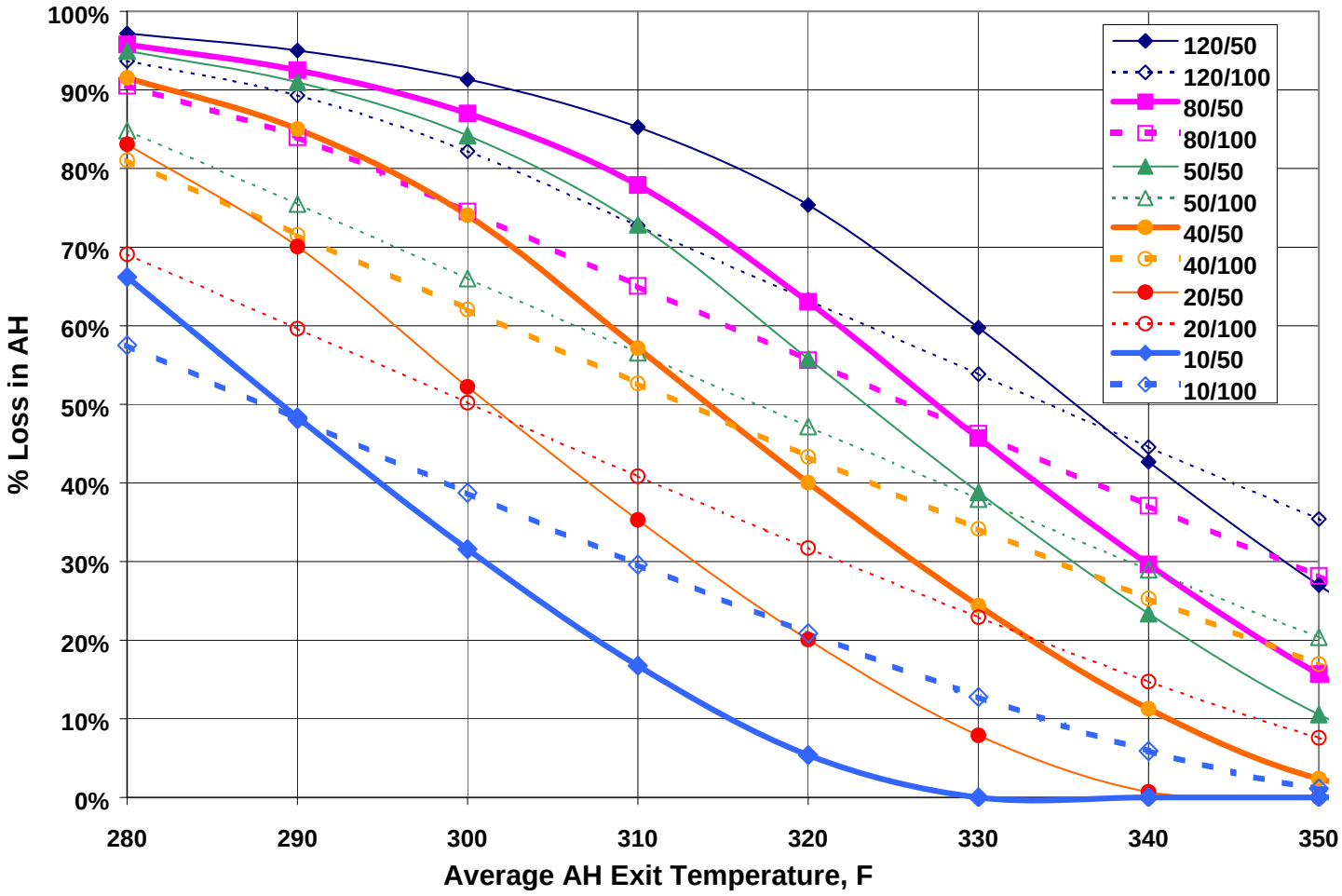

Figure 6.4. Estimated SO_3/H_2SO_4 losses across combustion air preheaters versus average air preheater exit temperature for a temperature offset of 30 °F. The first value of each pair in the legend is the preheater inlet SO_3/H_2SO_4 concentration in ppm and the second value of the pair is the spread in exit gas temperature between the cold side and the hot side of the preheater exit.

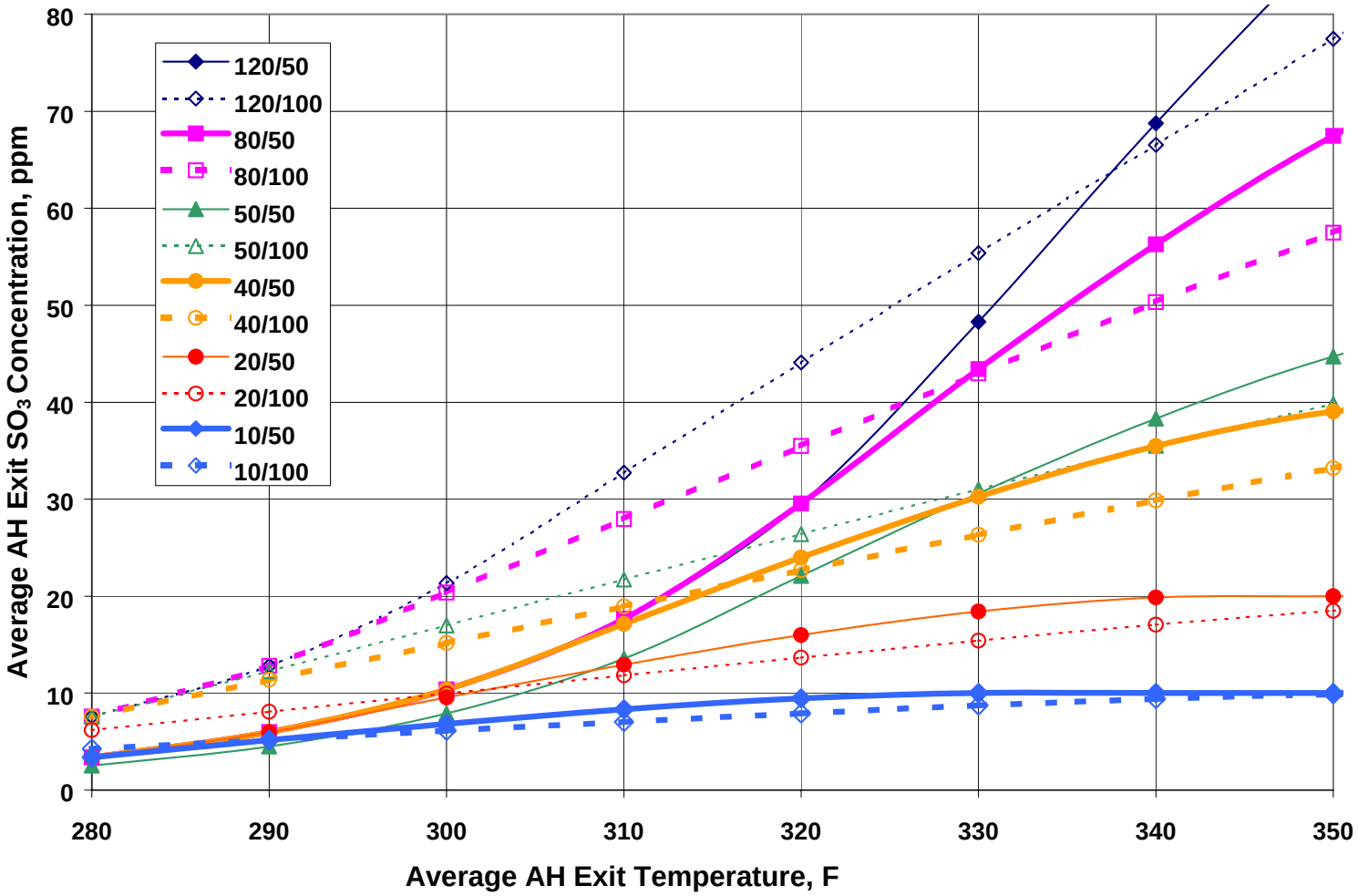

Figure 6.5. Estimated air preheater exit SO_3/H_2SO_4 concentration versus average air preheater exit temperature for a temperature offset of 30 °F. The first value of each pair in the legend is the preheater inlet SO_3/H_2SO_4 concentration in ppm and the second value of the pair is the spread in exit gas temperature between the cold side and the hot side of the preheater exit.

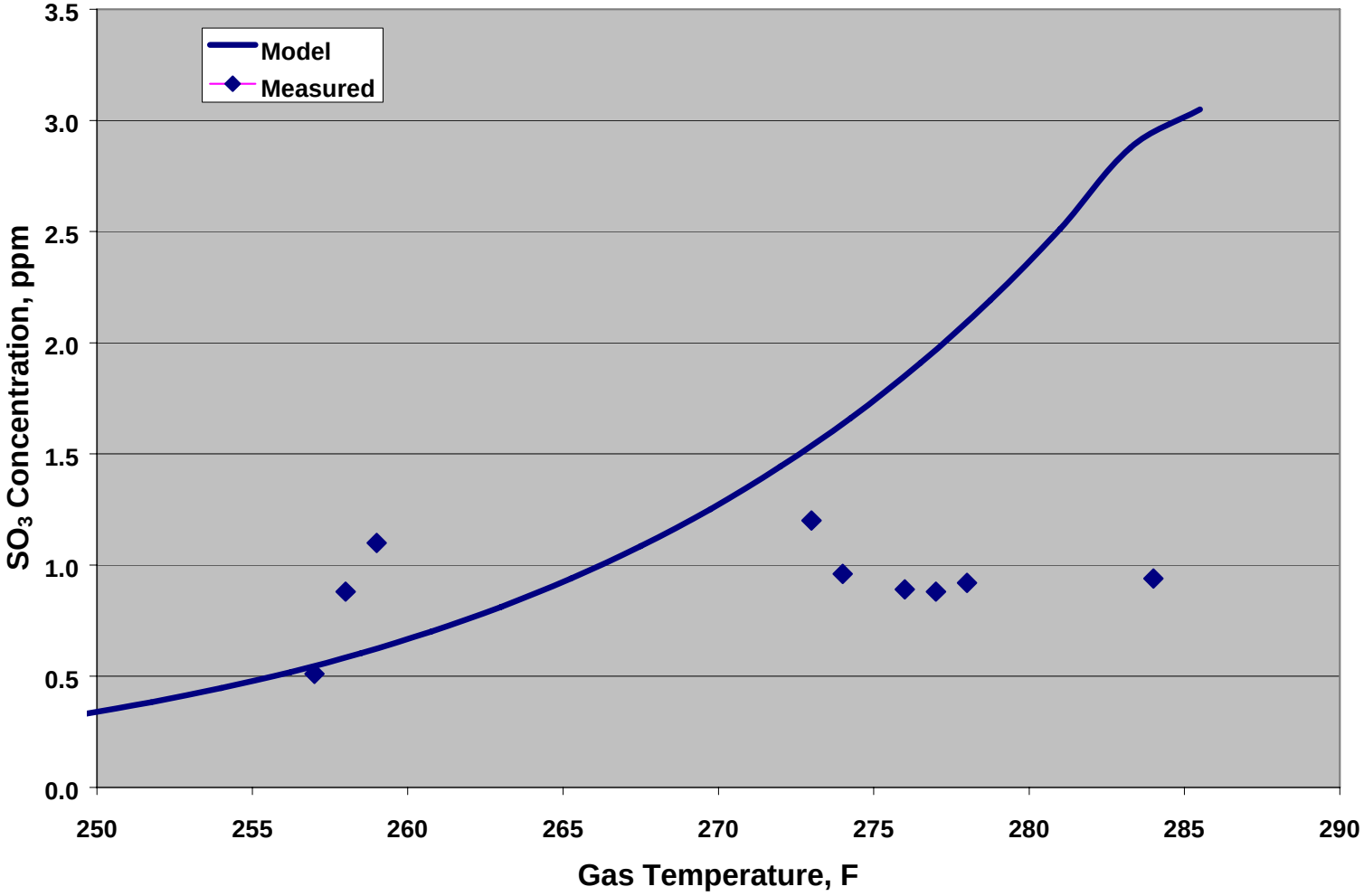

Figure 6.6. Comparison of predicted and measured SO_3 concentrations at the exit of rotary air heater No. 1 for a temperature offset of 30 °F. The measured inlet concentration was 3.1 ppm. The measured average was 0.9 ppm while the predicted average was 1.7 ppm.

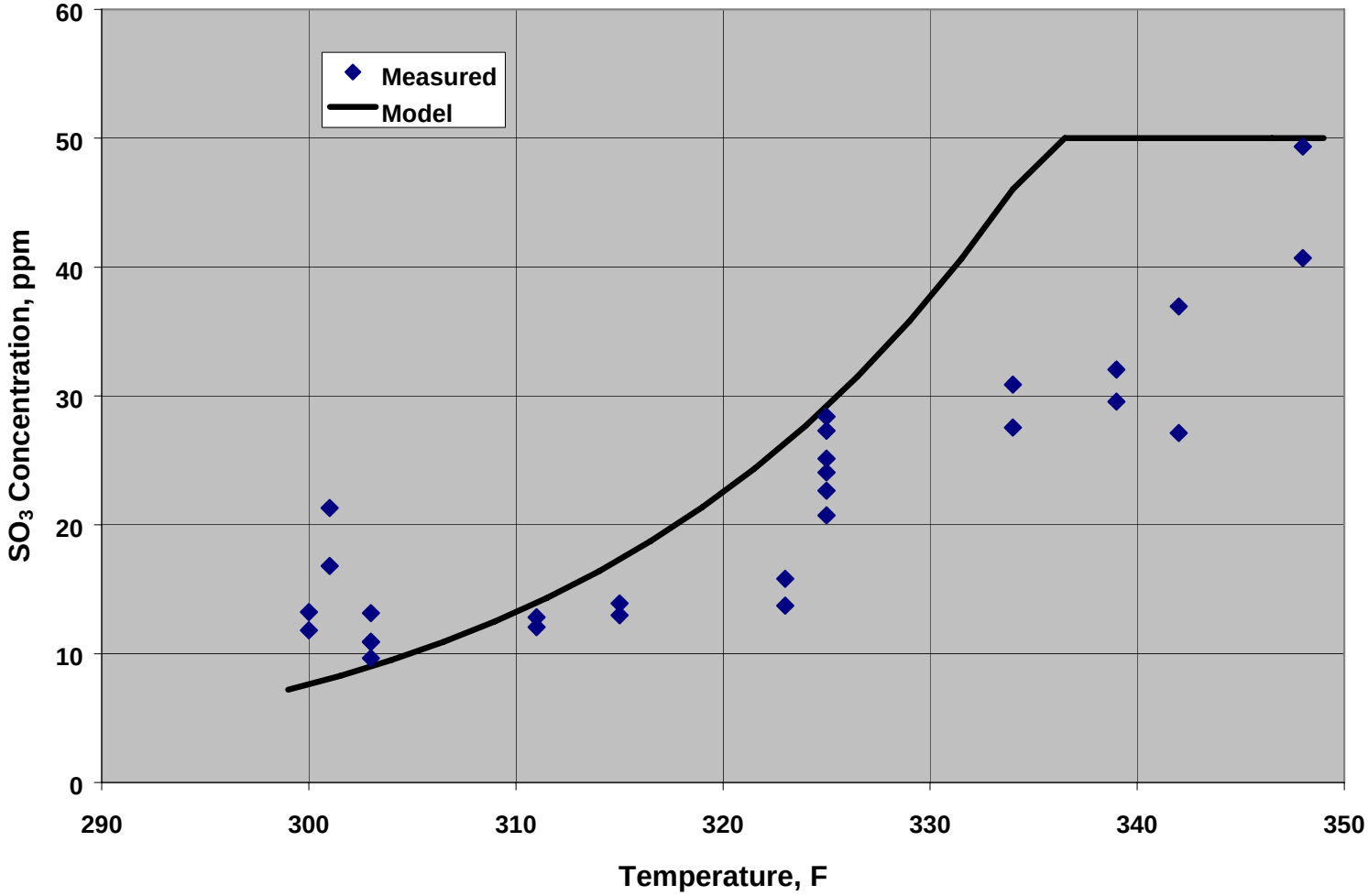

Figure 6.7. Comparison of predicted and measured SO_3 concentrations at the exit of rotary air heater No. 2 for a temperature offset of 30 °F. The inlet concentration was 50 ppm. The measured average was 23 ppm while the predicted average was 30 ppm.

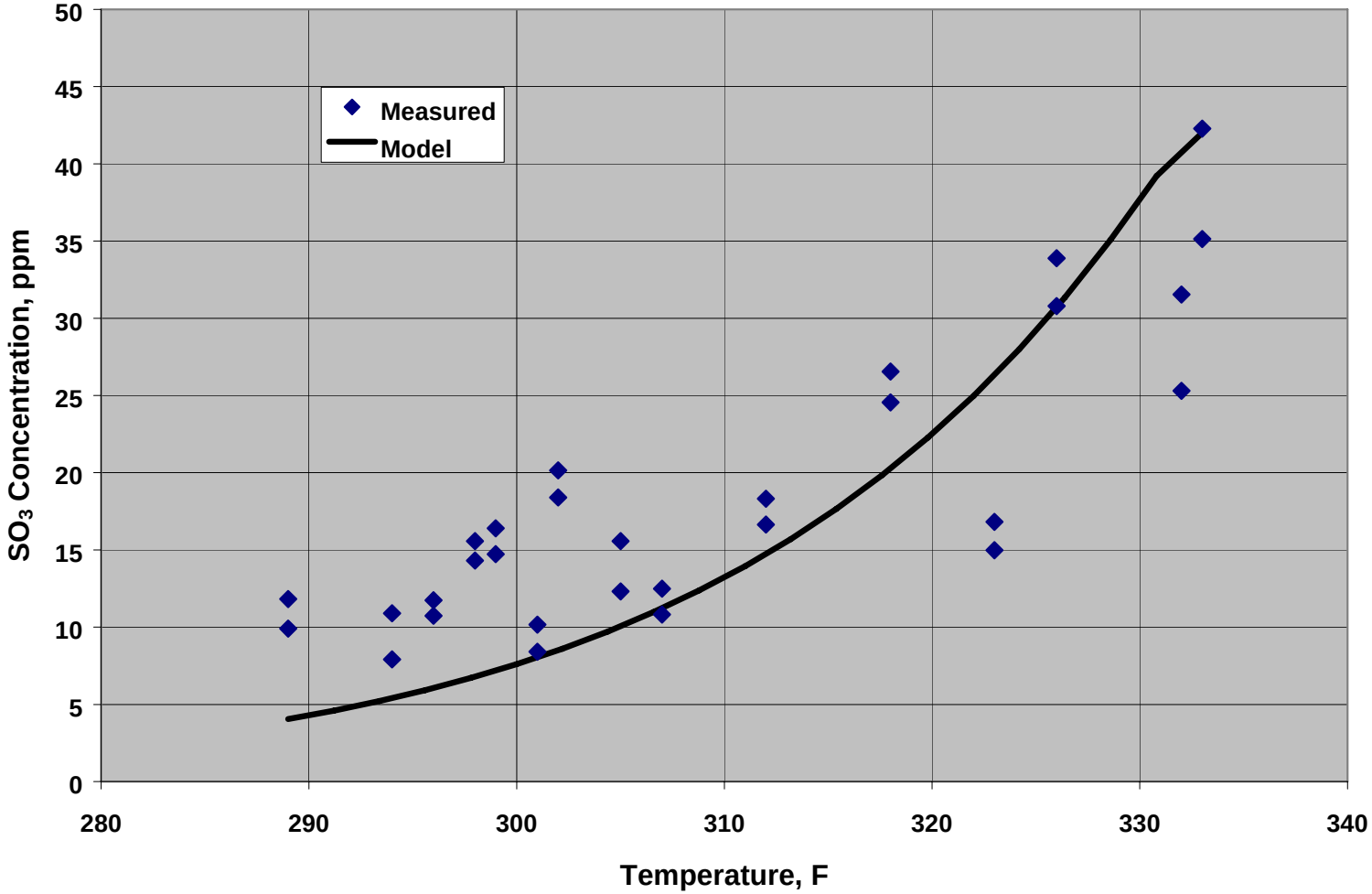

Figure 6.8. Comparison of predicted and measured SO_3 concentrations at the exit of rotary air heater No. 3 for a temperature offset of 33 °F. The inlet concentration was 42 ppm. The measured average was 18 ppm while the predicted average was 17 ppm.

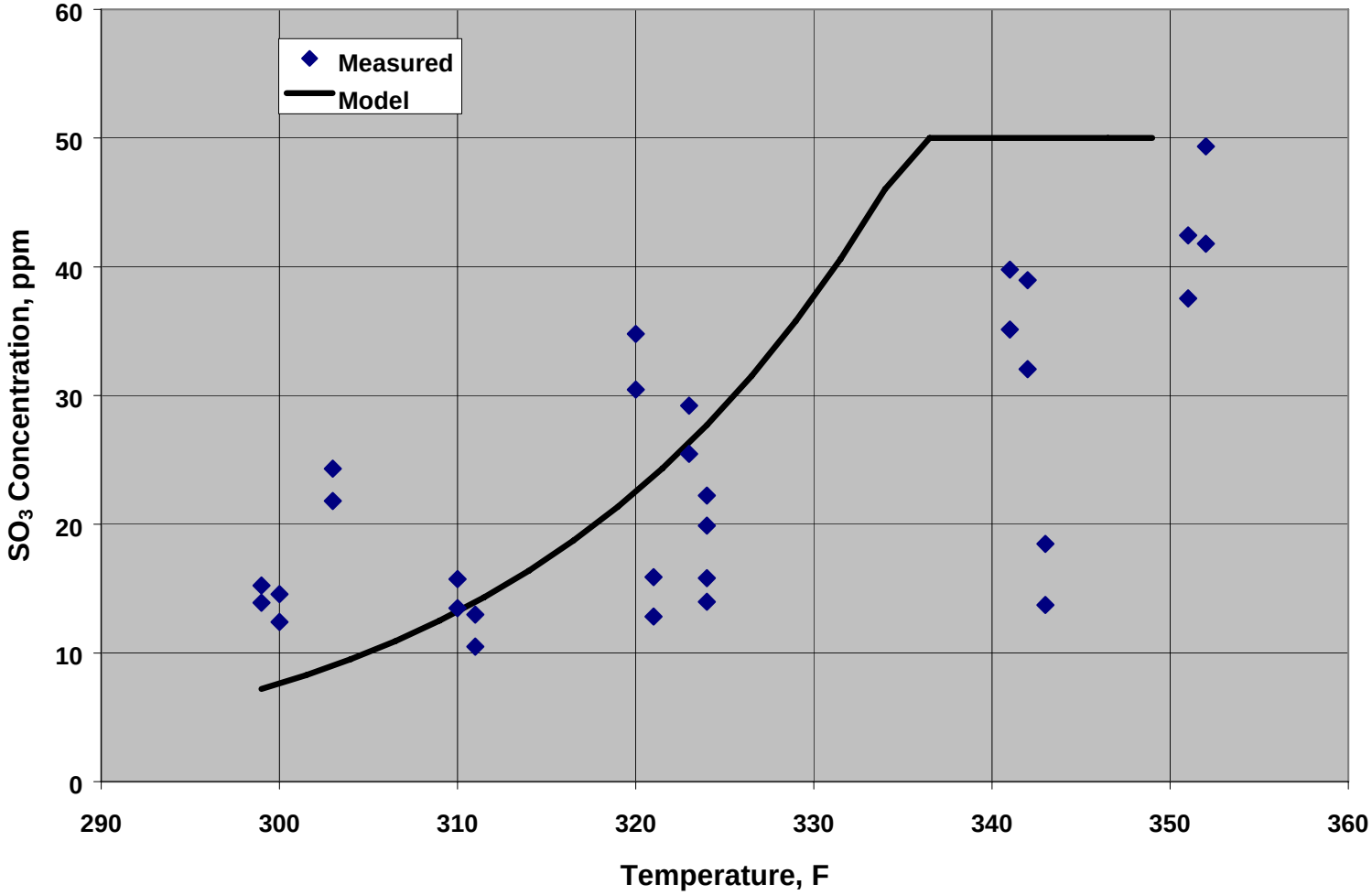

Figure 6.9. Comparison of predicted and measured SO_3 concentrations at the exit of rotary air heater No. 4 for a temperature offset of 30 °F. The inlet concentration was 50 ppm. The measured average was 24 ppm while the predicted average was 30 ppm.

7. EVOLUTION OF ACID MIST IN WET FLUE GAS DESULFURIZATION UNITS AND STACKS

In the initial EPA report on work conducted by SRI on SO_3 emissions, Farthing and coworkers assessed the effects of various pollution control technologies on sulfuric acid emissions and stack plume opacity.[2] Among the types of equipment and processes evaluated were ESPs, SCR, and wet FGD. Marked differences were noted in the behavior of buoyant, higher velocity plumes formed by hot stack gas in the absence of wet FGD and plumes formed by denser cold gas leaving a stack downstream from wet FGD equipment.

In the evaluation of anticipated acid emissions and light scattering coefficients of plumes, it was found that very few data are available on the behavior of acid mist in wet FGD. A calculation was presented by Farthing et al. showing the expected growth of acid droplets by coagulation following nucleation and condensation of the acid on cooling at the entrance to a scrubber.[2] The calculation assumed a fixed acid composition, neglecting the possibility for growth of the acid droplets by absorption of water vapor from the high humidity flue gas in the scrubber and stack.

To improve upon the accuracy of calculated acid mist properties, a more detailed analysis of acid mist evolution during wet FGD was conducted, considering coagulation of the acid droplets with each other, absorption of water vapor by the droplets, and coagulation of the acid droplets with spray droplets in the scrubber and with droplets carried over from the scrubber to the stack.[50] The principal findings of that work are summarized below.

Under the assumptions and conditions investigated, the principal role of a wet SO_2 scrubber, from the point of view of sulfuric acid mist, is to provide conditions for nucleation of acid droplets and a long residence time for their growth by coagulation and absorption of water vapor. Downstream from a wet FGD unit, the principal role of the stack, again from the point of view of sulfuric acid, is to provide additional residence time for growth of the acid mist by coagulation. Under all of the conditions examined, the mean size of acid droplets at the stack exit was predicted to have grown, through the combined effects of coagulation and absorption of water vapor, to sizes within the range able to scatter visible light.

According to the calculations and within the ranges of the parameters investigated, the only factor having significant influence on the volume fraction of acid mist leaving the stack was the original H_2SO_4 content of the flue gas. When the initial H_2SO_4 concentration was increased, the ultimate acid droplet volume fraction increased more rapidly than the H_2SO_4 concentration itself. Doubling the H_2SO_4 at the scrubber inlet from 10 to 20 ppmv increased the acid droplet volume fraction at the stack exit by a factor of 2.5, from 5.6 to 14 ppmv. The increased absorption of water vapor in the presence of higher acid concentration was due to the decrease in vapor pressure at the surfaces of the larger droplets that were formed, due to the Kelvin effect. The decrease in vapor pressure increased the rate of absorption of water vapor by the acid droplets.

In spite of the fact that the mechanism for the increase in volume fraction of acid mist in the scrubber is vaporization of water from scrubber droplets and absorption of the vapor by the acid, variation of the size of scrubber spray droplets over the range from 0.7 to 2 mm had hardly any influence on the properties of the acid. Transfer of water from the scrubber droplets to acid droplets appears to be regulated more by the dependence of the vapor pressure of the acid droplets on their H_2SO_4 content than on the specific surface area, mass transfer coefficient, or concentration of the scrubber spray.

The principal effect of decreasing the scrubber spray droplet size was to increase capture of acid by spray droplets in the scrubber, although the fractions of acid captured were not large enough to have significant influence on acid mist droplet size and volume fraction. The fraction of the original H_2SO_4 retained in the scrubber increased from 0.33% to 7.6% on decreasing the spray droplet size from 2 to 0.7 mm, due to increased mass transfer to the smaller droplets and to the increase in spray droplet concentration as the terminal velocity of the spray droplets approached the gas velocity. Spray droplets smaller than 0.7 mm were outside the range over which the model is applicable, because closer approach of the droplet terminal velocity to the gas velocity led to unrealistically high droplet concentrations characteristic of the "fluidized" regime.[51] It was noted that most of the acid capture was predicted to occur at very early times, when the acid nuclei are still small, so the calculated capture may be influenced by the assumption that acid nucleates immediately to form $H_2SO_4 \cdot H_2O$ on entering the scrubber.

According to the model, the source of water vapor that could be absorbed by acid mist in the stack is scrubber droplets carried over from the mist eliminator, not the water vapor present in the flue gas leaving the scrubber. This is because the acid at this stage is dilute (~ 1 wt% H_2SO_4), so the vapor pressure of water adjacent to acid mist droplets is not far from the vapor pressure over pure water. A continuous supply of water vapor is therefore needed if there is to be any significant uptake of water by the acid. Under the conditions investigated, an increase of 10 to 15% in acid mist volume fraction by absorption of water vapor in the stack was typical. Cooling of the stack gas, not taken into consideration in the calculation, is a possible mechanism by which water vapor could be maintained close to saturation in the presence of its absorption by acid mist. According to the model and calculations, the most important process occurring in the stack is the increase in droplet size due to coagulation. The acid droplet size was estimated to increase by 50% during 15 seconds of residence time in the stack.

The model exhibits some unexpected and counter-intuitive behavior, such as (1) a decrease in H_2SO_4 concentration in acid droplets at the stack exit on increasing the H_2SO_4 content of the flue gas, (2) insensitivity of acid volume fraction to scrubber spray droplet size, and (3) a decrease (though it is slight) in acid mist volume fraction on increasing the size of scrubber droplets passing the mist eliminator. The potential of such calculations to assist in the interpretation of observations of sulfuric acid behavior in the field would appear to justify further development of the model. To make the model a more powerful and useful simulation tool, the following refinements were proposed:

- Evaluate the effects of scrubber and stack temperature.

- Compare the results of the calculations with measurements of acid concentrations at the entrance and exit from wet FGD units.
- Using the scattering efficiency for visible light versus particle size, determine relative opacities for the acid mist at the stack exit for comparison of the effects of scrubber and stack conditions on plume visibility.
- Incorporate a droplet size distribution for the scrubber spray.
- Locate experimental data to improve confidence in the assignment of the value for the size of scrubber droplets passing the mist eliminator.
- Examine and refine, if necessary, the description of nucleation to provide a better model for droplet growth at short times and improve the simulation of capture of acid mist in the scrubber.
- Allow for cooling of flue gas as a driver for transfer of water vapor to acid mist in the stack.

Background

In a recent EPA report, Farthing et al. assessed the effects of various pollution control technologies on sulfuric acid emissions and stack plume opacity.[2] Among the types of equipment and processes evaluated were electrostatic precipitators (ESP), selective catalytic reduction (SCR), and wet flue gas desulfurization (FGD). Marked differences were noted in the behavior of buoyant, higher velocity plumes formed by hot stack gas in the absence of wet FGD and plumes formed by denser cold gas leaving a stack downstream from wet FGD equipment.

In the evaluation of anticipated acid emissions and light scattering coefficients of plumes, it was found that very few data are available on the behavior of acid mist in wet FGD. A calculation was presented by Farthing and coworkers, showing the expected growth of acid droplets by coagulation following nucleation and condensation of the acid on cooling at the entrance to a scrubber.[2] The calculation assumed a fixed acid composition, neglecting the possibility for growth of the acid droplets by absorption of water vapor from the high humidity flue gas in the scrubber and stack.

The present report describes calculations of acid mist evolution during wet FGD, considering coagulation of the acid droplets with each other, absorption of water vapor by the droplets, and coagulation of the acid droplets with spray droplets in the scrubber and with droplets carried over from the scrubber in the stack.

The type of SO_2 scrubber under consideration is a counterflow design, in which flue gas travels upward and scrubber spray droplets travel downward through the gas. The general outline of the model for the evolution of acid droplets in the scrubber and stack is as follows. Flue gas is cooled immediately to 333 K (140 ^{o}F) on entering the scrubber, causing nucleation of sulfuric acid. The acid nuclei travel upward through the scrubber at the average gas velocity, growing by coagulation with each other and by absorption of water vapor from the flue gas. Some acid droplets are removed from the flow by coagulation with scrubber spray droplets. The acid and scrubber spray droplets are

characterized using single, volume mean sizes. Temperature, gas velocity, and droplet velocity are considered to be uniform throughout the scrubber and stack.

At the outlet from the scrubber, the mist eliminator is assumed to remove all but 5 ppmv of the scrubber liquid flow. The droplets carried over are assumed to have a mean size of 10 μm under the conditions considered as the base case. Absorption of water vapor by acid mist droplets, coagulation of acid droplets with themselves, and coagulation of acid droplets with the remaining scrubber droplets continue in the stack.

In order to perform the calculations, we require the density and surface energy of sulfuric acid and the vapor pressure of water over sulfuric acid as functions of acid composition. The correlations for these properties, derived from data in the literature, are given in Appendix A.

Immediately after their nucleation, acid droplets grow very quickly by coagulation and condensation. Because growth at early times is so rapid, an exact calculation of the initial size of the acid nuclei was not thought to be necessary. A useful approximation is to take the initial size of the nuclei to be the diameter of single molecules of $H_2SO_4 \cdot H_2O$. This size was estimated by taking the diameter of a sphere having the volume occupied by the molecule, determined from the density of 84.5 wt % sulfuric acid, given by the correlation in Figure A1. Under this approximation, the initial number density of acid nuclei is simply the number concentration of sulfuric acid molecules in the flue gas. The initial diameter and values for the other constants used in the calculations are given in Table 7.1.

Development of Mist Behavior Equations

Coagulation of Acid Mist Droplets

The coagulation of acid droplets is described approximately by the rate expression for the decrease in number concentration of a monodisperse aerosol (Friedlander, p. 193):[52]

$$\frac{dN_{ad}}{dt} = -\frac{1}{2} k_{ad} N_{ad}^2 \tag{7.1}$$

where N_{ad} is the number concentration of acid mist droplets and k_{ad} is the rate coefficient for their coagulation. The rate coefficient is given, for uniform-size droplets, by (Seinfeld, p. 395;[53] Friedlander, p. 192[52]):

$$k_{ad} = 8 \pi d_{ad} D_{ad} \beta \tag{7.2}$$

in which d_{ad} is the diameter of the acid mist droplets and D_{ad} is their diffusion coefficient. The factor, β, in Eq. (7.3) describes the transition of droplet diffusion behavior from the continuum, through the transition, to the free molecule regime (Seinfeld, p. 395):[53]

$$\beta = \frac{1 + Kn_{ad,ad}}{1 + 2Kn_{ad,ad}(1 + Kn_{ad,ad})} \tag{7.3}$$

where $Kn_{ad,ad}$ is the Knudsen number for diffusion of acid droplets toward each other, equal to the ratio of the mean free path of the droplets, λ_{ad}, to the droplet radius, $d_{ad}/2$ (Seinfeld, p. 395):[53]

$$Kn_{ad,ad} = \frac{2\lambda_{ad}}{d_{ad}} \tag{7.4}$$

The mean free path of acid mist droplets in flue gas was evaluated using the form of the relationship between the mean speed of particles, their diffusion coefficient, and their mean free path required for consistency with the correction factor specified in Eq. (7.3), [Seinfeld (pp. 326, 335-338, 395)]:[53]

$$D_{ad} = \frac{1}{\sqrt{2}} c_{ad} \lambda_{ad} \tag{7.5}$$

in which c_{ad} is the mean speed of the droplets:

$$c_{ad} = \left(\frac{8k_B T}{\pi m_{ad}} \right)^{1/2} \tag{7.6}$$

The derivation by Seinfeld[53] (pp. 395-398) is for different-sized particles, for which the mean velocity is defined as $c_{12} = (c_1^2 + c_2^2)^{1/2}$. This introduces a factor of $\sqrt{2}$ in Eq. (7.5), when the particles are identical, and changes the equation from its more familiar form, $D = ½\, c\lambda$. The Knudsen number is then (Seinfeld, p. 395):[53]

$$Kn_{ad,ad} = \frac{2\sqrt{2} D_{ad}}{c_{ad} d_{ad}} \tag{7.7}$$

The diffusion coefficient for the droplets is given by the Stokes-Einstein relation with Cunningham correction (Seinfeld, p. 324):[53]

$$D_{ad} = \frac{k_B T C_c}{3\pi \mu_{fg} d_{ad}} \tag{7.8}$$

and the Cunningham correction factor, C_c, is (Seinfeld, p. 317) :[53]

$$C_c = 1 + \{Kn_{fg,ad} [1.257 + (0.4\, e^{-1.1/Kn_{fg,ad}})]\} \tag{7.9}$$

where $Kn_{fg,ad}$ is the Knudsen number for acid droplets in flue gas, the ratio of the mean free path of the average flue gas molecule to the droplet radius (Seinfeld, p. 326):[53]

$$Kn_{fg,ad} = \frac{2\lambda_{fg}}{d_{ad}} \tag{7.10}$$

The mean free path is determined from its relationship to the molecular speed and diffusion coefficient:

$$D_{w,fg} = \frac{1}{2} c_{fg} \lambda_{fg} \tag{7.11}$$

The molecular diffusion coefficient, $D_{w,fg}$ is estimated by treating the flue gas as a binary mixture of water vapor with the other combustion products. The mean speed of flue gas molecules is:

$$c_{fg} = \left(\frac{8RT}{\pi W_{fg}} \right)^{1/2} \tag{7.12}$$

and the Knudsen number is then:

$$Kn_{fg,ad} = \frac{4D_{w,fg}}{c_{fg} d_{ad}} \tag{7.13}$$

Absorption of Water Vapor from Flue Gas by Acid Mist Droplets

All the while that they are coagulating, the acid mist droplets may also absorb water vapor from the flue gas. Simultaneous evaporation of water from scrubber liquor droplets maintains the flue gas at high relative humidity. The process can be represented as follows:

$$H_2O(\text{scrubber spray droplets}) = H_2O(\text{vapor}) \tag{R 7.1}$$

$$H_2O(\text{vapor}) = H_2O(\text{acid mist droplets}). \tag{R 7.2}$$

The rate of change in concentration of scrubber liquor droplets, C_{sd} (kg/m^3 gas), due to evaporation of water from the droplets, is given by the expression describing diffusion of water vapor from the surface of a droplet, through the concentration boundary layer surrounding the droplet, and into the free stream:

$$\frac{dC_{sd}}{dt} = -\frac{Sh_{sd} D_{w,fg}}{d_{sd}} S_{sd} C_{sd} (C_{w,sd} - C_{w,\infty}) \tag{7.14}$$

in which Sh_{sd} is the Sherwood number for mass transfer between scrubber droplets and flue gas; $D_{w,fg}$ is the molecular diffusion coefficient in a pseudo-binary mixture of water vapor and flue gas, d_{sd} is the mean scrubber liquor droplet size; S_{sd} is the specific external surface area (m^2/kg) of scrubber liquor droplets; and $C_{w,sd}$ and $C_{w,\infty}$ are the concentrations

(kg/m^3 gas) of water vapor at the surface of scrubber liquor droplets and in the free stream, respectively. The Sherwood number was determined using the correlation of Frössling[54] and Ranz and Marshall[55] (please see the Nomenclature Section for definitions of symbols not mentioned here in the text):

$$Sh_{sd} = 2 + 0.6\, Re^{1/2}\, Sc^{1/3} \tag{7.15}$$

The rate of change in acid mist droplet concentration, C_{ad} (kg/m^3 gas), due to absorption of water vapor, is similarly described by the rate of diffusion of water vapor from the free stream, through the concentration boundary layer surrounding an acid mist droplet, to the surface of the droplet:

$$\frac{dC_{ad}}{dt} = \frac{Sh_{w,ad} D_{w,fg}}{d_{ad}} S_{ad} C_{ad} (C_{w,\infty} - C_{w,ad}). \tag{7.16}$$

where the symbols have definitions analogous to those in Eq. (7.14), but now refer to properties of the acid mist rather than scrubber spray droplets. During evolution of the acid mist, its droplets grow from the free molecule, through the transition, to the continuum regime. To account for mass transfer at all three stages, the Sherwood number was based on the interpolation relation of Dahneke,[56] given by Seinfeld (pp. 335-336):[53]

$$Sh_{w,ad} = 2\frac{1 + Kn_{w,ad}}{1 + 2Kn_{w,ad}(1 + Kn_{w,ad})} \tag{7.17}$$

in which $Kn_{w,ad}$ is the Knudsen number for water vapor molecules diffusing to acid mist droplets in flue gas, the ratio of the mean free path of H_2O to the droplet radius:

$$Kn_{w,ad} = \frac{2\lambda_w}{d_{ad}} \tag{7.18}$$

The mean free path of water vapor molecules in flue gas was evaluated using the same general relationship between mean speed, diffusion coefficient, and mean free path as before (Seinfeld, p. 338):[53]

$$D_{w,fg} = \frac{1}{2} c_w \lambda_w \tag{7.19}$$

in which c_{H_2O} is the mean speed of water vapor molecules:

$$c_w = \left(\frac{8RT}{\pi W_w} \right)^{1/2} \tag{7.20}$$

The Knudsen number is then:

$$Kn_{w,ad} = \frac{4D_{w,fg}}{c_w d_{ad}} \tag{7.21}$$

Assuming the system is close to its steady state throughout the scrubber, we can equate the net rate of change in water vapor concentration, represented by the sum of Eqs. (7.14) and (7.16), to zero and solve for the pseudo-steady concentration of water vapor in the free stream, $C_{w,\infty}$:

$$C_{w,\infty} = C_{w,sd} \frac{1 + \dfrac{\dfrac{Sh_{w,ad}}{d_{ad}} S_{ad} C_{ad} C_{w,ad}}{\dfrac{Sh_{sd}}{d_{sd}} S_{sd} C_{sd} C_{w,sd}}}{1 + \dfrac{\dfrac{Sh_{w,ad}}{d_{ad}} S_{ad} C_{ad}}{\dfrac{Sh_{sd}}{d_{sd}} S_{sd} C_{sd}}} \tag{7.22}$$

This expression is substituted for the free stream water vapor concentration in Eq. (7.16), which then becomes:

$$\frac{dC_{ad}}{dt} = \frac{C_{w,sd} - C_{w,ad}}{\dfrac{1}{\dfrac{Sh_{w,ad} D_{w,fg}}{d_{ad}} S_{ad} C_{ad}} + \dfrac{1}{\dfrac{Sh_{sd} D_{w,fg}}{d_{sd}} S_{sd} C_{sd}}} \tag{7.23}$$

Replacing the effective overall rate coefficient in Eq. (7.23) by the symbol, k_{sa}, and changing from concentrations to partial pressures of water vapor, we have:

$$\frac{dC_{ad}}{dt} = k_{sa}(P_{w,sd} - P_{w,ad}) \frac{W_w}{RT} \tag{7.24}$$

Because the curvature of the surface of the small acid droplets is so high, especially at early times, the equilibrium pressure of water vapor at the surfaces of the droplets is significantly higher than that over a flat liquid surface. The effect of curvature on the vapor pressure was evaluated using the relation presented by Equation 7 in Yue:[57]

$$P_{w,ad} = P_{w,af} \; exp\left\{ \frac{4\sigma_a W_w}{d_{ad} \rho_a RT} \left[1 + \frac{Y_a}{\rho_a} \frac{d\rho_a}{dY_a} - \frac{3}{2} \frac{Y_a}{\sigma_a} \frac{d\sigma_a}{dY_a} \right] \right\} \tag{7.25}$$

The density, ρ_a, and surface energy, σ_a, of sulfuric acid, and the equilibrium vapor pressure of water over a flat sulfuric acid surface, $P_{w,af}$, are given by the correlations in Figures A1, A2, and A3, respectively, of Appendix A. The derivatives of the density and surface energy with respect to composition were also evaluated using their respective

correlations. The vapor pressure of H_2SO_4 over aqueous sulfuric acid is negligible at the temperatures of interest here.

Coagulation of Acid Mist Droplets with Scrubber Liquor Droplets

The last process to be considered is the coagulation of acid droplets with the much larger scrubber spray droplets, treated as a diffusion process analogous to the vapor transport processes discussed above:

$$\frac{dC_{ad}}{dt} = -\frac{Sh_{sd} D_{ad}}{d_{sd}} S_{sd} C_{sd} C_{ad} \tag{7.26}$$

Coagulation of acid droplets with scrubber droplets changes the number density of the acid mist, as well as its mass concentration. The number density can be estimated by dividing the mass concentration by the average droplet mass, $N_{ad} = C_{ad}/m_{ad}$, therefore, from Eq. (7.26) we have, approximately, for uniform-size acid mist droplets:

$$\frac{dN_{ad}}{dt} = -\frac{Sh_{sd} D_{ad}}{d_{sd}} S_{sd} C_{sd} N_{ad} \tag{7.27}$$

in which the Sherwood number for the scrubber liquor droplets, Sh_{sd}, is given by Eq. (7.15) and the diffusion coefficient for the acid mist droplets, D_{ad}, by Eq. (7.8).

Calculation Procedure

The mass concentration of acid mist is increased due to absorption of water vapor by the droplets, but decreased due to loss of acid mist droplets to scrubber liquor. Adding the contributions from these two processes, according to Eqs. (7.24) and (7.26):

$$\frac{dC_{ad}}{dt} = k_{sa}(P_{w,sd} - P_{w,ad})\frac{W_w}{RT} - \frac{Sh_{sd} D_{ad}}{d_{sd}} S_{sd} C_{sd} C_{ad} \tag{7.28}$$

This equation was integrated approximately over small increments of time, Δt, as follows:

$$C_{ad}(t+\Delta t) = C_{ad}(t) + \left\{ k_{sa}(t)\left[P_{w,sd} - P_{w,ad}(t)\right]\frac{W_w}{RT} - \frac{Sh_{sd} D_{ad}(t)}{d_{sd}} S_{sd} C_{sd} C_{ad}(t) \right\} \Delta t \tag{7.29a}$$

$$C_{ad} = C_{ad0} \quad \text{at} \quad t = 0 \tag{7.29b}$$

Coagulation of acid droplets with themselves does not change their mass concentration.

The number density of acid droplets, on the other hand, is decreased both by coagulation of the droplets with themselves and by their coagulation with scrubber spray droplets. Adding the contributions from these two processes, according to Eqs. (7.1) and (7.27):

$$\frac{dN_{ad}}{dt} = -\frac{1}{2}k_{ad}N_{ad}^2 - \frac{Sh_{sd}D_{ad}}{d_{sd}}S_{sd}C_{sd}N_{ad} \tag{7.30}$$

This equation was integrated approximately over small increments of time, Δt, as follows:

$$N_{ad}(t+\Delta t) = N_{ad}(t) - \left[\frac{1}{2}k_{ad}(t)N_{ad}^2(t) + \frac{Sh_{sd}D_{ad}(t)}{d_{sd}}S_{sd}C_{sd}N_{ad}(t)\right]\Delta t \tag{7.31a}$$

$$N_{ad} = N_{ad0} \text{ at } t = 0 \tag{7.31b}$$

Following the addition of an increment in time and calculation of new mass and number concentrations using Eqs. (7.29a) and (7.31a), the new average acid droplet mass is found from:

$$m_{ad}(t) = \frac{C_{ad}(t)}{N_{ad}(t)} \tag{7.32}$$

The cumulative fraction of the original acid captured by scrubber spray droplets is found from:

$$f_{cap}(t+\Delta t) = f_{cap}(t) + \frac{Sh_{sd}D_{ad}(t)}{d_{sd}}S_{sd}C_{sd}C_{ad}(t)\frac{Y_a(t)}{C_{H_2SO_4}}\Delta t \tag{7.33a}$$

$$f_{cap} = 0 \text{ at } t = 0 \tag{7.33b}$$

The new acid composition, resulting from its dilution by absorption of water vapor, is given by:

$$Y_a(t) = [1 - f_{cap}(t)]\frac{C_{H_2SO_4}}{C_{ad}(t)} \tag{7.34a}$$

$$Y_a = 0.845 \text{ at } t = 0 \tag{7.34b}$$

where $Y_a = 0.845$ is the mass fraction of H_2SO_4 in the first acid nuclei formed, assumed to have composition, $H_2SO_4 \cdot H_2O$.

Evolution of Acid Mist in the Stack

The same processes of acid mist coagulation, absorption of water by acid droplets, evaporation of water from scrubber droplets, and coagulation of acid mist with scrubber droplets continue in the stack, downstream from the wet scrubber and mist eliminator. However, the characteristics of the system are changed in the following ways: (1) there are marked decreases in scrubber droplet mass concentration and droplet size across the mist eliminator, and (2) the remaining scrubber droplets have approximately the same

velocity as the gas and therefore have Sherwood numbers for mass transfer equal approximately to 2. The effects of lower Sherwood number and smaller concentration on mass transfer are offset somewhat by the smaller droplet size so, depending upon the conditions in a particular situation, the net change in rates of evaporation of water vapor from scrubber droplets carried over and coagulation of acid droplets with the scrubber droplets may be less than might be expected.

In contrast to the situation in the scrubber, where acid mist droplets coagulating with scrubber spray droplets are removed from the flue gas, acid captured by carried-over scrubber droplets in the stack is emitted as sulfate, though in a different particle size range from acid mist.

Results and Discussion

The results of the calculations of acid mist properties as functions of time through a wet SO_2 scrubber and stack are shown in Figures 7.1 to 7.5. The results for a base case are presented in Figure 7.1, followed by figures showing the effects of changing individual parameters characterizing the H_2SO_4 concentration entering the scrubber, the scrubber spray quality, and mist eliminator performance. The parameters and their values were: H_2SO_4 concentration, 10 and 20 ppmv; scrubber spray droplet size, 0.7, 1, and 2 mm; and size of droplets leaving the mist eliminator, 10 and 20 μm. Droplet size was chosen as the indicator of mist eliminator performance because its influence is stronger than that of collection efficiency. The flue gas residence time in the scrubber was fixed at 5 seconds, followed by up to 15 seconds of residence time in the stack. Identical scales are used on the ordinates of the figures, for ease of comparison of acid properties under the various sets of conditions.

Base Case

The following conditions were assigned for the base case: H_2SO_4 volume fraction in flue gas entering the scrubber, 10 ppmv; scrubber spray droplet size, 1 mm; and size of droplets passing the mist eliminator, 10 μm. The values of the other parameters used in the calculations are given in Table 7.1. The evolution of acid mist properties in the scrubber and stack under the base case conditions is shown in Figure 7.1. The individual panels in the figure are, from the top: (a) the acid mist droplet size; (b) mass fraction of H_2SO_4 in the acid mist droplets; (c) the number concentration of acid mist droplets; (d) the volume fraction of acid mist (m^3 droplets/m^3 flue gas); and (e) the cumulative fraction of the original acid captured by coagulation of acid mist with scrubber spray droplets.

Both coagulation and absorption of water vapor contribute to the growth of acid mist in the scrubber, shown at the left in Figure 7.1a. The progress of coagulation is best seen in the decline in number concentration with time, shown on a logarithmic scale in Figure 7.1c. Growth by coagulation is most rapid at early times, when the number concentration is high and the droplets are small. Absorption of water vapor has no direct effect on number concentration, though it influences the rate of coagulation through its effects on the volume fraction of acid mist and its droplet size.

The progress of absorption of water vapor is best seen in Figure 7.1d, showing the increase in volume fraction of acid mist with time. Absorption of water vapor by the

droplets is most rapid at early times, when the acid concentration in the droplets is high and the equilibrium vapor pressure of water at the surfaces of the droplets is low, so there

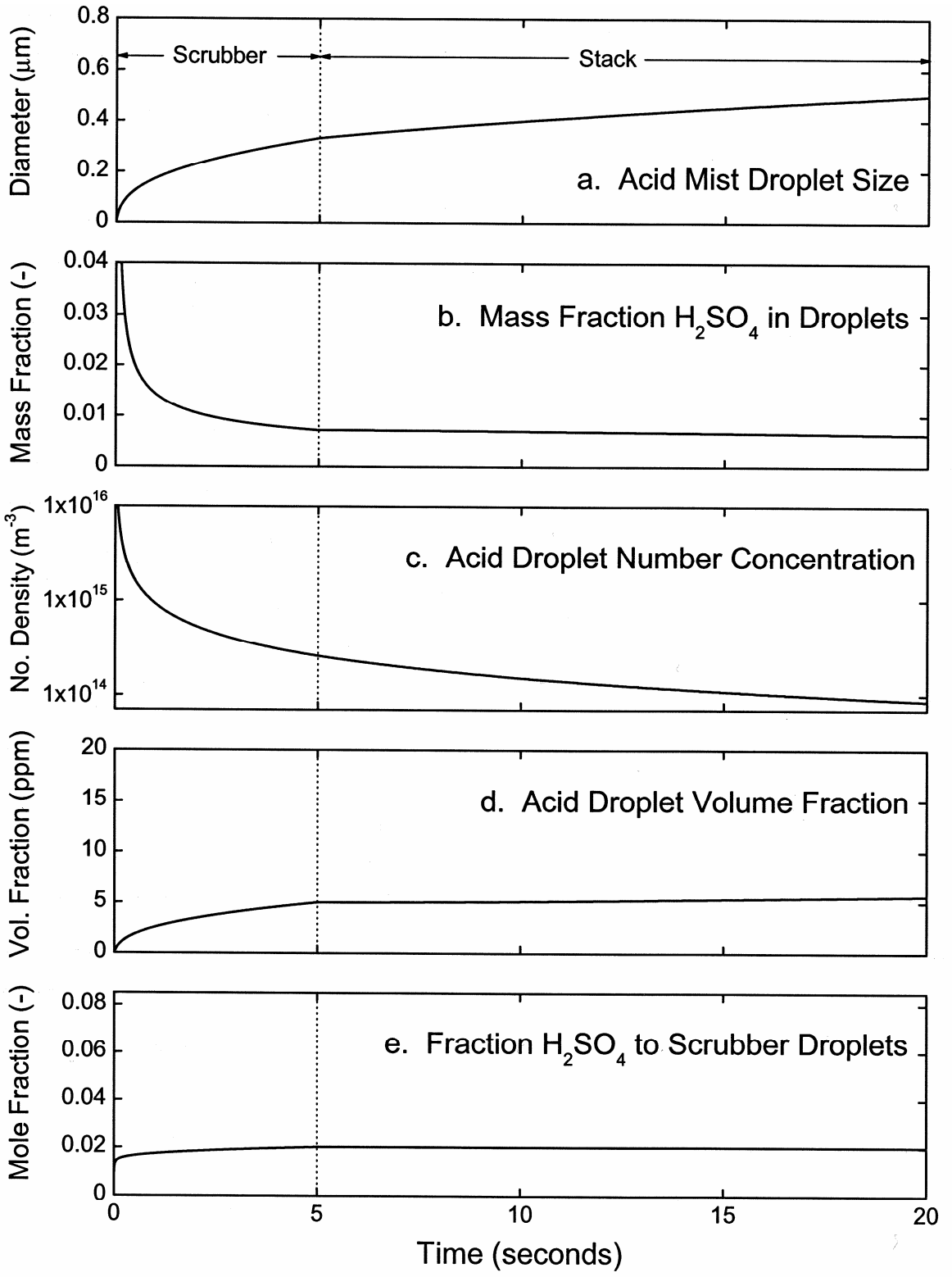

Figure 7.1. Properties of acid mist as a function of time in the SO_2 scrubber and stack—base case:
H_2SO_4 entering scrubber, 10 ppmv
mean spray droplet size, 1 mm
mean droplet size passing the mist eliminator, 10 μm

is a large difference in water vapor concentration between the free stream and acid droplet surfaces. The importance of this can be seen by examination of Figure 7.1b, showing the decline in acid concentration in the acid mist droplets with time due to dilution by absorbed water vapor. The initial condensation nuclei are assumed to contain 84.5 wt % H_2SO_4. During only 5 seconds of residence time in the scrubber, this concentration is reduced by absorption of water vapor to 0.71 wt%. Corresponding to this change in composition, the vapor pressure of water adjacent to the acid droplets rises from approximately 0 to 19954.8 Pa, compared with 19955.5 Pa at the surface of the scrubber spray droplets, which are the source of water vapor. At an acid concentration of 0.71 wt % there is less than 1 Pa of partial pressure difference driving the transfer of water from scrubber droplets to acid mist so, by the time they reach the scrubber exit, the absorption of water vapor by acid droplets has become relatively slow. Coagulation of acid mist droplets with each other has no direct effect on the volume fraction of acid mist (m^3 acid droplets/m^3 flue gas), though it influences the rate of absorption of water vapor through its effects on droplet size and the consequent effects on water vapor pressure at the droplet surfaces (Kelvin effect) and mass transfer coefficient.

The evolution of the ability of the scrubber spray to capture acid mist is shown in Figure 7.1e. According to the model, only 2% of the original sulfuric acid is retained in the scrubber. Most of the capture occurs at very early times, when the sizes of the acid condensation nuclei are still small and have large diffusion coefficients and high rates of mass transfer to the much larger scrubber droplets. Because the properties of the acid mist at short times are evidently so important to this process, the result may be sensitive to the assumption that all of the H_2SO_4 nucleates as $H_2SO_4 \cdot H_2O$ instantaneously on entering the scrubber.

Evolution of acid mist in the stack, shown in the right-hand three-quarters of the panels in Figure 7.1, is dominated by coagulation. Because the mist eliminator removes most of the scrubber droplets and greatly reduces the source of water vapor, the free stream water vapor partial pressure drops to only 0.002 Pa above the partial pressure of water vapor adjacent to the dilute acid droplet surfaces, shutting off the transfer of water from scrubber droplets to acid. There is little increase in the volume fraction of acid mist in the stack, as shown in Figure 7.1d, and little further dilution of the acid in the mist, as shown in Figure 7.1b. Coagulation, however, continues in the stack, as shown by the factor of three decrease in number concentration (Figure 7.1c) and 50% increase in droplet size (Figure 7.1a) from stack entrance to exit. Coagulation of acid mist with the low concentration of scrubber droplets passing the mist eliminator is not significant in the stack (Figure 7.1e). At the stack exit, under the base case conditions, the acid mist droplets are estimated to have a mean size of 0.5 μm, are expected to contain 0.6 wt % H_2SO_4, and occupy 6 ppm by volume of the stack gas.

Effect of H_2SO_4 Concentration

Increasing the initial H_2SO_4 from 10 to 20 ppmv changes the properties of the acid mist as shown in Figure 7.2. The number concentration of acid droplets at the scrubber and stack exits is only slightly increased (Figure 7.2c), by 16 and 12%, respectively, because higher initial number concentration increases their coagulation rate. On the other hand, the volume fraction of acid mist at the scrubber outlet is increased from 5 ppm (base case) to 13 ppm, a factor significantly larger than the doubling in initial H_2SO_4

Table 7.1. Values of the parameters used in the calculations for the base case.

Property	Symbol	Value	Source
Temperature in scrubber	T	333.15 K (140 ^{o}F)	typical
Average molecular weight of flue gas	W_{fg}	30	typical
Flue gas velocity in scrubber	u_{fg}	3.7 m/s (12 ft/s)	typical
Scrubber spray droplet downward velocity, relative to the scrubber	u_{sd}	1.5 m/s (5 ft/s)	typical
Liquid-to-gas ratio in scrubber	LG	0.02 m^3/actual m^3 (150 gal/1000 acf)	typical
Drag coefficient for the scrubber droplets	C_D	0.54	a
Scrubber liquor spray droplet diameter	d_{sd}	1 mm	b
Density of scrubber spray droplets	ρ_{sd}	1225 kg/m^3	15 wt% solids
Initial mass fraction of H_2SO_4 in $H_2SO_4 \cdot H_2O$, the condensation nuclei	Y_{a0}	$W_{H2SO4}/W_{H2SO4 \cdot H2O}$ = 0.845	
Density of sulfuric acid	ρ_a	Figure A1	c
Surface energy of sulfuric acid	σ_a	Figure A2	d
Equilibrium vapor pressure of steam over a flat sulfuric acid surface	$P_{w,af}$	Figure A3	c
Initial diameter of acid condensation nuclei	d_{ad0}	0.597 nm	e
Viscosity of flue gas	μ_{fg}	$\frac{1.458x10^{-6}\ T^{1.5}}{T+110.4}$ kg/(m·s)	f
Molecular diffusion coefficient in water vapor - flue gas mixture	$D_{w,fg}$	$1.87x10^{-10}\ T^{2.072}$ m^2/s	g
Fraction of scrubber liquor flow rate passing the mist eliminator	--	5 x 10^{-6}	h
Mean size of scrubber liquor droplets passing the mist eliminator	--	10 μm	estimate
Flue gas residence time in scrubber	--	5 s	typical

a. Michalski, 2000.[51]
b. Adjusted to give a terminal velocity for the scrubber spray droplets of 5.2 m/s (17 ft/s), equal to $u_{fg} + u_{sd}$, using the drag coefficient of Michalski, 2000.[51]
c. Perry et al., 1984, pp. 3-65, 3-66, and 3-237.[58]
d. Morgan and Davis, 1969[59]; Myhre et al., 1998.[60]
e. Diameter of a sphere having the volume occupied by one molecule of $H_2SO_4 \cdot H_2O$ liquid at 333.15 K.
f. Approximated using the viscosity of nitrogen from Hilsenrath et al., 1955.[61]
g. Approximated using the binary diffusion coefficient for water vapor-nitrogen from Marrero and Mason, 1972.[62]
h. 300 MW unit, liquid-to-gas ratio of 150 gal/1000 acf, emission limit of 0.03 lb/10^6 Btu, slurry is 15 wt% solids, and ½ of particulate matter in stack is scrubber solids.

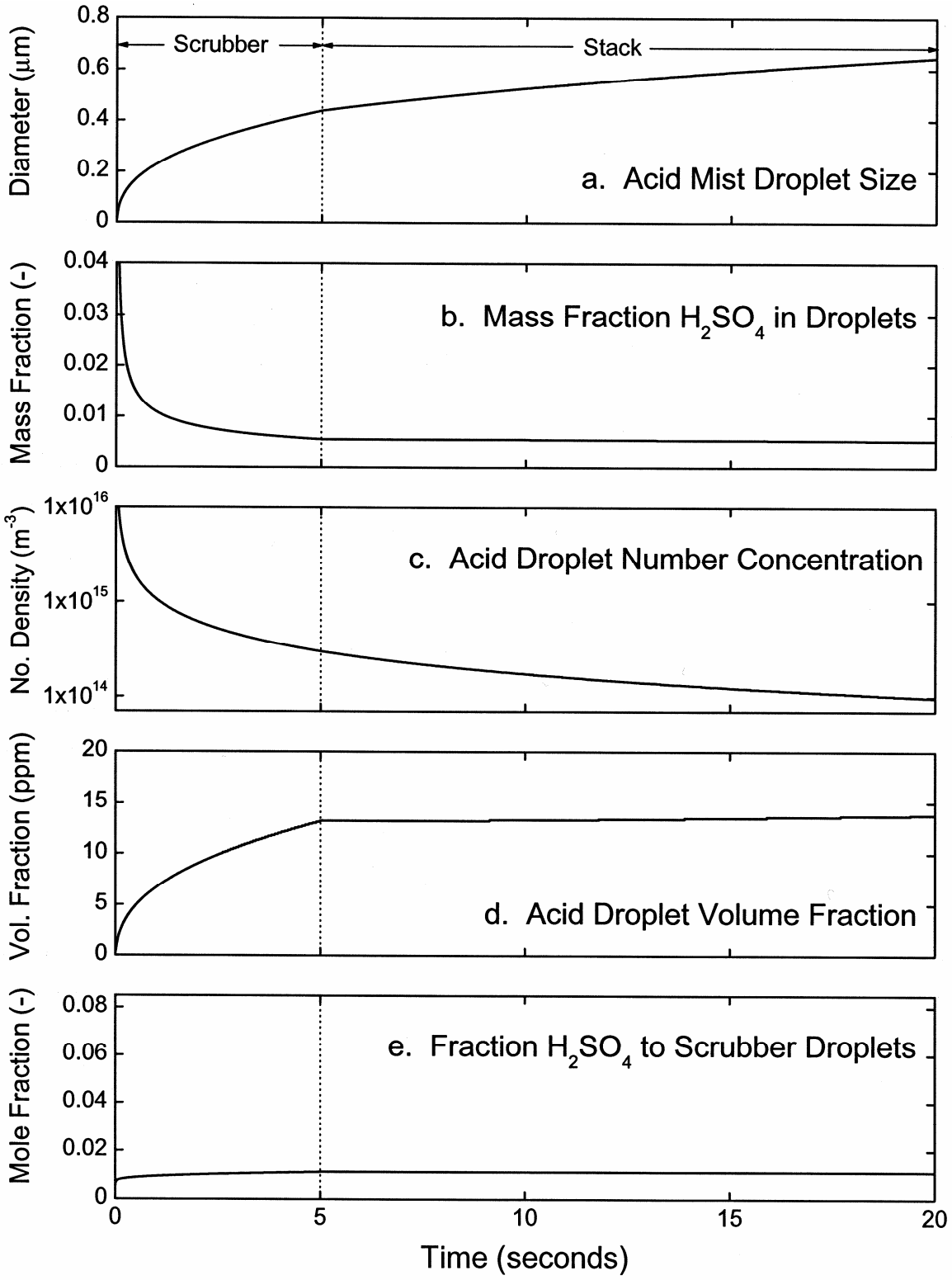

Figure 7.2. Properties of acid mist as a function of time in the SO_2 scrubber and stack—increased H_2SO_4 case:

H_2SO_4 entering scrubber, 20 ppmv
mean spray droplet size, 1 mm
mean droplet size passing the mist eliminator, 10 µm

concentration. The increase in volume fraction, due to increased absorption of water vapor, is consistent with increased dilution of the acid, as shown by comparison of Figures 7.1b and 7.2b. The mass fraction of H_2SO_4 in the acid mist at the scrubber outlet is now only 0.55 wt %, compared with 0.71 wt % at the same location under the base case conditions. The higher absorption of water vapor in the present case is driven by the lower vapor pressure of water at surfaces having larger radii of curvature, characteristic of the larger acid droplets (Kelvin effect[57]). The combination of increased amounts of condensing species and small change in droplet number concentration result in a significant increase in mean acid mist droplet size at the scrubber outlet, from 0.33 μm in the base case to 0.44 μm on doubling the H_2SO_4 concentration. The fraction of the acid captured in the scrubber (Figure 7.2e) decreases in inverse proportion to the increase in initial H_2SO_4 concentration, from 2% in the base case (Figure 7.1e) to only 1%.

As in the base case, there is little absorption of water by acid mist in the stack, because the mist eliminator removed of most of the scrubber droplets, which were the source of water vapor in the scrubber. Neither the droplet composition (Figure 7.2b) nor the droplet volume fraction (Figure 7.2d) changes significantly in the stack. Coagulation of the acid mist, however, continues in the stack, increasing the mean droplet size from 0.44 μm at the scrubber outlet to 0.65 μm at the stack exit, a fractional increase similar to that observed in the base case. Little coagulation of acid mist with scrubber droplets passing the mist eliminator is expected (Figure 7.2e).

Scrubber Droplet Size

The effects of increasing the mean scrubber spray droplet size from 1 mm to 2 mm and decreasing it to 0.7 mm are shown in Figures 7.3 and 7.4, respectively. Compared with the base case, Figure 7.1, there are no large changes in acid mist droplet size, composition, number concentration, or volume fraction in either the scrubber or the stack. The properties of acid mist leaving the stack are practically the same in all three cases. According to the model, the only significant change in the behavior of the system is an increase in the capture of H_2SO_4 in the scrubber as the spray droplet size decreases, shown by comparison of Figures 7.1e, 7.3e, and 7.4e. The fraction of the original H_2SO_4 captured by 2-mm spray droplets was 0.33%, the fraction captured by 1-mm droplets was 2%, and the fraction captured by 0.7-mm droplets was 7.6%. A corresponding slight reduction in the volume fraction of acid mist leaving the stack can also be seen (Figures 7.1d, 7.2d, and 7.3d).

Further reduction in the size of the scrubber spray droplets below 0.7 mm is outside the range of application of the model. The terminal fall velocity of 0.5 mm droplets is 3.7 m/s, equal to the upward gas velocity in the scrubber. As the spray droplet size approaches 0.5 mm, the calculated concentration of droplets increases to physically unrealistic levels. In practice this corresponds to the "fluidized" regime,[51] not described by the present model. The calculated volume fractions of droplets in the scrubber were 2, 5, and 11% for the spray droplet sizes of 2, 1, and 0.7 mm, respectively. The increase in acid capture with decreasing size is due to the combined effects of increasing specific surface area and increasing concentration of the spray droplets.

We note that, according to the calculation, capture of acid by scrubber spray droplets occurs primarily at early times when the acid nuclei are still very small and have high

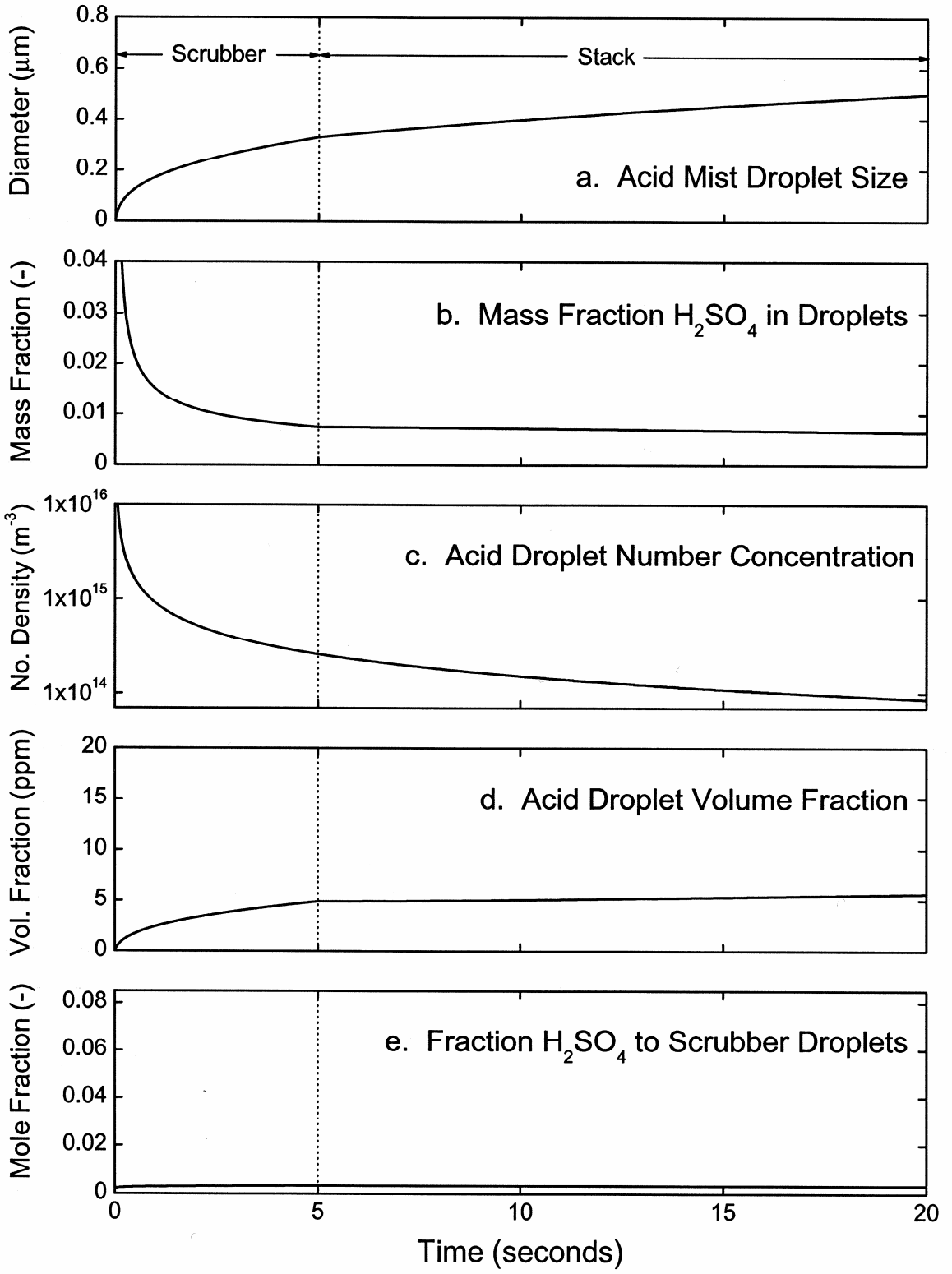

Figure 7.3. Properties of acid mist as a function of time in the SO_2 scrubber and stack—increased scrubber droplet size case:

H_2SO_4 entering scrubber, 10 ppmv
mean spray droplet size, 2 mm
mean droplet size passing the mist eliminator, 10 µm

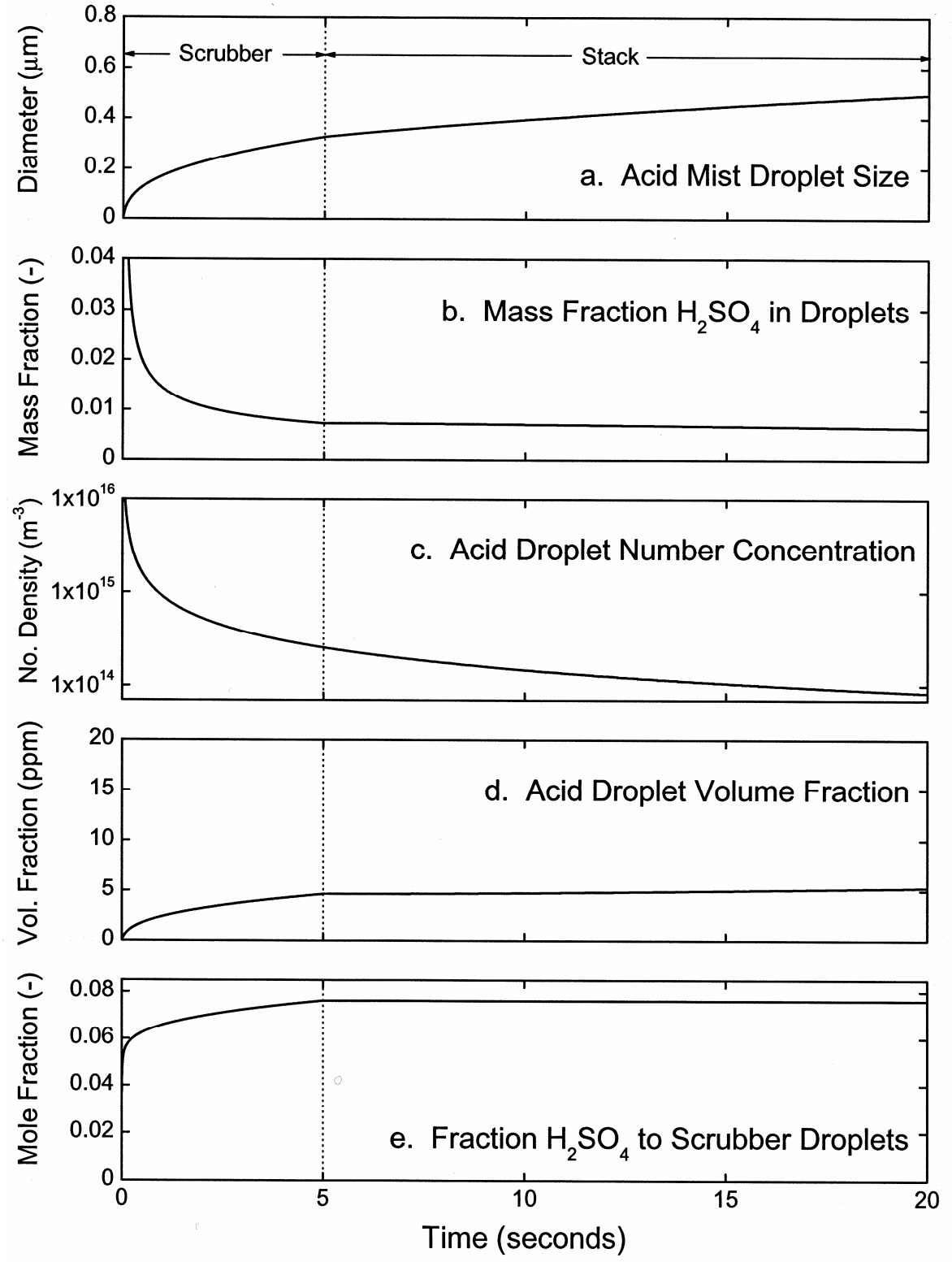

Figure 7.4. Properties of acid mist as a function of time in the SO_2 scrubber and stack—decreased scrubber droplet size case:

H_2SO_4 entering scrubber, 10 ppmv
mean spray droplet size, 0.7 mm
mean droplet size passing the mist eliminator, 10 µm

diffusion coefficients. This is shown by the rapid rise in the fraction of H_2SO_4 captured near time = 0 in Figure 7.4e. The present estimates of acid capture in the scrubber may be influenced by the assumption that nucleation of acid begins with instantaneous formation of $H_2SO_4 \cdot H_2O$ at the inlet. A more detailed description of the nucleation of acid droplets may be needed to achieve high accuracy in the calculation of acid removal by the scrubber. The presence of a distribution of droplet sizes in the scrubber spray also needs to be considered, including a mechanism for removal of droplets having terminal velocities near the gas velocity, so their concentrations are properly bounded. Possible mechanisms for removal of droplets near the critical size are coalescence of the droplets and a distribution of gas velocities in the scrubber.

Performance of the Mist Eliminator

The last case to be considered is the effect of spoiling the performance of the mist eliminator. We chose to simulate this by increasing the mean size of scrubber droplets passing the mist eliminator, rather than decrease the collection efficiency, because the base case already assumes that one-half of the particulate matter emissions limit is contributed by scrubber solids (Table 7.1, footnote h), so there is little room left for adjustment of the efficiency. The effect of increasing the mean size of scrubber droplets in the stack from 10 to 20 μm is shown in Figure 7.5. Interestingly, the most visible effect, compared with the base case, is a small decrease in the acid mist volume fraction at the stack exit with increasing droplet size. This is due to the decrease in rate of supply of water vapor to the free stream from the larger size scrubber droplets, limiting the transfer of water from the scrubber droplets to the acid mist. The acid concentration in the mist droplets at the exit from the stack is slightly higher, and the droplet size slightly smaller, than in the base case. With respect to acid mist, and under the conditions investigated, the function of scrubber droplets not collected by the mist eliminator is to provide a small supply of water vapor to increase the volume fraction of acid mist in the stack. An increase of 10 to 15% in acid mist volume fraction by absorption of water vapor in the stack was typical. The concentration of scrubber droplets is too low, and both acid mist and scrubber droplets are too large, for the scrubber droplets to be effective as scavengers of acid mist in the stack. Larger increases in the volume fraction of acid mist by absorption of water vapor or capture of acid mist by scrubber droplets in the stack might be possible under some conditions, for example in the presence of low efficiency of mist removal at the scrubber exit or unusually small size of droplets passing the mist eliminator.

Comparisons of Predicted and Measured Acid Droplet Size Distributions

Over the past several years Southern Research has developed a technique for analyzing the material collected on the stages of cascade impactors to separately ascertain the size distributions of the primary sources of the material collected in the various size fractions: fly ash, scrubber solids, and condensed H_2SO_4. Examples of these breakdowns by constituent are shown in Figures 7.6 through 7.8. As can be seen, the bulk of the condensed H_2SO_4 is found in particles having diameters of a few tenths of a micrometer. Comparisons of the volume mean diameter of the condensed acid from the model to extrapolations from the measured values of the diameters of the acid are shown in Figure 7.9. The extrapolations were made by assuming constant number concentrations with the

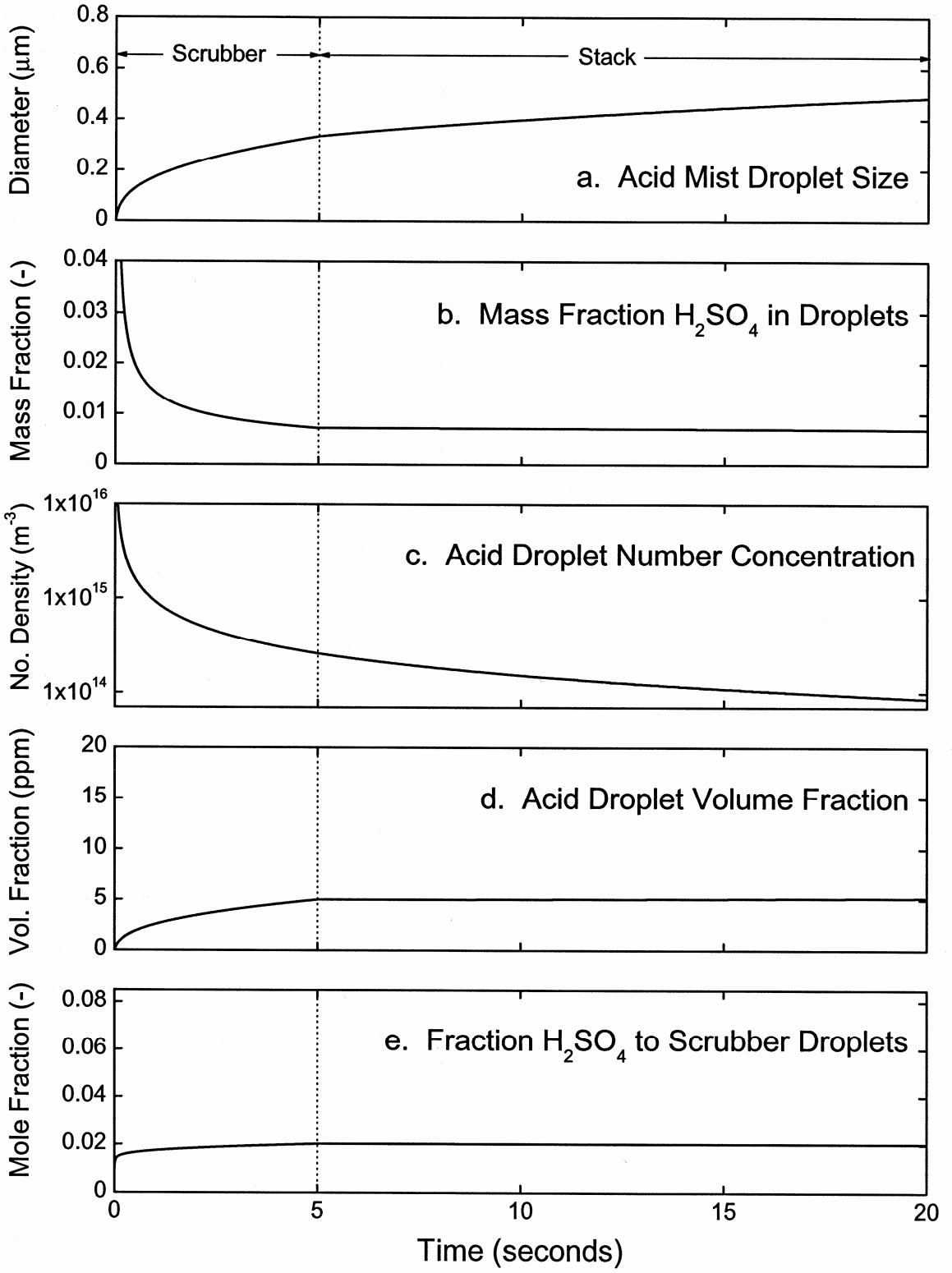

Figure 7.5. Properties of acid mist as a function of time in the SO_2 scrubber and stack—increased size of droplets passing the mist eliminator case:

H_2SO_4 entering scrubber, 10 ppmv
mean spray droplet size, 1 mm
mean droplet size passing the mist eliminator, 20 μm

diameters being proportional to the cube root of the SO_3 concentration. As can be seen, the predictions compare favorably with values based on measurement. The validity of the predictions are further strengthened when predicted opacities in the plume from a 1300 MW coal-fired using a wet scrubber for SO_2 control are compared with those measured by a certified "smoke reader" as shown in Figure 7.10. The predictions and measurements in the latter case were made for the point downwind of the stack at which the condensed water fog had evaporated.

Conclusions and Recommendations

Under the assumptions and conditions investigated, the principal role of a wet SO_2 scrubber, from the point of view of sulfuric acid mist, is to provide conditions for nucleation of acid droplets and a long residence time for their growth by coagulation and absorption of water vapor. Downstream from a wet FGD unit, the principal role of the stack, again from the point of view of sulfuric acid, is to provide additional residence time for growth of the acid mist by coagulation. Under all of the conditions examined, the mean size of acid droplets at the stack exit is predicted to have grown, through the combined effects of coagulation and absorption of water vapor, to sizes within the range able to scatter visible light.

According to the calculations and within the ranges of the parameters investigated, the only factor having significant influence on the volume fraction of acid mist leaving the stack was the original H_2SO_4 content of the flue gas. When the initial H_2SO_4 concentration was increased, the ultimate acid droplet volume fraction increased more rapidly than the H_2SO_4 concentration itself. Doubling the H_2SO_4 at the scrubber inlet from 10 to 20 ppmv increased the acid volume fraction at the stack exit by a factor of 2.5, from 5.6 to 14 ppmv. The increased absorption of water vapor in the presence of higher acid concentration was due to the decrease in vapor pressure at the surfaces of the larger droplets that were formed, due to the Kelvin effect. The decrease in vapor pressure increased the rate of absorption of water vapor by the acid droplets.

In spite of the fact that the mechanism for the increase in volume fraction of acid mist in the scrubber is vaporization of water from scrubber droplets and absorption of the vapor by the acid, variation of the size of scrubber spray droplets over the range from 0.7 to 2 mm had hardly any influence on the properties of the acid. Transfer of water from the scrubber droplets to acid droplets appears to be regulated more by the dependence of the vapor pressure of the acid droplets on their H_2SO_4 content than on the specific surface area, mass transfer coefficient, or concentration of the scrubber spray.

The principal effect of decreasing the scrubber spray droplet size was to increase capture of acid by spray droplets in the scrubber, although the fractions of acid captured were not large enough to have significant influence on acid mist droplet size and volume fraction. The fraction of the original H_2SO_4 retained in the scrubber increased from 0.33% to 7.6% on decreasing the spray droplet size from 2 to 0.7 mm, due to increased mass transfer to the smaller droplets and to the increase in spray droplet concentration as the terminal velocity of the spray droplets approached the gas velocity. Spray droplets smaller than 0.7 mm were outside the range over which the model is applicable, because closer approach of the droplet terminal velocity to the gas velocity led to unrealistically high droplet concentrations characteristic of the "fluidized" regime.[51] It was noted that most

of the acid capture was predicted to occur at very early times, when the acid nuclei are still small, so the calculated capture may be influenced by the assumption that acid nucleates immediately to form $H_2SO_4 \cdot H_2O$ on entering the scrubber.

According to the model, the source of water vapor that could be absorbed by acid mist in the stack is scrubber droplets carried over from the mist eliminator, not the water vapor present in the flue gas leaving the scrubber. This is because the acid at this stage is dilute (~ 1 wt % H_2SO_4), so the vapor pressure of water adjacent to acid mist droplets is not far from the vapor pressure over pure water. A continuous supply of water vapor is therefore needed if there is to be any significant uptake of water by the acid. Under the conditions investigated, an increase of 10 to 15% in acid mist volume fraction by absorption of water vapor in the stack was typical. Cooling of the stack gas, not taken into consideration in the present calculation, is a possible mechanism by which water vapor could be maintained close to saturation in the presence of its absorption by acid mist. According to the present model and calculations, the most important process occurring in the stack is the increase in droplet size due to coagulation. The acid droplet size was estimated to increase by 50% during 15 seconds of residence time in the stack.

The model exhibits some unexpected and counter-intuitive behavior, such as the decrease in H_2SO_4 concentration in acid droplets at the stack exit on increasing the H_2SO_4 content of the flue gas (Figures 7.1b and 7.2b), the insensitivity of acid volume fraction to scrubber spray droplet size (Figures 7.3d and 7.4d), and the decrease (though it is slight) in acid mist volume fraction on increasing the size of scrubber droplets passing the mist eliminator (Figures 7.1d and 7.5d). The potential of such calculations to assist in the interpretation of observations of sulfuric acid behavior in the field would appear to justify some further development of the model. To make the calculation a more powerful and useful simulation tool, the following refinements are proposed:

- Evaluate the effects of scrubber and stack temperature.
- Compare the results of the calculations with measurements of acid concentrations at the entrance and exit from wet FGD units.
- Using the scattering efficiency for visible light versus particle size, determine relative opacities for the acid mist at the stack exit for comparison of the effects of scrubber and stack conditions on plume visibility.
- Incorporate a droplet size distribution for the scrubber spray.
- Locate experimental data to improve confidence in the assignment of the value for the size of scrubber droplets passing the mist eliminator.
- Examine and refine, if necessary, the description of nucleation to provide a better model for droplet growth at short times and improve the simulation of capture of acid mist in the scrubber.
- Allow for cooling of flue gas as a driver for transfer of water vapor to acid mist in the stack.

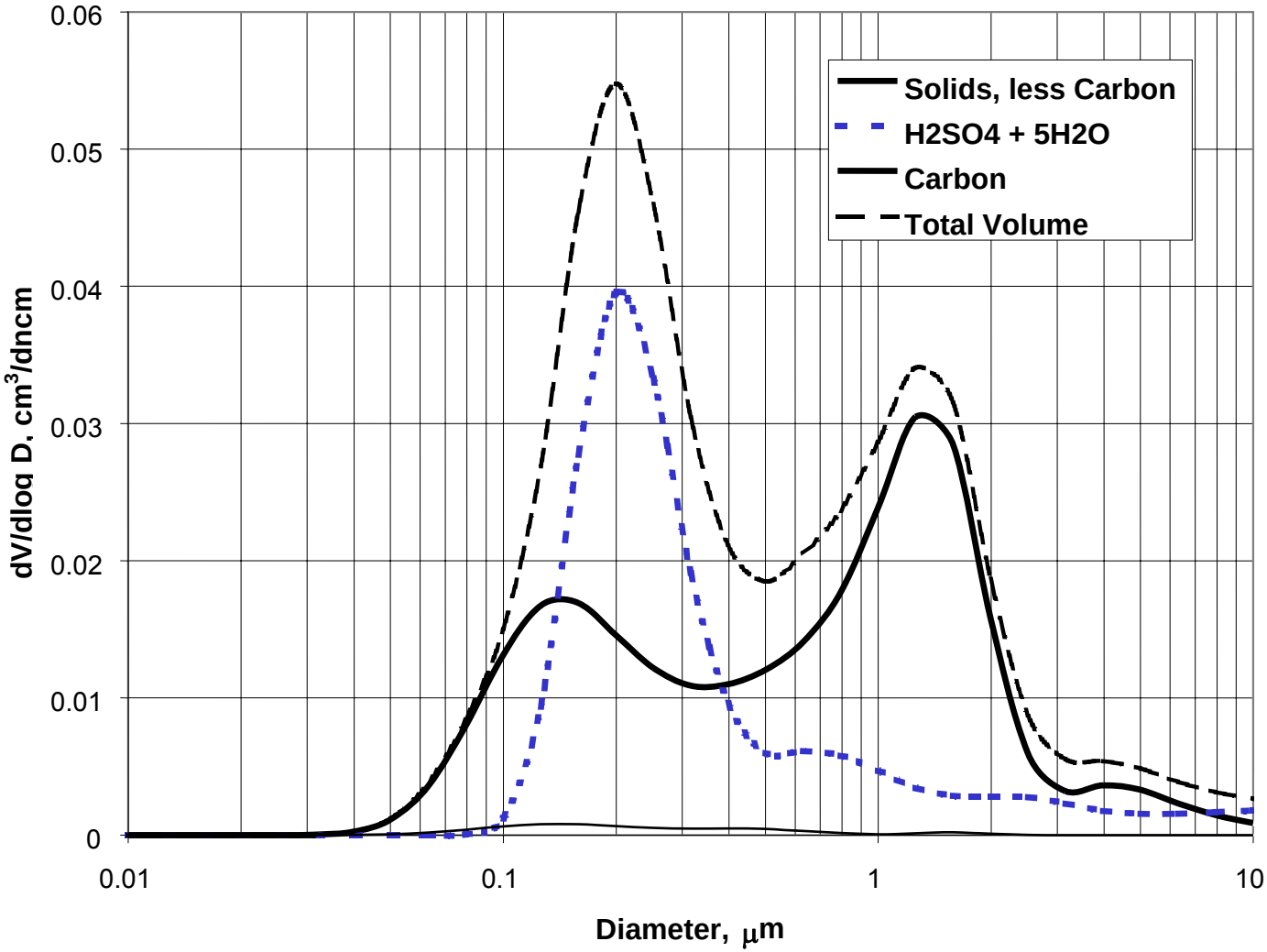

Figure 7.6. Measured size distributions of acid mist and other particulate components downstream of scrubber module "A." Concentrations are shown on the basis of particle volume. The H_2SO_4 concentration in the flue gas was 2.6 ppmv.

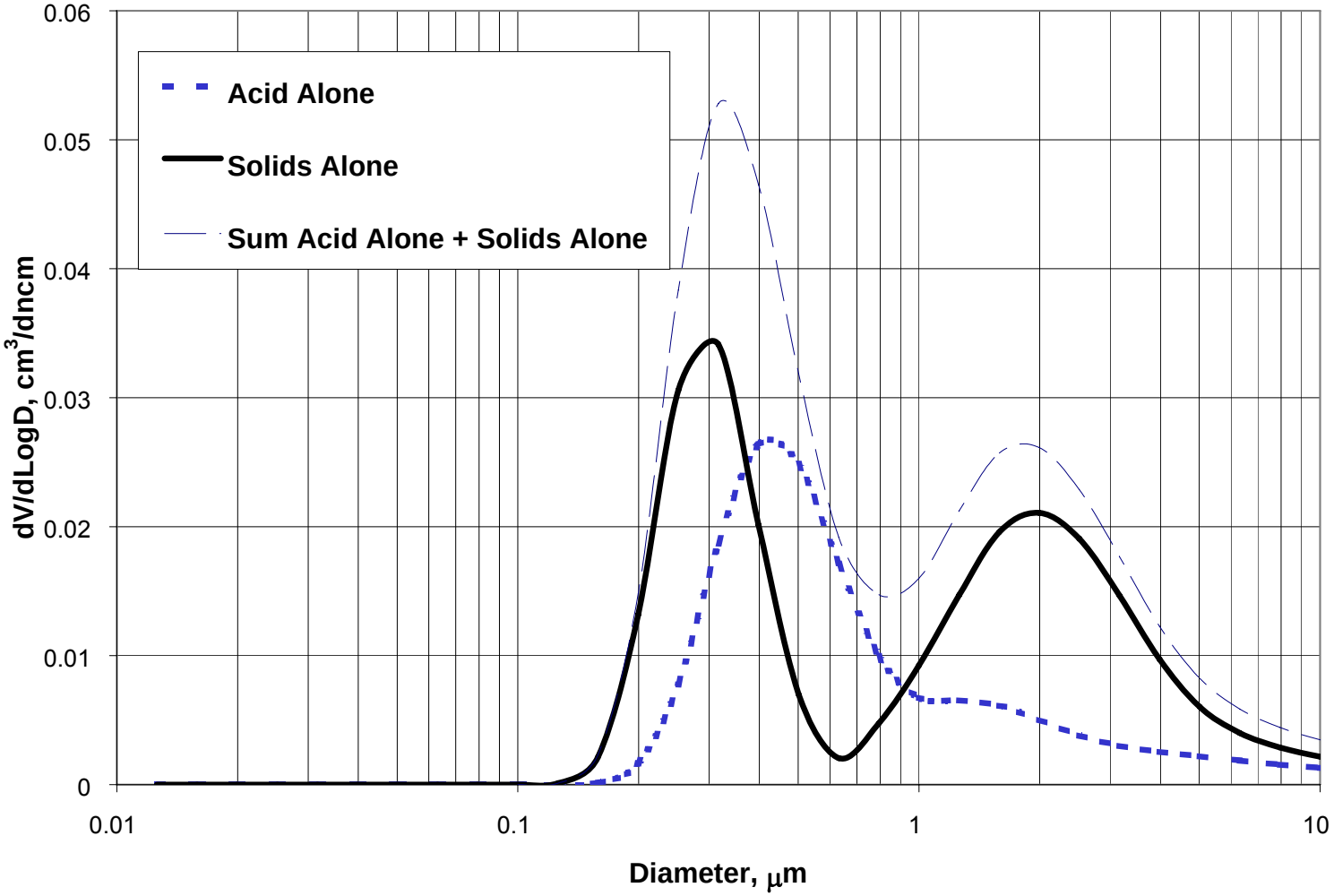

Figure 7.7. Measured size distributions of acid mist and other particulate components in the stack downstream of a scrubber system. Concentrations are shown on the basis of particle volume. The H_2SO_4 concentration in the flue gas was 2.3 ppmv.

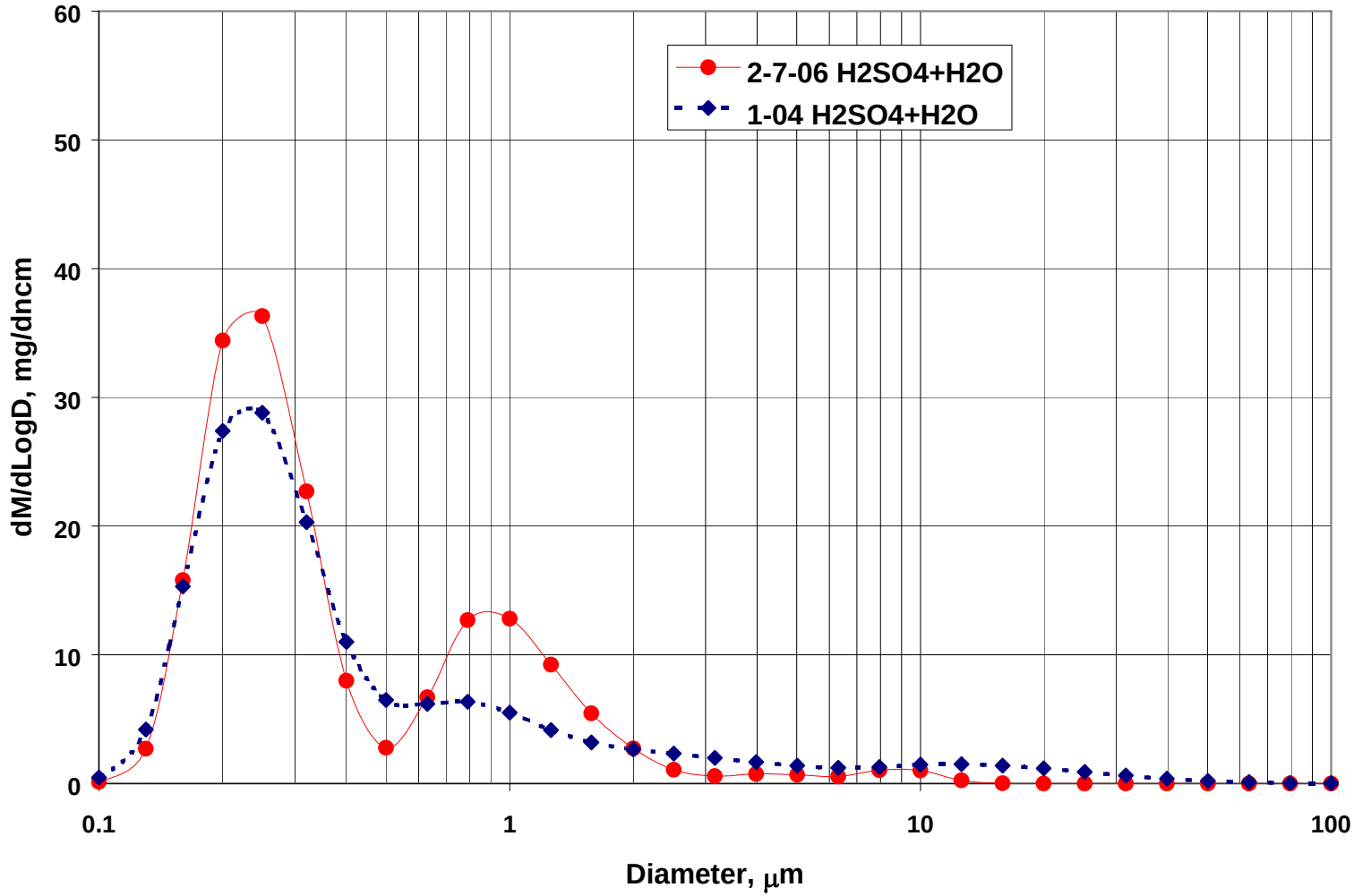

Figure 7.8. Measured size distributions of acid mist in the stack as shown in Figure 7.7 after replacement of the scrubber system with one of a different type. Concentrations here are shown on the basis of particle mass.

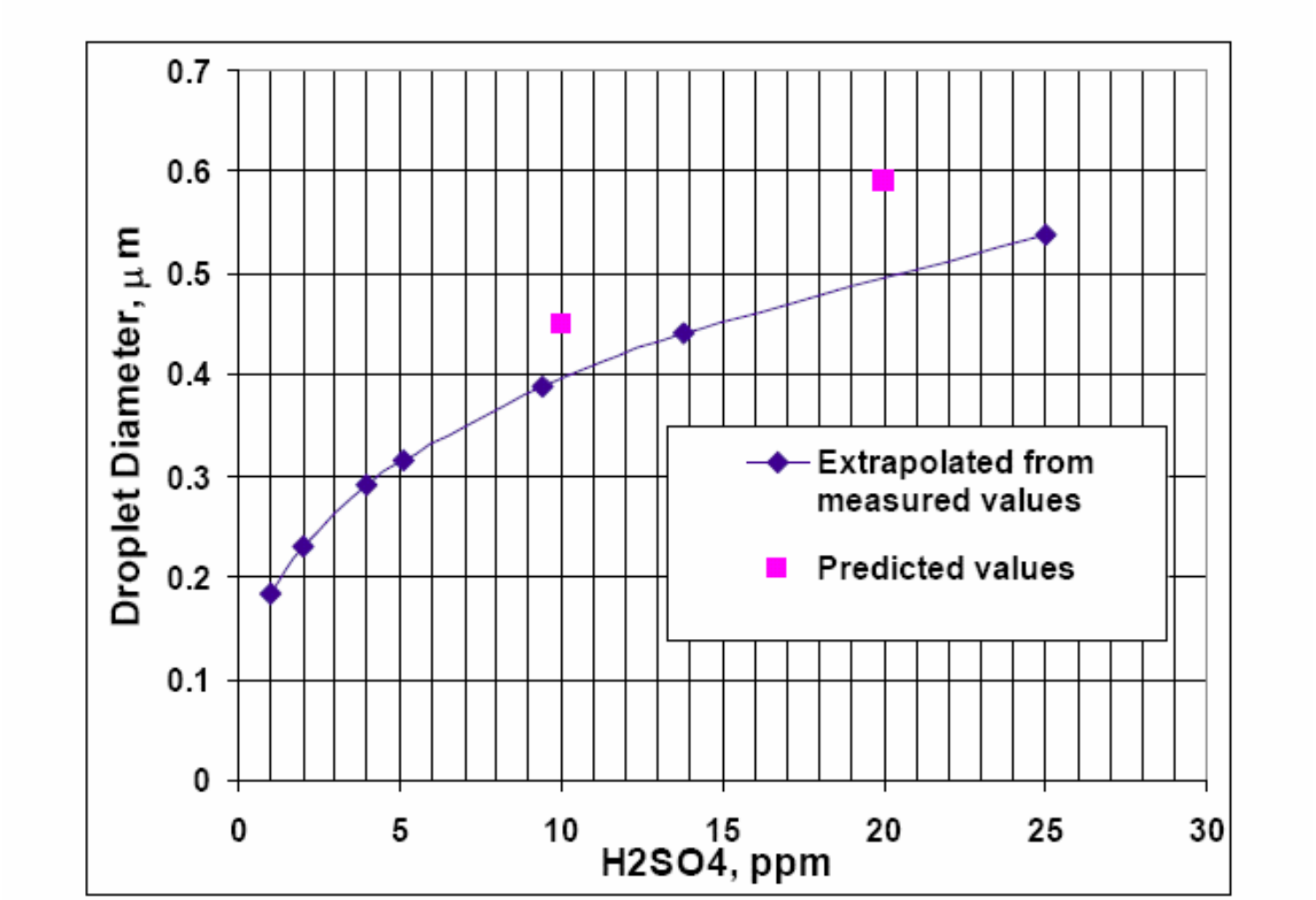

Figure 7.9. Comparison of droplet diameters extrapolated from measurements with those predicted by the model. The extrapolations were made by assuming constant number concentrations with the diameters being proportional to the cube root of the SO_3 concentration.

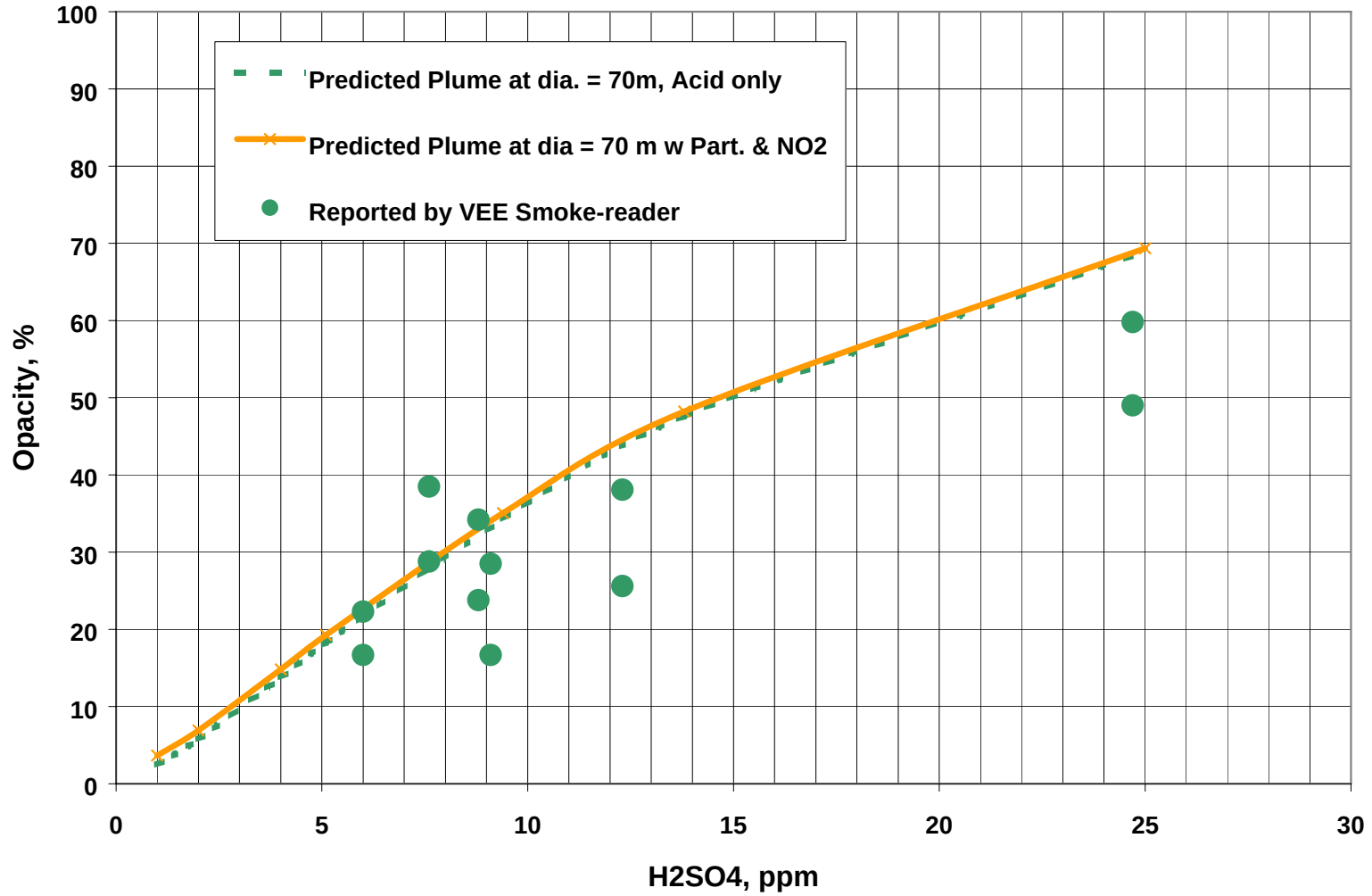

Figure 7.10. Comparison of predicted plume opacities versus H_2SO_4 concentration with those measured by a certified "smoke reader" for a 1300 MW unit with a pollution control system consisting of an SCR followed by a cold-side ESP and an SO_2 scrubber.

8. REFERENCES

1. U.S. Environmental Protection Agency, "Rule To Reduce Interstate Transport of Fine Particulate Matter and Ozone (Clean Air Interstate Rule)," *Federal Register*, Vol. 70, pp. 25162-25405, 2005.
2. Farthing, W.E., P.M. Walsh, J.P. Gooch, J.D. McCain, W.S. Hinton and R.F. Heaphy, *Identification of (and Responses to) Potential Effects of SCR and Wet Scrubbers on Submicron Particulate Emissions and Plume Characteristics*, Office of Research and Development, EPA-600/R-04-107, Research Triangle Park, NC, August, 2004.
3. Leikauf, G., D.B. Yeates, K.A. Wales, D. Spektor, R.E. Albert and M. Lippmann, "Effects of sulfuric acid aerosol on respiratory mechanics and mucociliary particle clearance in healthy nonsmoking adults," *AIHA Journal*, Vol. 42, pp. 273 - 282, 1981.
4. Wyzga, R.E. and L.J. Folinsbee, "Health effects of acid aerosols," *Water, Air, & Soil Pollution*, Vol. 85, pp. 177 - 188, 1995.
5. Folinsbee, L.J., "Human health effects of exposure to airborne acid," *Environmental Health Perspectives*, Vol. 79, pp. 195-199, 1989.
6. Schlesinger, R.B., J.T. Zelikoff, L.C. Chen and P.L. Kinney, "Assessment of toxicologic interactions resulting from acute inhalation exposure to sulfuric acid and ozone mixtures," *Toxicology and Applied Pharmacology*, Vol. 115, pp. 183-190, 1992.
7. Jakab, G.J., R.W. Clarke, D.R. Hemenway, M.V. Longphre, S.R. Kleeberger and R. Frank, "Inhalation of acid coated carbon black particles impairs alveolar macrophage phagocytosis," *Toxicological Letters*, Vol. 88, pp. 243-248, 1996.
8. New Jersey Department of Health and Senior Services, Sulfur Trioxide Hazardous Substance Fact Sheet, http://www.state.nj.us/health/eoh/rtkweb/1767.pdf, accessed February 2005, 2005.
9. Downing, B., "Power Plant Releases Clouds Of Sulfuric Acid," Akron Beacon Journal, Akron, OH, p. 1, Sect. A, August 2, 2001.
10. U.S. Environmental Protection Agency Region 5, "Request for the ATSDR to evaluate air monitoring data and assess any adverse human health effects on the residents of Cheshire, Gallia County, Ohio," to Senior Regional Representative, Agency for Toxic Substances and Disease R., Chicago, IL, July 24, 2001.
11. Agency for Toxic Substances and Disease Registry, Health Consultation: Gavin Power Plant, Cheshire, Gallia County, Ohio, http://www.atsdr.cdc.gov/HAC/PHA/gavinpower/gpp_p1.html, accessed July 10, 2006.
12. Zetlmeisl, M.J., K.J. McCarthy and D.F. Laurence, "Investigation of some factors affecting nonflame generation and suppression of SO_3," *Industrial Engineering and Chemistry Product Research and Development*, Vol. 22, pp. 710-716, 1983.
13. Srivastava, R.K., C.A. Miller, C. Erickson and R. Jambhekar, "Emissions of sulfur trioxide from coal-fired power plants," *Journal of the Air & Waste Management Association*, Vol. 54, pp. 750-762, 2004.

14. U.S. Department of Energy, *Annual Steam-Electric Plant Operation and Design Data*, Energy Information Administration, Form EIA-767, Washington, DC, 2002.
15. U.S. Environmental Protection Agency, 2002 National Emissions Inventory Data & Documentation, ftp://ftp.epa.gov/EmisInventory/2002finalnei/point_sector_data/national/, August 7, 2006.
16. The McIlvaine Company, Utility Environmental Upgrade Tracking System, The McIlvaine Company, http://www.mcilvainecompany.com/, 2006.
17. Hardman, R., R. Stacey and E. Dismukes, "Estimating sulfuric acid aerosol emissions from coal-fired power plants," presented at DOE-FETC Conference on Formation, Distribution, Impact, and Fate of Sulfur Trioxide in Utility Flue Gas Streams, Pittsburgh, PA, March, 1998.
18. U.S. Environmental Protection Agency, *Analysis in Support of the Clean Air Interstate Rule Using the Integrated Planning Model*, Office of Air and Radiation, Clean Air Markets Division, Washington, DC, May 28, 2004.
19. "Madigan, Kaid comment on lawsuit filed Monday against Cinergy/PSI," Daily Republican Register, Mt. Carmel, IL, August 10, 2004.
20. Cassell, B., "Murray to expand Galatia Coal operation in Illinois into high-sulfur steam," SNL Energy Coal Report, Charlottesville, VA, January 24, 2005.
21. Cassell, B., "Alliance Resource Partners works on major high-sulfur mine project," SNL Energy Coal Report, Charlottesville, VA, January 24, 2005.
22. Barber, W., "Cinergy emissions control spending grows to $465 million in 2005," SNL Energy Coal Report, Charlottesville, VA, January 24, 2005.
23. Cassell, B., "Numerous scrubbers to cut SO2 emissions, boost high-sulfur coal," SNL Energy Coal Report, Charlottesville, VA, January 31, 2005, 2005.
24. Cassell, B., "LG&E, KU to remake coal market with new coal unit, scrubbers," SNL Energy Coal Report, Charlottesville, VA, January 31, 2005.
25. Cassell, B., "PPL boosts high-sulfur coal with Brunner, Montour scrubbers," SNL Energy Coal Report, Charlottesville, VA, February 28, 2005.
26. Monroe, L. and K. Harrison, *An Updated Method for Estimating Total Sulfuric Acid Emissions from Stationary Power Plants*, Southern Company Services, Research & Environmental Affairs, Internal Report, Birmingham, AL, March, 2003.
27. U.S. Environmental Protection Agency, "Method 8 - Determination of Sulfuric Acid and Sulfur Dioxide Emissions from Stationary Sources," *Code of Federal Regulations, Title 40 Part 60 (Appendix A-4)*, 2004.
28. Cheney, J. and J. Homolya, *Characterization of Combustion Source Sulfate Emissions with a Selective Condensation Sampling System*, Office of Air Quality Planning and Standards, EPA-600/9-78-020a, Research Triangle Park, NC, 1978.
29. Maddalone, R. and N. Garner, *Process Measurement Procedures - H_2SO_4 Emissions*, Office of Air Quality Planning and Standards, EPA-600/7-79-156, Research Triangle Park, NC, 1979.
30. Blythe, G., C. Galloway, C. Richardson and R. Rhudy, "Improvements to the controlled condensation measurement method for sulfuric acid," presented at EPRI-DOE-EPA Combined Utility Air Pollution Control Symposium: The Mega Symposium, Atlanta, GA, August 16-20, 1999.

31. Blythe, G., C. Galloway and R. Rhudy, "Flue gas sulfuric acid measurement method improvements," presented at AWMA EPRI-DOE-EPA Combined Utility Air Pollution Control Symposium: The Mega Symposium, Chicago, IL, August 20-23, 2001.
32. McCain, J.D., R.S. Saltzman and B. Carney, "Development of a low maintenance, field ruggedized SO_3 CEM," presented at Air Quality V, Arlington, VA, September 19-21, 2005.
33. McCain, J.D., *Development of Particle Size Test Methods for Sampling High Temperature and High Moisture Source Effluents*, Southern Research Institute, California Air Resources Board Contract A132-084, Birmingham, AL, June, 1994.
34. U.S. Environmental Protection Agency, "Method 17 - Determination of Particulate Matter Emissions from Stationary Sources," *Code of Federal Regulations, Title 40 Part 60 (Appendix A-6)*, pp. 426-431, 2004.
35. Bickelhaupt, R.E., *Measurement of Fly Ash Resistivity Using Simulated Flue Gas Environments*, Industrial Energy Research Laboratory, EPA-600/7-78-035, Research Triangle Park, NC, March, 1978.
36. Bickelhaupt, R.E., *A Technique for Predicting Fly Ash Resistivity*, U.S. Environmental Protection Agency, Industrial Energy Research Laboratory, EPA-600/7-79-204, Research Triangle Park, NC, August, 1979.
37. Walsh, P.M., *Properties of Particles Formed during Combustion of Residual Fuel Oils*, Empire State Electric Energy Research Corp., Research Report EP90-15, New York, NY, October, 1996.
38. Walsh, P.M., T.E. DeJohn, E.T. Bower and M. Rahimi, *Measurements of Sulfur Trioxide and Sulfate in the Products of Coal Combustion in a Traveling Grate Stoker*, Pennsylvania State University, University Park, PA, June, 1994.
39. Walsh, P.M., D.J. Mormile and B.F. Piper, "Sulfur trioxide formation in the presence of residual oil ash deposits in a electric utility boiler," *American Chemical Society, Division of Fuel Chemistry*, Vol. 38, pp. 294-300, 1993.
40. Merryman, E.L. and A. Levy, "Sulfur trioxide flame chemistry - H_2S and COS flames," *Thirteenth Symposium (International) on Combustion*, The Combustion Institute, Pittsburgh, PA, pp. 427-436, 1971.
41. Cullis, C.F. and M.F.R. Mulcahy, "The kinetics of combustion of gaseous sulphur compounds," *Combustion and Flame*, Vol. 18, pp. 225-292, 1972.
42. Smith, O.I., S.-N. Wang, S. Tseregounis and C.K. Westbrook, "The sulfur catalyzed recombination of atomic oxygen in a CO/O_2/Ar flame," *Combustion Science and Technology*, Vol. 30, pp. 241-271, 1983.
43. Walsh, P.M., W.F. Farmayan, T. Kolb and J.M. Beér, "Sulfur trioxide formation in high sulfur residual oil flames," *American Chemical Society, Division of Fuel Chemistry*, Vol. 31, pp. 112-121, 1986.
44. Urbanek, A. and M. Trela, "Catalytic oxidation of sulfur dioxide," *Catalysis Reviews, Science and Engineering*, Vol. 21, pp. 73-133, 1980.
45. Wickert, K., *The Oil-Firing Yearbook*, Kopf, Stuttgart, 1963.
46. Squires, R.T., "The kinetics of SO_3 formation in oil-fired boilers," *Journal of the Institute of Energy*, Vol. 55, pp. 41-46, 1982.

47. Walsh, P.M., A.N. Sayre and J.M. Beér, *Reduction of Particulate Emissions from High Asphaltene Heavy Fuel Oil Flames*, Empire State Electric Energy Research Corp., Research Report EP85-21, Albany, NY, November, 1988.
48. Shareef, G.S., J. Homolya and D.J. Mormile, "SO_3 formation over fuel oil fly ash deposits," presented at the 1990 SO_2 Control Symposium, New Orleans, LA, May 8-11, 1990.
49. Piper, B.F. and T. Kokoska, *Opacity study - data to support SO_3 formation analysis*, KVB, Inc., KVB 81-21620-1447, prepared for Consolidated Edison Company of New York, 1983.
50. Walsh, P.M., *Formation of Acid Mist and Evolution of its Properties in the Wet SO2 Scrubber and Stack of a Coal-Fired Electric Utility Boiler*, University of Alabama at Birmingham, Report prepared for Southern Research Institute, Birmingham, AL, April 5, 2005.
51. Michalski, J.A., "Development of droplet size distribution in FGD spray towers," *Atomization and Sprays*, Vol. 10, pp. 105, 2000.
52. Friedlander, S.K., *Smoke, Dust, and Haze: Fundamentals of Aerosol Dynamics*, Oxford University Press, New York, 2000.
53. Seinfeld, J.H., *Atmospheric Chemistry and Physics of Air Pollution*, John Wiley & Sons, New York, NY, 1986.
54. Frossling, N., "Uber die Verdunstung fallender Tropfen (The evaporating of falling drops)," *Gerlands Beitrage zur Geophysik*, Vol. 52, pp. 170-216, 1938.
55. Ranz, W.E. and W.R. Marshall, Jr., "Evaporation from drops, Parts I and II," *Chemical Engineering Progress*, Vol. 48, pp. 141-146, 173-180, 1952.
56. Dahneke, B., "Simple kinetic theory of Brownian diffusion in vapors and aerosols," in Theory of Dispersed Multiphase Flow, Mayer, R.E. (ed.), Academic Press, New York, NY, 1983.
57. Yue, G.K., "A quick method for estimating the equilibrium size and composition of aqueous sulfuric acid droplets," *Journal of Aerosol Science*, Vol. 10, pp. 75-86, 1979.
58. Perry, R.H., D.W. Green and J.O. Maloney (eds.), *Perry's Chemical Engineers' Handbook*, McGraw-Hill, New York, NY, 1984.
59. Morgan, J.L.R. and C.E. Davis, "The properties of mixed liquids. I. Sulfuric acid-water mixtures," *Journal of the American Chemical Society*, Vol. 38, pp. 555-568, 1916.
60. Myhre, C.E.L., C.J. Nielsen and O.W. Saastad, "Density and surface tension of aqueous H2SO4 at low temperature," *Journal of Chemical Engineering Data*, Vol. 43, pp. 617-622, 1998.
61. Hilsenrath, J., C.W. Beckett, W.S. Benedict, L. Fano, H.J. Hoge, J.F. Masi, R.L. Nuttall, Y.S. Touloukian and H.W. Woolley, *Tables of Thermal Properties of Gases Comprising Tables of Thermodynamic and Transport Properties of Air, Argon, Carbon Dioxide, Carbon Monoxide, Hydrogen, Nitrogen, Oxygen, and Steam*, U.S. Department of Commerce, National Bureau of Standards, NBS Circular 564, Gaithersburg, MD, 1955.
62. Marrero, T.R. and E.A. Mason, "Gaseous diffusion coefficients," *Journal of Physical and Chemical Reference Data*, Vol. 1, pp. 3-118, 1972.

APPENDIX A. CORRELATIONS FOR SULFURIC ACID DENSITY, SULFURIC ACID SURFACE ENERGY, AND THE VAPOR PRESSURE OF WATER OVER SULFURIC ACID AT 333.15 K (140 °F).

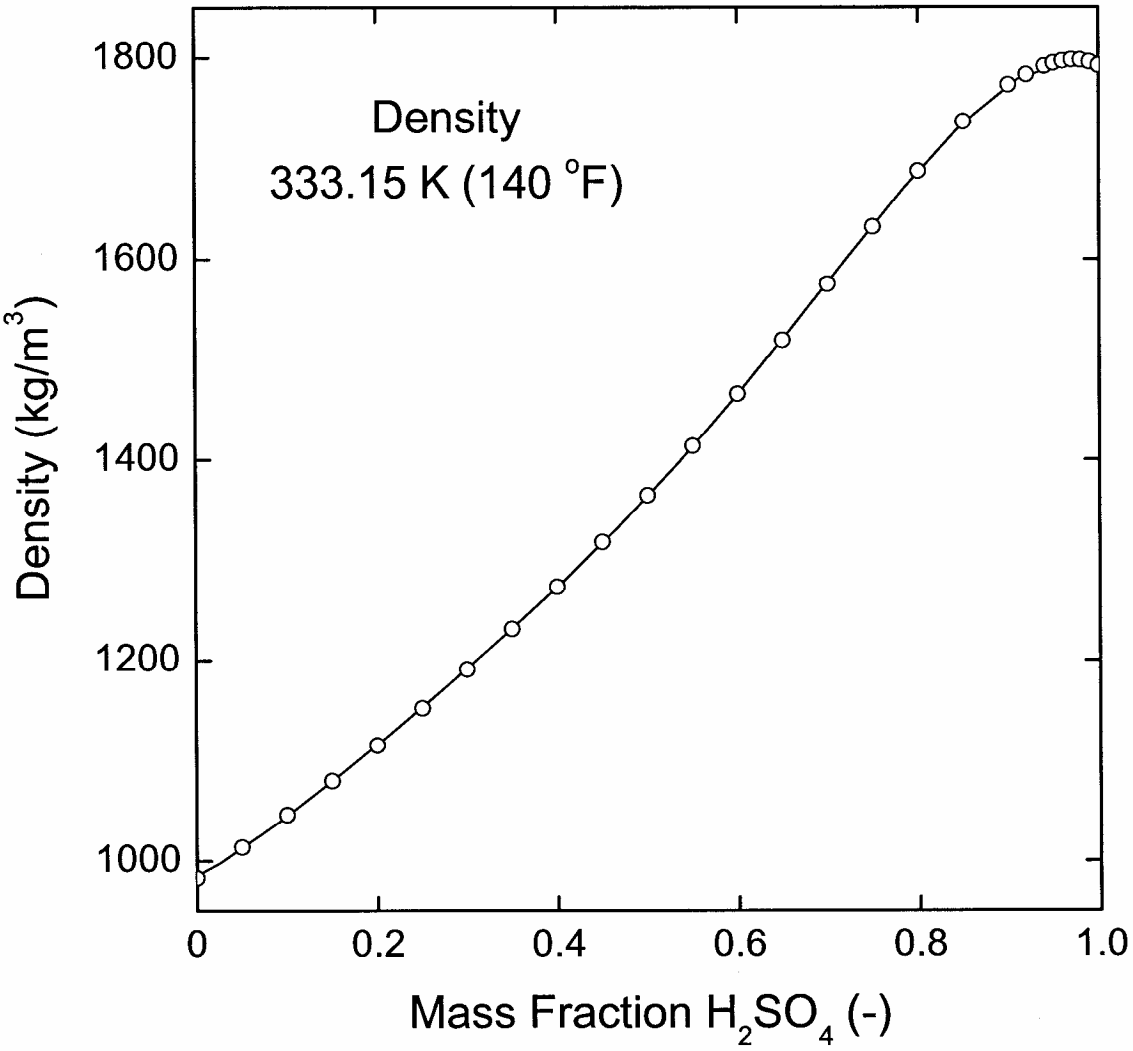

$$\rho_a = 984.38623 + 508.41087\, Y_a + 1291.75158\, Y_a^2 - 3787.52718\, Y_a^3 + 6008.2008\, Y_a^4 - 3211.78493\, Y_a^5$$

Perry's Chemical Engineers' Handbook, 6th ed.,
D. W. Green and J. O. Maloney (Eds.), McGraw-Hill,
New York, 1984, pp. 3-76, 3-85, and 3-86.

Figure A1

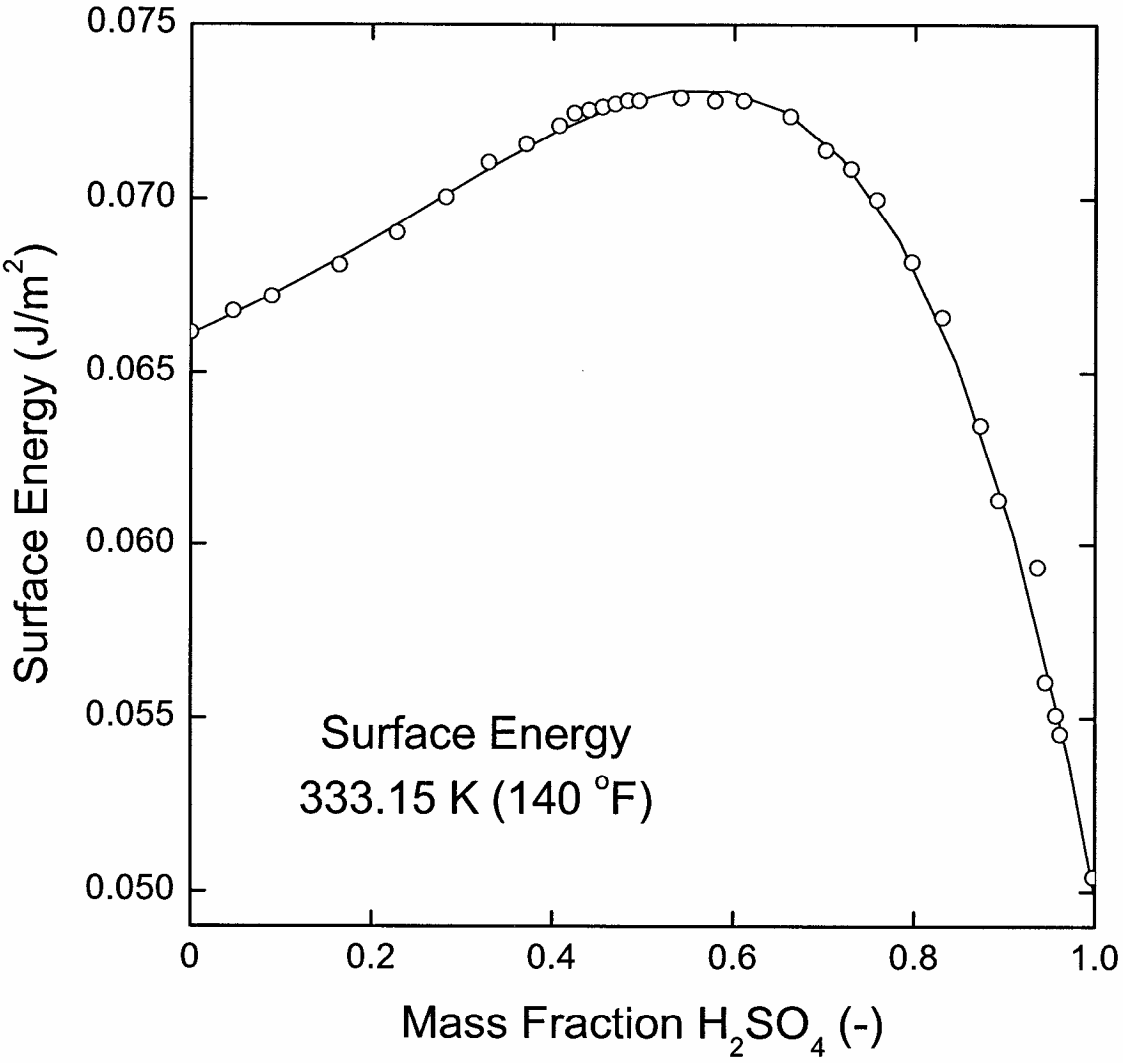

$$\gamma_a = 0.0661 + 0.01206\, Y_a + 0.00552\, Y_a^2 + 0.02411\, Y_a^3 - 0.05772\, Y_a^4$$

Morgan and Davis, *J. Am. Chem. Soc. 38* (1916) 555.
Corrected by Myhre, Nielsen, and Saastad,
J. Chem. Eng. Data 43 (1998) 617, and extrapolated
from 323 to 333 K.

Figure A2

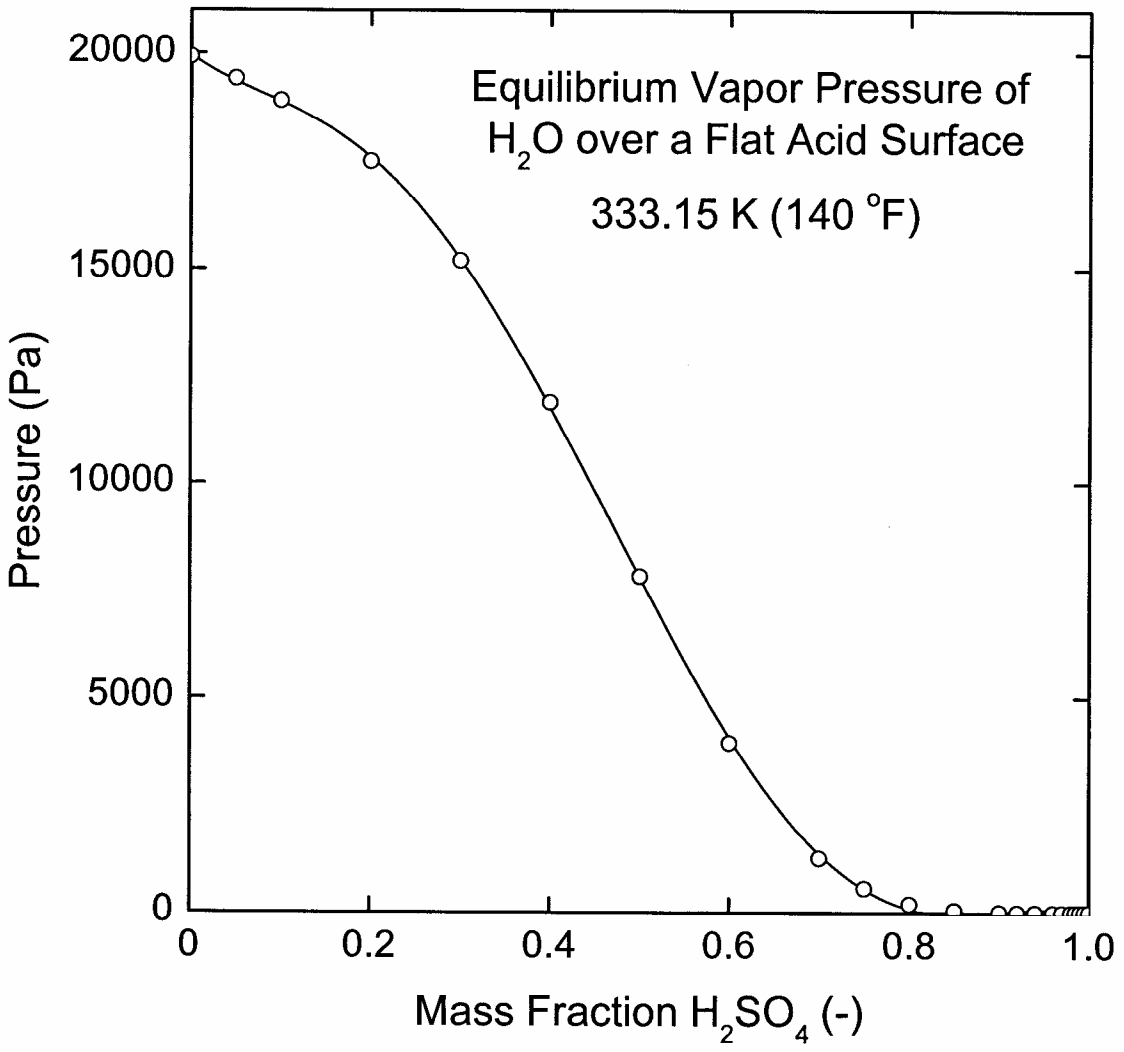

$$p_{w/a} = 19955.45586 - 15325.75513\ Y_a + 84410.70689\ Y_a^2 - 446027.0626\ Y_a^3 + 607784.80457\ Y_a^4 - 250883.30342\ Y_a^5$$

Perry's Chemical Engineers' Handbook, 6th ed.,
D. W. Green and J. O. Maloney (Eds.), McGraw-Hill,
New York, 1984, pp. 3-65, 3-66, and 3-237.

Figure A3

APPENDIX B. COMPUTER CODE FOR THE CALCULATION OF ACID MIST PROPERTIES IN THE SCRUBBER AND STACK.

```
// Calculates the evolution of acid mist droplet size and composition following
// nucleation of sulfuric acid on quenching of flue gas at the entrance to
// a wet scrubber.  The starting point is individual molecules of H2SO4.H2O.
// Growth is by coagulation of acid mist droplets with each other and absorption
// of water vapor by the acid droplets.  Evaporation of water from scrubber spray
// droplets maintains a steady water vapor concentration in the flue gas.
// Coagulation of acid mist droplets with the scrubber droplets is also included.

#include <stdio.h>
#include <math.h>
#include <stdlib.h>

#define  PI  3.1415927
#define  R  8314.51  //J/kmol K  universal gas constant
#define  TSCRB  333.15  //K  = 140 deg F
#define  WA  98.08  //kg/kmol  molecular weight H2SO4
#define  WW  18.01534  //kg/kmol  molecular weight H2O
#define  WFG  30.  //approximate average molecular weight of flue gas
#define  KB  1.38e-23  //J/K  Boltzmann constant
#define  P0  101325.  //Pa  atmospheric pressure
#define  N0  6.022e26  //kmol-1  Avogadro's number
#define  PWW  19955.5  //Pa  equilibrium vapor pressure of steam over flat water surface, from fi
t to data.
#define  UFG  3.7  //m/s  flue gas velocity (12 ft/s)
#define  LG  150.  //liquid-to-gas ratio in scrubber, gallon per 1000 actual cubic feet
#define  CD  0.54  //Drag coefficient for scrubber spray droplets, Michalski, 2000.

double  ya, y, seplus, rhoaplus, seminus, rhoaminus, dsedy, drhoady, rhoady, rhoa, se, pwaf, pwa;
double  rhofg, nad0, ttot, cma0, cma, tres, nad, da, mad, mad0, mufg, dw, Rew, Scw, Shw, swdw;
double  difw, kw, kn, Sha, ka, cad2, cad, ccad, difad, knad, cfg2, cfg, knfg, beta, kad, dnadca;
double  dnadcw, dcmadw, dcmacw, da3, volfr, rh, acap, ppm0, time, udwt, udwt2, cw, cw2, knw;
int     I;

    void main(void)
{
    FILE *outfile;
    outfile = fopen("cout1.dat", "w");

    //Adjustable parameters
    ppm0 = 10.e-6;  //mole fraction H2SO4 in flue gas
    dw =  0.001;  //m  scrubber spray droplet diameter
```

```
    //Initialize integration variables and properties of acid mist nuclei.
    //Calculate physical properties.
    I = 1;
    tres = 0.;
    ttot = 0.;
    ya = WA / (WA + WW);  //mass fraction H2SO4 in H2SO4.H2O = 0.845
    y = ya;
    rhoa = 984.4 + 508.4 * y + 1292. * pow(y, 2.) - 3788. * pow(y, 3.) + 6008. * pow(y, 4.) - 321
2. * pow(y, 5.);
    mad = (WA + WW) / N0;  //Mass of H2SO4.H2O molecule
    da3 = (mad / rhoa) * 6. / PI;
    da = pow(da3, (1./3.));  //Diameter of H2SO4.H2O molecule
    rhofg = P0 * WFG / (R * TSCRB);
    nad0 = ppm0 * P0 * N0 / (R * TSCRB);
    cma0 = ppm0 * P0 * WA / (R * TSCRB);
    cma = cma0/ya;
    nad = nad0;
    mad0 = cma / nad;
    mad = mad0;
    mufg = 14.58e-7 * pow(TSCRB, 1.5) / (TSCRB + 110.4);
    difw = 0.187e-9 * pow(TSCRB, 2.072);  //Marrero and Mason, H2O-N2, 282-373 K
    Scw = mufg / (rhofg * difw);

    //Set parameters depending upon scrubber spray quality
    udwt2 = 4. * 1225 * 9.8 * dw / (3. * CD * rhofg);
    udwt = pow(udwt2, 0.5);  //terminal velocity of water droplets
    Rew = rhofg * udwt * dw / mufg;  //water droplet Reynolds number
    Shw = 2. + 0.6 * pow(Rew, 0.5) * pow(Scw, (1./3.));  //Frossling and Ranz and Marshall correl
ation
    swdw = (LG * 0.0001337 * UFG / fabs(udwt - UFG)) * (6. / dw);  //m-1  product of specific sur
face area and concentration
    kw = (Shw * difw / dw) * swdw;  //mass transfer coefficient for water vapor moving away from
water droplets

    while (ttot < 5.)
    {
        if (ttot <= 1.e-9)
            tres = 0.01e-9;
        if (ttot > 1.e-9)
            tres = 0.1e-9;
        if (ttot >= 10.e-9)
            tres = 1.e-9;
```

```
        if (ttot >= 100.e-9)
            tres = 10.e-9;
        if (ttot >= 100.e-6)
            tres = 0.1e-6;
        if (ttot >= 5.e-3)
            tres = 1.e-6;
        if (ttot >= 50.e-3)
            tres = 10.e-6;
        if (ttot >= 0.5)
            tres = 0.0001;

        y = ya + 0.0005;
        seplus = 0.0661 + 0.01206 * y + 0.00552 * pow(y, 2.) + 0.02411 * pow(y, 3.) - 0.05772 * p
ow(y, 4.);
        rhoaplus = 984.4 + 508.4 * y + 1292. * pow(y, 2.) - 3788. * pow(y, 3.) + 6008. * pow(y, 4
.) - 3212. * pow(y, 5.);
        y = ya - 0.0005;
        seminus = 0.0661 + 0.01206 * y + 0.00552 * pow(y, 2.) + 0.02411 * pow(y, 3.) - 0.05772 *
pow(y, 4.);
        rhoaminus = 984.4 + 508.4 * y + 1292. * pow(y, 2.) - 3788. * pow(y, 3.) + 6008. * pow(y,
4.) - 3212. * pow(y, 5.);
        dsedy = (seplus - seminus) / 0.001;
        drhoady = (rhoaplus - rhoaminus) / 0.001;
        y = ya;
        rhoa = 984.4 + 508.4 * y + 1292. * pow(y, 2.) - 3788. * pow(y, 3.) + 6008. * pow(y, 4.) -
 3212. * pow(y, 5.);
        se = 0.0661 + 0.01206 * y + 0.00552 * pow(y, 2.) + 0.02411 * pow(y, 3.) - 0.05772 * pow(y
, 4.);
        pwaf = PWW - 15326. * y + 84411. * pow(y, 2.) - 446027. * pow(y, 3.) + 607785. * pow(y, 4
.) - 250883. * pow(y, 5.);
            if (pwaf < 0.)
                pwaf = 0.;
        pwa = pwaf * exp((4. * se * WW / (da * rhoa * R * TSCRB)) * (1. + (ya * drhoady / rhoa) -
 (3. * ya * dsedy / (2. * se))));
        cw2 = 8. * R * TSCRB / (PI * WW);
        cw = pow(cw2, 0.5);
        knw = 4. * difw / (cw * da);
        Sha = 2. * ((1. + knw) / (1. + 2. * knw * (1. + knw)));
        ka = (Sha * difw / da) * (6. / (rhoa * da)) * cma;
        cad2 = 8. * KB * TSCRB / (PI * mad);
        cad = pow(cad2, 0.5);
        cfg2 = 8. * R * TSCRB / (PI * WFG);
```

```
        cfg = pow(cfg2, 0.5);
        knfg = 4. * difw / (cfg * da);
        ccad = 1. + (knfg * (1.257 + (0.4 / exp(1.1 / knfg))));  //Cunningham correction
        difad = KB * TSCRB * ccad / (3. * PI * mufg * da);
        knad = 2. * pow(2., 0.5) * difad / (cad * da);
        beta = (1. + knad) / (1. + 2. * knad * (1. + knad));
        kad = 8. * PI * da * difad * beta;
        dnadca = (kad / 2.) * pow(nad, 2.) * tres;
                 //Decrease in acid droplet number concentration by coagulation with themselves
        dcmadw = ((PWW - pwa) * WW * tres) / (R * TSCRB * ((1./ka) + (1./kw)));
                 //Increase in acid droplet concentration by addition of water by diffusion
        dcmacw = (Shw * difad / dw) * swdw * cma * tres;
                 //Loss of acid droplets by coagulation with water spray droplets
        cma = cma + dcmadw - dcmacw;
        dnadcw = dcmacw / mad;  //Loss in acid droplet number concentration to water spray drople
ts
        nad = nad - dnadca - dnadcw;
        acap = acap + dcmacw * ya / cma0;  //Cumulative fraction of original acid captured by wat
er spray
        mad = cma / nad;
        ya = cma0 * (1. - acap) / cma;
        y = ya;
        rhoa = 984.4 + 508.4 * y + 1292. * pow(y, 2.) - 3788. * pow(y, 3.) + 6008. * pow(y, 4.) -
 3212. * pow(y, 5.);
        da3 = (mad / rhoa) * 6. / PI;
        da = pow(da3, (1./3.));
        volfr = cma / rhoa;
        rh = (1. + (ka * pwa / (kw * PWW))) / (1. + (ka / kw));
        ttot = ttot + tres;

        if (I == 100)
        {
            printf("\n%9.6lf %9.6lf %9.6lf  %9.6e  %9.3e %8.3lf %8.5lf", ttot, da*1.e6, ya, nad,
volfr, rh*100., acap);
            fprintf(outfile, "\n%10.6e %10.6lf %10.6lf %10.3e %10.3e %8.5lf", ttot, da*1.e6, ya,
nad, volfr, acap);
            I = 0;
        }
        I = I + 1;
    }

    //Enter stack; change water droplet size
```

```
    dw =  10.e-6;  //m  droplet diameter downstream from the mist eliminator
    Shw = 2.;  //Droplets move with stack gas
    swdw = (LG * 0.0001337 * 1.) * (6. / dw);  //m-1  product of specific surface area and concen
tration
    swdw = 5.e-6 * swdw;  //5 wt ppm of scrubber liquor passes the mist eliminator
    kw = (Shw * difw / dw) * swdw;  //mass transfer coefficient for water vapor moving away from
water droplets

    while (ttot < 20.)
    {
        tres = 0.0001;
        y = ya + 0.0005;
        seplus = 0.0661 + 0.01206 * y + 0.00552 * pow(y, 2.) + 0.02411 * pow(y, 3.) - 0.05772 * p
ow(y, 4.);
        rhoaplus = 984.4 + 508.4 * y + 1292. * pow(y, 2.) - 3788. * pow(y, 3.) + 6008. * pow(y, 4
.) - 3212. * pow(y, 5.);
        y = ya - 0.0005;
        seminus = 0.0661 + 0.01206 * y + 0.00552 * pow(y, 2.) + 0.02411 * pow(y, 3.) - 0.05772 *
pow(y, 4.);
        rhoaminus = 984.4 + 508.4 * y + 1292. * pow(y, 2.) - 3788. * pow(y, 3.) + 6008. * pow(y,
4.) - 3212. * pow(y, 5.);
        dsedy = (seplus - seminus) / 0.001;
        drhoady = (rhoaplus - rhoaminus) / 0.001;
        y = ya;
        rhoa = 984.4 + 508.4 * y + 1292. * pow(y, 2.) - 3788. * pow(y, 3.) + 6008. * pow(y, 4.) -
 3212. * pow(y, 5.);
        se = 0.0661 + 0.01206 * y + 0.00552 * pow(y, 2.) + 0.02411 * pow(y, 3.) - 0.05772 * pow(y
, 4.);
        pwaf = PWW - 15326. * y + 84411. * pow(y, 2.) - 446027. * pow(y, 3.) + 607785. * pow(y, 4
.) - 250883. * pow(y, 5.);
            if (pwaf < 0.)
                pwaf = 0.;
        pwa = pwaf * exp((4. * se * WW / (da * rhoa * R * TSCRB)) * (1. + (ya * drhoady / rhoa) -
 (3. * ya * dsedy / (2. * se))));
        cw2 = 8. * R * TSCRB / (PI * WW);
        cw = pow(cw2, 0.5);
        knw = 4. * difw / (cw * da);
        Sha = 2. * ((1. + knw) / (1. + 2. * knw * (1. + knw)));
        ka = (Sha * difw / da) * (6. / (rhoa * da)) * cma;
        cad2 = 8. * KB * TSCRB / (PI * mad);
        cad = pow(cad2, 0.5);
        cfg2 = 8. * R * TSCRB / (PI * WFG);
```

```
        cfg = pow(cfg2, 0.5);
        knfg = 4. * difw / (cfg * da);
        ccad = 1. + (knfg * (1.257 + (0.4 / exp(1.1 / knfg))));  //Cunningham correction
        difad = KB * TSCRB * ccad / (3. * PI * mufg * da);
        knad = 2. * pow(2., 0.5) * difad / (cad * da);
        beta = (1. + knad) / (1. + 2. * knad * (1. + knad));
        kad = 8. * PI * da * difad * beta;
        dnadca = (kad / 2.) * pow(nad, 2.) * tres;
        dcmadw = ((PWW - pwa) * WW * tres) / (R * TSCRB * ((1./ka) + (1./kw)));
        dcmacw = (Shw * difad / dw) * swdw * cma * tres;
        cma = cma + dcmadw - dcmacw;
        dnadcw = dcmacw / mad;
        nad = nad - dnadca - dnadcw;
        acap = acap + dcmacw * ya / cma0;
        mad = cma / nad;
        ya = cma0 * (1. - acap) / cma;
        y = ya;
        rhoa = 984.4 + 508.4 * y + 1292. * pow(y, 2.) - 3788. * pow(y, 3.) + 6008. * pow(y, 4.) -
 3212. * pow(y, 5.);
        da3 = (mad / rhoa) * 6. / PI;
        da = pow(da3, (1./3.));
        volfr = cma / rhoa;
        rh = (1. + (ka * pwa / (kw * PWW))) / (1. + (ka / kw));
        ttot = ttot + tres;

        if (I == 100)
        {
            printf("\n%9.6lf %9.6lf %9.6lf  %9.6e  %9.3e %8.3lf %8.5lf", ttot, da*1.e6, ya, nad,
volfr, rh*100., acap);
            fprintf(outfile, "\n%10.6e %10.6lf %10.6lf %10.3e %10.3e %8.5lf", ttot, da*1.e6, ya,
nad, volfr, acap);
        I = 0;
        }
        I = I + 1;
    }

return;
}
```